MODELING AND CONTROL OF A TILT-DUCT VTOL UAV

A THESIS SUBMITTED TO
THE GRADUATE SCHOOL OF NATURAL AND APPLIED SCIENCES
OF
THE MIDDLE EAST TECHNICAL UNIVERSITY

BY

AYCAN OKAN

IN PARTIAL FULFILLMENT OF THE REQUIREMENTS FOR THE DEGREE OF
MASTER OF SCIENCE
IN
THE DEPARTMENT OF AERONAUTICAL ENGINEERING

DECEMBER 2000

Approval of the Graduate School of Natural and Applied Sciences.

Prof. Dr. Tayfur ÖZTÜRK
Director

I certify that this thesis satisfies all the requirements as a thesis for the degree of Master of Science.

Prof. Dr. H. Nafiz ALEMDAROĞLU
Head of Department

This is to certify that I have read this thesis and that in my opinion it is fully adequate, in scope and quality, as a thesis for the degree of Master of Science.

Assoc. Prof. Dr. Ozan TEKİNALP
Supervisor

Examining Committee Members

Prof. Dr. İ. Sinan AKMANDOR

Prof. Dr. Ersin TULUNAY (Chairman)

Assoc. Prof. Dr. Mehmet Ş. KAVSAOĞLU

Assoc. Prof. Dr. Ozan TEKİNALP (Supervisor)

Dr. Volkan NALBANTOĞLU

ABSTRACT

MODELING AND CONTROL OF A TILT-DUCT VTOL UAV

OKAN, Aycan
M. S., Department of Aeronautical Engineering
Supervisor: Assoc. Prof. Dr. Ozan TEKİNALP

December 2000, 138 pages

In this thesis, first the new tilt-duct VTOL UAV concept, which is an original work of a research group where the author is an active member, is presented. The conceptual design study process carried out until now is summarized under related topics and some geometric and performance characteristics are given. Then, flight mechanics equations for this VTOL UAV are derived. Trim flight conditions at various flight regimes are obtained using these nonlinear equations. For this purpose a trim program, which finds the trim conditions by solving relevant optimization problems. Various trim conditions for hover, transition and cruise flight modes are obtained. The nonlinear equations are linearized at these trim flight conditions and the aircraft stability is investigated. The automatic flight control system designed by using classical root locus analyses as well as linear quadratic regulator design is presented.

Keywords: Unmanned aerial vehicle (UAV), tilt-duct, vertical takeoff and landing (VTOL), flight mechanics, hover, stability, trim, transition, feedback, control.

ÖZ

HAREKETLİ KANAL TİPİNDE DİKİNE KALKIP İNEBİLEN BİR İNSANSIZ HAVA ARACININ MODELLENMESİ VE DENETİMİ

OKAN, Aycan
Yüksek Lisans, Havacılık Mühendisliği Bölümü
Tez Yöneticisi: Doç. Dr. Ozan TEKİNALP

Aralık 2000, 138 sayfa

Bu tezde, öncelikle yazarın da faal bir üyesi olduğu araştırma grubunun özgün bir çalışması olan, hareketli kanal tipinde yeni bir dikine kalkıp inebilen insansız hava aracı kavramı sunulmuştur. Gerçekleştirilen kavramsal tasarım çalışması özetlenmiş ve bazı geometrik ve performans karakteristikleri ilgili tablolarda verilmiştir. Tasarlanan insansız hava aracı için uçuş mekaniği denklemleri çıkarılmıştır. Doğrusal olmayan yunuslama yönündeki denklemler kullanılarak değişik uçuş bölgeleri için çeşitli trim (denge) şartları elde edilmiştir. Bu amaçla, trim (denge) şartlarını eniyileme yoluyla hesaplayan bir program geliştirilmiştir. Bu program yardımıyla, dikine hareket, geçiş bölgesi ve geleneksel uçuş için trim (denge) koşulları elde edilmiştir. Doğrusal olmayan uçuş denklemleri bu noktalarda doğrusallaştırılmış ve hava aracının kararlılık çözümlemesi gerçekleştirilmiştir. Kök yeri grafiği vb. klasik denetim yöntemleri ve

doğrusal ikinci dereceden düzenleyici tasarımı gibi teknikler kullanılarak tasarlanan otomatik uçuş denetim dizgesi sunulmuştur.

Anahtar Kelimeler: İnsansız hava aracı (İHA), hareketli kanal, dikine kalkıp inebilme yetisi, uçuş mekaniği, dikine hareket, kararlılık, denge hali, geçiş bölgesi, geri besleme, denetim.

This study is dedicated to my mother, father and grandmother.

ACKNOWLEDGMENTS

I would like to express my gratitude to Assoc. Prof. Dr. Ozan Tekinalp for his supervision, guidance, encouragement and patience during all the stages of this thesis.

I would also like to thank to Assoc. Prof. Dr. Mehmet Ş. Kavsaoğlu and Prof. Dr. Ersin Tulunay for their helpful comments and suggestions.

Thanks are also extended to Ms. Özlem Armutcuoğlu for her support in the group study, all of my friends for their encouragement, and all of the members of the Department of Aeronautical Engineering, METU.

Finally, I would like to express all my love to my family for their support and patience during this study and my life.

TABLE OF CONTENTS

LIST OF TABLES

TABLE

LIST OF FIGURES

FIGURES

CHAPTER 1

INTRODUCTION

1.1 The Aim of the Thesis

The aim of this thesis is to introduce the new tilt-duct vertical takeoff and landing (VTOL) unmanned aerial vehicle (UAV) concept developed and represent the flight mechanics modeling of this new concept as well as to present the analysis carried out to investigate aircraft stability. Also automatic flight control system designed for this new concept is presented.

This study is a part of a research activity being carried out in the research group, with members from the Department of Aeronautical Engineering and the Department of Electrical and Electronics Engineering, Middle East Technical University. The group introduced in Section 1.5 decided to work on UAVs due to the challenging issues and considerable interest on UAVs in our country. The core of the team consists of three faculty members and two research assistants. The project had started in 1998. The main purpose of the group is to develop an autonomously controlled VTOL UAV, which can takeoff and land vertically as helicopter and convert to a propeller driven airplane in forward flight mode by tilting its ducted propellers forward. In this way, the aircraft will not need a runway for takeoff or landing besides it can reach higher speeds than a conventional helicopter in forward flight.

1.2 Overview of Related Work on VSTOL Aircraft

Since vertical flight became accessible in the mid 1940's, better safety, and performance, and higher speed have always been desired. A great deal of work has been done in search of these goals, especially in the last twenty years with the advances in computing of tiltrotor aircraft. Many different vertical/short takeoff and landing (VSTOL) concepts have been researched. Several have been built and flown, and even more have been studied in depth with theoretical analysis, wind tunnel tests and other means.

There are two primary methods by which VSTOL aircraft are classified by mission and by propulsive lift concept.

By propulsive lift concept, the VSTOL aircraft can be listed in order of descending disk loading as following, [2]

i) Direct Lift (Deflected Thrust)
ii) Jet Augmented Lift
iii) Fan-in-wing
iv) Propeller (tilt-propeller, tilt-wing and tilt-duct)
v) Rotor (compound helicopter, tilt-rotor, rotor-wing concept, stoppable and stowable rotor concepts,

Direct lift concepts are those, which use turbojet or turbofan engines to provide all lift required for vertical takeoff and substantial lift for short takeoff and landing operation of this type of aircraft. Such engines have vertical thrust and selective lift/cruise thrust generation applications.

The X-14, a small research aircraft built by Bell was an early version of this type. Thrust diverter vanes in the tailpipes located below the pilot at about the c.g. direct the exhaust gas down for hover. This method for thrust vectoring may be called as deflected thrust or jet concept. The Harrier, having four rotating nozzles

is also direct lift aircraft. The VJ-101 from Germany, which has tilting engines mounted in wing tip pods can be classified as tilt-jet concept. In tilt-jet concept, two main models were used. The jet engines could be mounted so that they tilt, or they can be fixed, with control over the thrust vector by vanes in the jet exit. By either method, the direction of thrust can be varied by a separate control, from vertical to horizontal at the will of the pilot. The Bell X-14 VTOL shown in Figure 1.1, was one such aircraft that has been tested extensively. The ShortSC. 1 and the French Dassault Balzac, proposed Mirage 3V also used separate lift and cruise engines. [2]

In the jet augmented lift concept (i.e., jet ejector concept), the engine exhaust gases are ejected downward through an ejector nozzle, pulling additional air through the ejector to augment the basic jet thrust by about 35-40 percent. The Lockheed XV-4A Hummingbird was built to investigate this concept and could achieve nearly half of the desired thrust augmentation in the flight test [2].

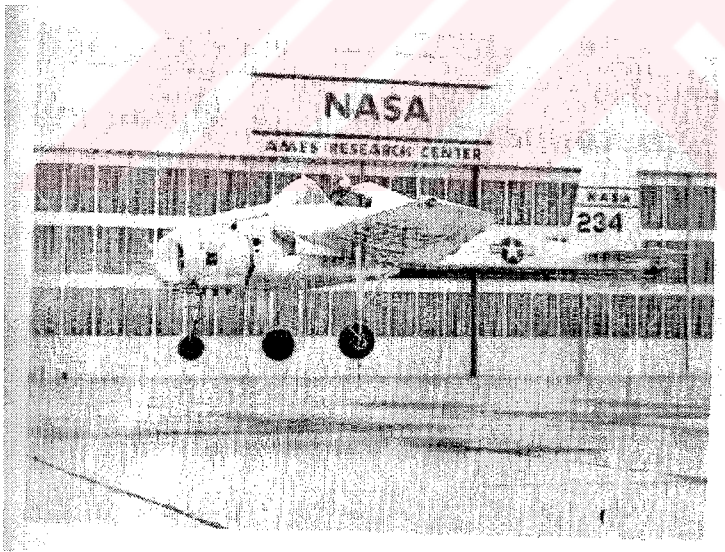

Figure 1.1 The Bell X-14 VTOL aircraft [3]

In fan-in-wing concept, the Ryan XV-5, shown in Figure 1.2, was a unique configuration. Two large fans, covering much of the planform, were mounted on

each side of the airplane in the wing. These fans were driven by turbine blades mounted directly to a ring around the fan blade tips. For vertical takeoff, panels on the wing surface was opened and the engine exhaust was diverted to drive the tip turbines. After transition phase from hovering to forward flight, the panels were closed to form solid wing surface and the engine exhaust directed rearward [4].

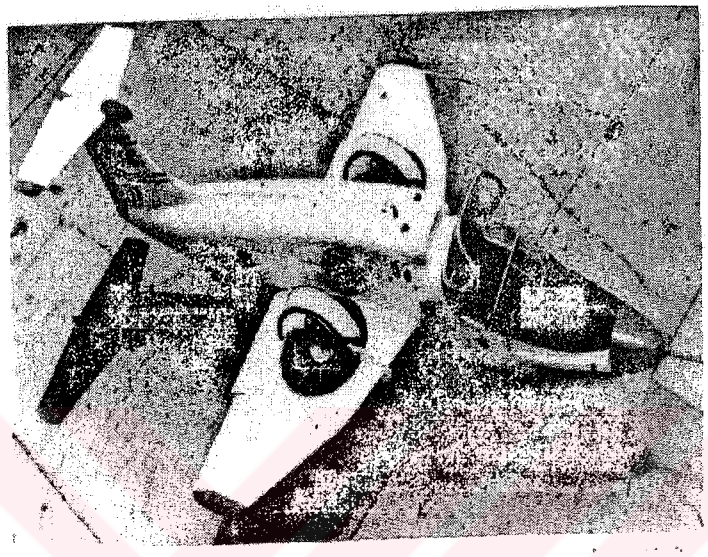

Figure 1.2 The Ryan XV-5, a fan-in-wing VTOL aircraft [4]

There are basically three types of propeller type VSTOL aircraft. These are tilt-propeller, tilt-wing and the tilt-duct propeller concepts.

In tilt propeller concept, the wing is fixed and only the propellers of the aircraft tilt between a roughly vertical direction for hover and horizontal direction for forward flight. In hover mode, pitch and yaw control was provided by the jet deflection at the tail, and roll control was achieved by differential pitch between two propellers. In forward flight conventional control surfaces were used. The Curtiss-Wright X-100 VTOL aircraft, shown in Figure 1.3 is a typical example of this concept. [2]

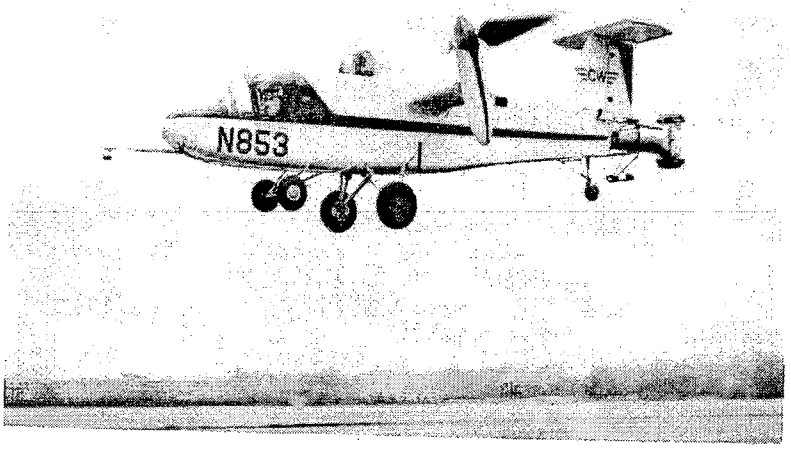

Figure 1.3 The Curtiss-Wright X-100 VTOL aircraft [3]

When the entire wing is immersed in the propeller slipstream and tilts with the propellers, the aircraft is known as tilt-wing. Two early models designed to investigate the feasibility of this concept were Hiller X-18 and the Boeing Vertol VZ-2. The VZ-2 aircraft, shown in Figure 1.4, used flapping rotors mounted on a tilting wing. In hover mode, control, with the wing vertical, was cyclic pitch for longitudinal moments, differential collective for roll moments, and tail rotor collective pitch for yawing moments. With the wing tilted over, the aircraft gains higher speed and the conventional control surfaces could be used. The Canadair CL-84, the LTV XC-142, Kaman K-16 were important examples for this type [3].

With the idea of improving hover performance of propeller VSTOL aircraft, the solution is to enclose the propellers in ducts. It is effective for hover but it adds drag at high cruise speeds. The Doak VZ-4DA, shown in Figure 1.5 had a ducted propeller at each wing tip. The second tilt-duct VSTOL aircraft was the Bell Aerospace X-22A.It had four ducted propellers. The Doak VZ-4DA had highly loaded ducted propellers on the wing tips support the aircraft in hovering,

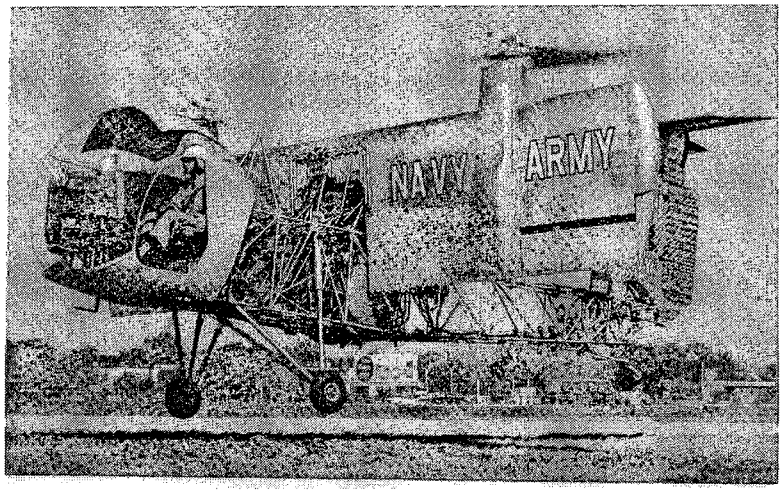

Figure 1.4 The Boeing Vertol VZ-2 VTOL aircraft [4]

and rotate forward to produce forward thrust in cruise flight mode. In this mode, the conventional controls were used. In hover mode, yaw and pitch control were achieved by deflection of the jet exhaust at the tail. Roll was controlled by differential thrust between two propellers [3,4].

There are few types of the rotor type VSTOL aircraft. These are compound helicopters, tilt-rotor concepts, rotor-wing concept, stoppable and stowable rotor concepts.

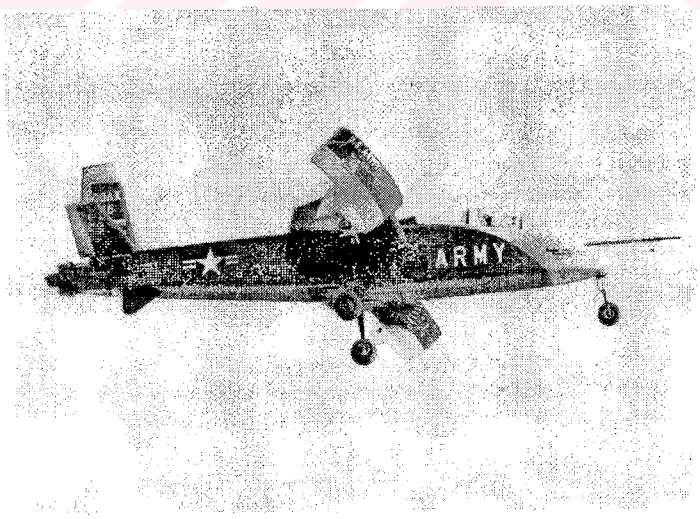

Figure 1.5 The Doak VZ-4DA VTOL aircraft [3]

When some forward thrust device is used in addition to the main rotor, a helicopter can be defined as a compound helicopter. These auxiliary thrust devices may be rotors, propellers or jet engines, and may be powered by the main power plants or separate engines entirely. The rotor can be operated at lower lift coefficients or "unloaded" if part of the aircraft weight can be supported by small wings. The compound version of UH-1 was developed by the Bell Helicopter Company. Also Lockheed AH-56A Cheyenne was an example of this type of the aircraft [2].

Tilt-rotor aircraft are another and maybe the most important class of the VSTOL aircraft powered by the rotors. Such rotors are mounted near the wing tips. In the 1940s The Transcendental Aircraft Co. designed and built the Model 1-G, shown in Figure 1.6, the first tilt-rotor VTOL aircraft. It was a single place, research aircraft with a gross weight of 794 kg and two 5.2 m diameter, tilting rotors [2,4].

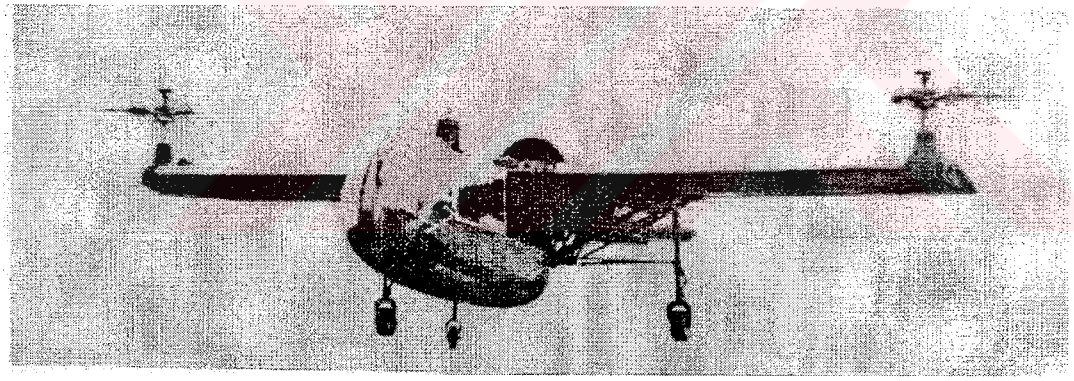

Figure 1.6 The Transcendental 1-G, the first tilt-rotor VTOL aircraft [4]

In the mid 1950's, Bell Helicopter and Boeing involvement in the design and test of tiltrotor vehicles and models started. Beginning with the XV-3, shown in Figure 1.7, Bell's initial tiltrotor design, and maturing with the XV-15, many different engineering methods have been used to prepare these aircraft to fly safely and efficiently. The XV-15 is a fully researched tiltrotor aircraft. It was subject to detailed analyses, simulations and full-scale wind tunnel tests. The program began

in the early 1970's and continued into the 1990's. The success of the XV-15's program and Boeing advances in composite structures and rotors, electronic flight controls and aerodynamics demonstrated the maturity of the technology and provided the necessary confidence that led to the most extensive tiltrotor program supported by the United States government to date, the V-22 Osprey world's first production tiltrotor [2,3,4,5].

V-22 Osprey, shown in Figure 1.8 is the first military version tiltrotor and is currently in production and initial deliveries of its over 500 orders to United States Navy, began in 1999. It has an empty weight of 15025 kg and can carry 24 combat troops or up to 9070 kg of cargo. The BA 609 Civil Tiltrotor is similar in size to the XV-15, but it is much more sophisticated because of the maturing technology gained from the V-22 project. It has maximum gross weight of 7254 kg

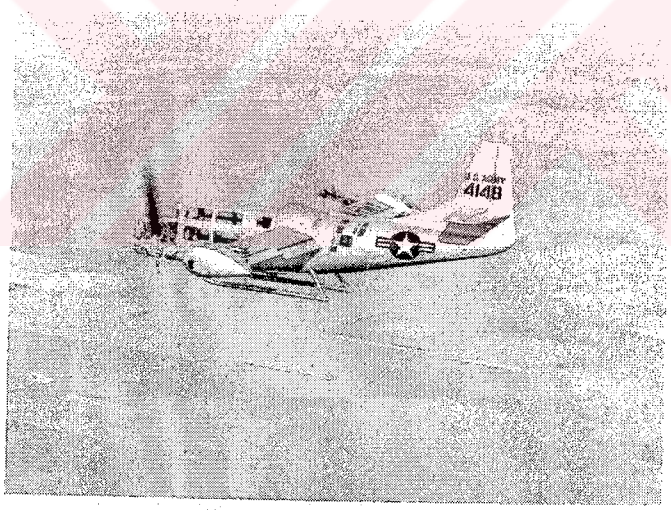

Figure 1.7 The Bell XV-3 VTOL aircraft [3]

Two PT-6 turboshaft engines will be used. The corporate version will allow for 6 to 9 passengers. It may also be used as an emergency vehicle for critical patients. The 609 is also proposed for non-civil Coast Guard service as the HV-609 [5].

Figure 1.8 The Bell-Boeing V-22 Osprey, a tilt-rotor VTOL aircraft [4]

Stopped and stowed rotors are more advanced rotor concepts. It would be desirable to takeoff, land and hover with a large rotor due to its good hovering efficiency, but it would also be desirable to get rid of it for forward flight. One way to solve this problem is stopping the rotor after takeoff procedure. Then, it might be used as a wing, such as the Hughes Hot Cycle rotor-wing concept [2].

Another possibility is to fold up the rotor and stow it in a streamlined compartment after it has been stopped. It would be unstowed, unfolded and started up again for landing.

Besides these listed concepts, there are two more original concepts in the literature. These are tail-sitters and propulsive wing concepts.

The second primary method of classifying VSTOL aircraft is by mission. Pure research vehicles, military prototypes and/or concept development testbeds, operational military vehicles and commercial aircraft can be listed.

1.3 Uninhabited Aerial Vehicles (UAVs) with Vertical Takeoff and Landing (VTOL) Capability

Uninhabited aerial vehicles (UAV) have attracted considerable interest from the military mainly for reconnaissance and surveillance purposes. It is important to gather information without endangering the lives of pilots. Additionally they should be much cheaper than a traditional reconnaissance aircraft. UAVs can be cheap because, without the need to carry life support, instruments, and escape systems for a pilot, they can be any size and can stay aloft or violently maneuver far beyond the limits of human endurance [1]. The absence of aircrew cuts significantly into life-cycle cost. Civilian uses, such as, aerial surveys for agriculture, traffic monitoring, pollution control, meteorological data collection, pipeline survey, early forest fire detection, security, natural resource inspection, overnight package delivery are also attracting interest.

This type of aircraft combines the vertical takeoff and landing (VTOL) capability of the helicopters with the superior forward flight performance of the fixed-wing conventional type of airplane. Their vertical flight capabilities may come from the various concepts that are listed in the previous section.

VTOL UAVs have their own characteristics and are generally more difficult to pilot than either conventional aircraft or helicopters. However, they can be operated without a need for a runway and launch-recovery system. Also, with the recent developments in automatic flight control systems, guidance techniques, sensor technology including electro-optical sensors, data-processing hardware, software techniques and navigation instruments (such as GPS), it is now possible to develop autonomous flight capability.

1.4 Unmanned (Uninhabited) Aerial Vehicles (UAVs)

Uninhabited aerial vehicles are commonly known by the acronym UAV and nearly everybody knows what it means. The word, "uninhabited" is, especially in Europe frequently substituted by "unmanned". This terminology is some

misleading nowadays, because as a matter of fact, "unmanned" implies that there is no possibility for human intervention, once vehicle is flying. At present, a remote pilot can intervene to cancel or to modify the mission at all times during the flight. So "uninhabited" is more appropriate [6].

Today, there are some special types of UAVs. In general, UAVs concern pilotless aircraft of small and medium size, mainly used for day and night observation equipped with necessary data link and sensors. If the topic is covered in details, it can be written that micro aerial vehicles (MAVs), tactical uninhabited aerial vehicles (TUAVs) and uninhabited combat aerial vehicles (UCAVs) are the members of this huge family.

Due to recent technological progress, especially in electro-optical sensors, UAVs have become very useful tool. At present the main accent is on military applications. However, it is beyond any doubt that there is an important potential for civil applications as well. Applications of UAVs in the civil and commercial markets and regulating the flight of these types are important discussion topics in aviation society.

UAVs have been used to achieve different missions for many years in both military and civil services. Some programs can be listed as, Predator, Pioneer, Perseus B, Darkstar, Outrider, Pathfinder, Apex, Hunter, Aquilla, Hermes, Global Hawk, Scout and Searcher, Altus where most of the programs are from USA [1,6].

Pioneer, shown in Figure 1.9, based on Israeli design, is manufactured in USA to provide imagery intelligence for tactical commanders on land and sea. It has a wingspan of 5.18 m and fuselage length of 4.27 m. Maximum takeoff weight is 204 kg and its payload capacity (TV/FLIR) amounts to 45 kg. It has a radius of action of 180 km and it can stay aloft for 5 hrs [6].

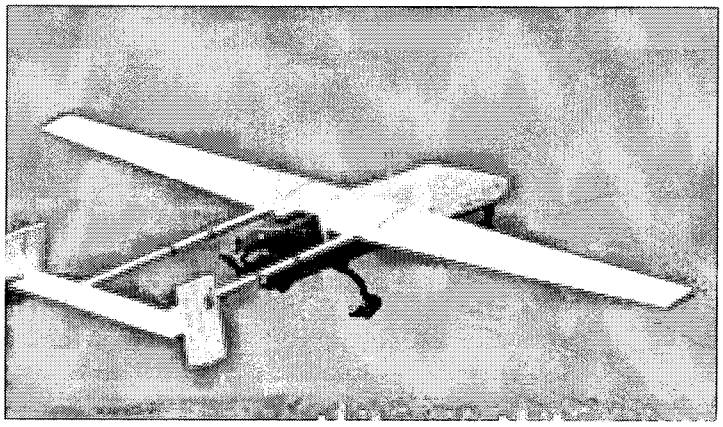

Figure 1.9 Pioneer UAV [1]

The UAV Eagle Eye Tiltrotor, shown in Figure 1.10 is also being researched in a flight demonstration program by Bell Helicopter. It has a maximum speed of 103 m/s (200 knots) and a controllable radius of 926 km (500 nautical miles) [5].

Since the very beginnings of aviation, the idea of a "remotely-piloted vehicle" has never been far from the minds of inventors and military strategists. The development of UAVs over the years has focused on target and training drones and, as technology has become more sophisticated, reconnaissance vehicles. In order to understand trend in UAVs from USA perspective, Figure 1.11 is very useful.

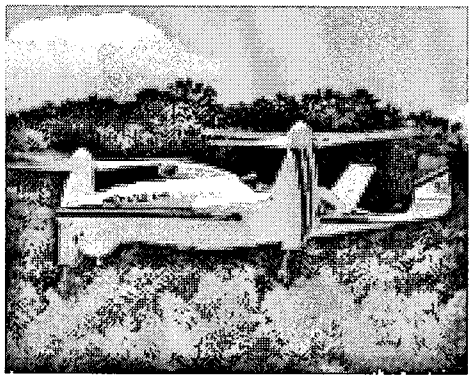

Figure 1.10 The Bell Helicopter Eagle Eye
(UAV flight demonstration program) [1]

Many other nations have recognized the utility of UAVs and are moving rapidly to develop their own capabilities. The Israelis were one of the firsts to go full-scale into the UAV business. Having a different geographic and geopolitical situation in Middle East and needing to multiply their forces by applying technology, the Israelis initially used UAV with considerable success. Israel has long been the preeminent developer of tactical UAVs, but with many more countries beginning to develop UAVs, its position has diminished. UAV development efforts in Western Europe have experienced many of the problems such as serious funding problems. The Franco-German Brevel program has similar problem. The Crecerelle of France has proven to be attractive. Also, it serves as the basis for the new Dutch Sperwer, and for a new Swedish program. Britain's Phoenix UAV is in production after a long series of delays. Switzerland took a more conservative route and based its new Ranger UAV on Israeli technology. Italy has an ambitious UAV program with its Mirach Meteor effort, but it remains to be seen whether the budget will permit fulfillment of this program. Spain has entered the UAV arena with its new SIVA program, and a related civil effort called ALO. UAV programs have also sprung up in Central and Eastern Europe. Russia has a long-standing interest in UAVs, though many of their vehicles were secret until recently. The Russian army has begun to deploy a new tactical UAV system called the Sterkh, and the air force has several programs underway including a new Tupolev air vehicle to replace its Reys system. The Czech Republic has developed the Sojka system, and has been offering it on the world export market. Japan has an active UAV program with both military and civil aspects. A helicopter drone is under development, both as a possible army surveillance platform, and as a possible agricultural sprayer. India has a number of UAV development efforts, though its recent purchase of Israeli UAVs suggests that these have not been entirely fruitful. Iran has been attempting to develop a UAV industry [1].

In Turkey, UAVs have attracted interest, too. Turkish Aerospace Industries, Inc. (TAI) has made some research activities on conventional type uninhabited aerial vehicle, UAV X-1 for reconnaissance and surveillance missions. However,

this program could not reach to the success and ended because of the different reasons. Nowadays, a new work is still continuing on UAVs including autopilot integration into the target drone, TAI-UKHU, produced by TAI previously [7]. Also, EES, Inc. produces Doğan and Kırlangıç UAVs, bought with licenses from Israel, in the Ankara facilities of the company. Also, our army is dealing with UAVs for military purposes.

As a result, there have been increasing demands in modern world to use UAV systems as intelligence, reconnaissance, surveillance, target acquisition and etc. Although requirements for UAVs change based on the missions to be carried, expectations are generally similar for each type. Cost effectiveness, reliability, maintainability, usefulness, operational availability, mobility, transportability, deployability, sustainability, survivability, vulnerability, growth potential, interchangeability and modularity are general requirements that all systems should have. UAVS are not only vehicle, they are more than this. It has subsystems such as air vehicle, ground control station, payloads (LCD camera, etc.), data link and support equipment. Performance parameters are closely interrelated and usually shape these subsystems. At the beginning of the program definition phase, requirements are always beyond the technological advances. However, an optimum cost-performance, system definition can be reached by adequate trade-off studies, taking operational concepts and technological capabilities as parameters [8].

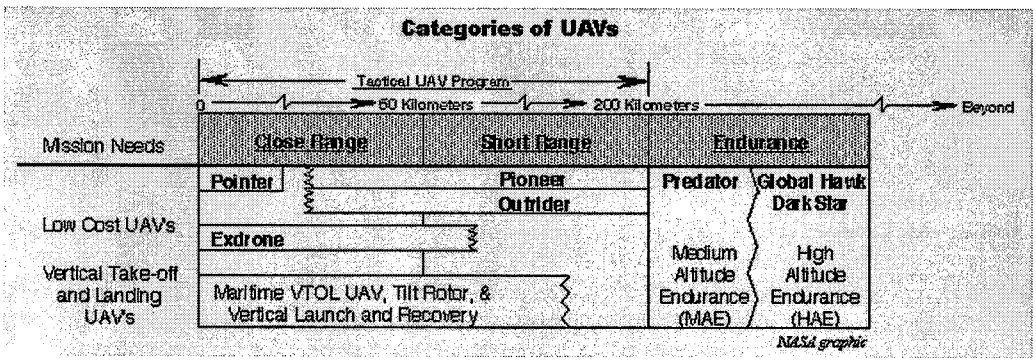

Figure 1.11 The categories of UAVs, from USA perspective [1]

1.5 Members of the UAV Design Group

The members of the design group are listed below.

Prof. Dr. Ersin Tulunay (EE), *Project Director*
Assoc. Prof. Dr. Mehmet Ş. Kavsaoğlu (AEE), *Supervisor*
Assoc. Prof. Dr. Ozan Tekinalp (AEE), *Supervisor*
Graduate Research Assistant Aycan Okan (AEE), *Researcher*
Graduate Research Assistant Özlem Armutcuoğlu (AEE), *Researcher*

1.6 Contents of this Study

In the following, the detailed summary of the conceptual design study of this new concept is discussed under related topics, such as airfoil and geometry selection, initial sizing, propulsion and fuel system integration, etc. The evaluated characteristics of this aircraft are presented in the relevant tables. Three view drawings in hover and cruise flight modes are presented.

In third chapter, the flight mechanics equations of motion are presented in order to model this aircraft. Usual rotational equations are modified to take account into the angular momentum changes due to moving parts, i.e. ducts and propellers.

In fourth chapter, trim flight conditions are obtained. For this purpose a trim program is written which minimizes a cost function. Various trim flight conditions for hover, transition and cruise are obtained and the aircraft stability at these particular flight conditions is discussed.

In fifth chapter, automatic flight control system designed with classical design techniques including block diagram representations and root locus analyses and modern control techniques including eigenvalue assignment and linear quadratic regulator design is presented. Finally, conclusions are given.

CHAPTER 2

CONCEPTUAL DESIGN STUDY OF TILT-DUCT VTOL UAV

2.1 Introduction

Conceptual design is a very fluid process. New ideas and problems are very likely to emerge as further detailed calculations are performed on a design. As new decisions are made and relevant modifications are required, these should be reflected to the current design where the procedure could be seen in Figure 2.1.

Although similar in many respects to conventional aircraft design, VTOL concept presents some key differences and challenges.

It is quite self-evident that vertical takeoff and landing capability brings many operational benefits to an aircraft. While the conventional transportation

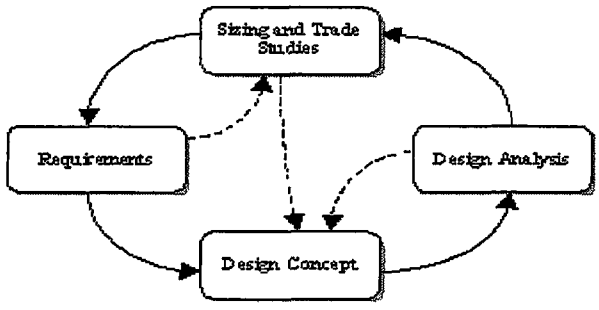

Figure 2.1 Interactive Design Process [9]

depends on airports and long paved runways, VTOL can be performed in a quite compact area. It should be also taken into account how rare airports exist and how crowded they usually are, causing delays in the air and on the ground.

The first type of VTOL aircraft developed was the helicopter. Although, it proved to be quite useful in rescue operations and short range point-to-point transportation, it carries the disadvantages of having speed and range limitations.

At this point tilt-duct concept comes into view offering a compromise between helicopter-like vertical flight and efficient wing-borne cruise.

Tilt-duct concept has some basic differences than the tilt-rotor concept; such that the propellers are located in the ducts attached to the tip of the wings. This brings an advantage of 'end-plate' effect and a protection for the propellers against strong side winds. Another difference is that, the propellers require no hinge or swash-plate design and manufacturing. Such details require too much expertise that conflicts with one of the main objectives of this design, 'cheap and easy manufacturing'. This design has also the purpose to combine the advantages of VTOL capability with a UAV.

Since, this UAV is designed for civilian uses and will be manufactured in an university type environment, it is aimed to be cheap and easy to manufacture.

In this chapter, summary of the design study is mainly based on the thesis study, which is being carried out by research group member, Ms. Armutcuoğlu. The steps taken during this conceptual design will be presented under related sub-titles. The results and sketches related with the topics will be presented immediately at the relevant section. The main characteristics of the aircraft are presented without going into details as in [10].

2.2 Basic VSTOL Definitions

Basic VSTOL definitions, which are still being used and will be used in further chapters are given as follows; [2]

VTOL: Vertical takeoff and landing.

VSTOL: Verical and short takeoff and landing.

Powered Lift Flight Regime: That flight regime of any aircraft in which controlled level flight is possible below the power off stall speed and in which part of all of the lift and for control moments are derived directly from power plant(s).

Hovering flight: Flight primarily supported by power plant(s) derived lift.

Hover: To remain stationary relative to the air mass.

Translation: Horizontal movement in any direction relative to a fixed point.

Transition flight: Flight at airspeeds below the power off stall speed, where lift is derived both from power plant(s) and the dynamic pressure resulting from forward flight.

Transition: The act of going from the powered lift flight regime to the aerodynamic flight regime and vice versa.

Aerodynamic flight mode (Conventional-cruise flight mode): Flight primarily supported by the forward flight dynamic pressure acting on non-revolving aerodynamic surfaces (wings) at airspeeds above the power off stall speed.

2.3 Competitors Study

Before starting the conceptual design process first a literature survey is performed to investigate similar aircraft, if exists, and have obtain an impression about the market potential for a UAV of these characteristics.

When the market search is narrowed down to UAVs, only a limited number of VTOL UAVs are found to exist in the market; e.g. CL-327 from Canada; Camcopter 5.1 from Austria and Eagle Eye from USA, and some more. The main characteristics of these aircraft are tabulated in Table 2.1. The interesting point is that only Eagle Eye has the tilt-rotor characteristics. Other UAVs may be considered as helicopter type VTOLs.

As a result, it is concluded that a 'tilt-duct' VTOL UAV will be unique in the market.

Table 2.1 Some Competitor UAVs Properties [11]

AIRCRAFT	*Kırlangıç**	*Mini- Vanguard**	*RPG-Midjet MKII**	*Searcher*	*CL-327*	*Camcopter 5.1*
Country	TURKEY	USA	SWEEDEN	ISRAEL	CANADA	AUSTRIA
Type	UAV	UAV	UAV	UAV	VTOL, UAV	VTOL, UAV
Payload Weight (N)	275.8	111	196	615	980	245
Empty Weight (lb)	-	-	-	-	1467	262
Max. Gross Weight (N)	1325	445	783	3650	3425	511
Power Plant	2*13 hp	1*12 hp, gasoline	1*18 hp, *Aerrow A200S*	1*47 hp, *Limbach*	1*100 shp, *WTS-117-5*, heavy fuel	1*10 hp, petrol engine
Wing Span (m)	4.9	2.13	2 (rotor diam.)	7.2	4 (rotor diam.)	3 (rotor diam.)
Length (m)	2.9	1.7	2.1	5.1	0.83	2.28
Height (m)	-	1	1.2	-	1.8	0.8
Cruise Speed (km/h)	111-120	216.7	30-150	194.5	157	90
Operation Height (m)	6100 (max)	5100 (max)	-	4572	5500	-
Endurance (hr)	8	3	3-4	12	6.25	7
Range (km)	150	49.9	100	120	100	10-80
Guidance / Tracking	GPS, auto. flight control, pre-programmable	GPS, OMAR	GPS, autopilot, manual manoeuvrability, auto & pre-programmed flight	real time payload & UAV control, GPS	GPS, auto. flight, waypoint navigation, inertial auto. Flight	fully autonomous, waypoint, INS & DGPS navigation
Launch / Recovery	wheeled take-off and landing	conventional wheeled take-off and landing (auto)	nearVTOL(1m)/wheeledTO (10-20 m.)- wheeled landing<10 m. (45 deg.)	wheeled take-off & landing	automatic VTOL	VTOL
Payload / sensors	FLIR, daylight camera	thermal camera-28V electrical power	CCD/IR camera	IAI / Tamam, MOSP, TV/TV&FLIR	TV camera, FLIR, EW, SAR	IR / colour CCD camera, real time video link
Use(s)	reconnaissance, surveillance, civil	commercial , para-military, military surveillance	reconnaissance, surveillance, artillery correction	surveillance, reconnaissance, target acquisition	surveillance, reconnaissance, target acquisition	surveillance, reconnaissance, target acquisition, env. monitor.

2.4 Mission Requirements

First, a mission profile, shown in Figure 2.2 is selected. In this figure, various segments of the mission are numbered, with zero denoting the start of the mission with takeoff and seven denoting the end of mission with landing. The mission requirements of the design are:

Operational Altitude (h) = 2000 m

- Cruise speed (V_c) > 38 m/s (124 ft/s & 73.42 knots)
- Stall Speed (V_s) = 29 m/s (50 knots) at h=1000 m.
- Payload weight (W_p); 20 kg > W_p >10 kg
- Simple structure and sub-systems, easy manufacturing

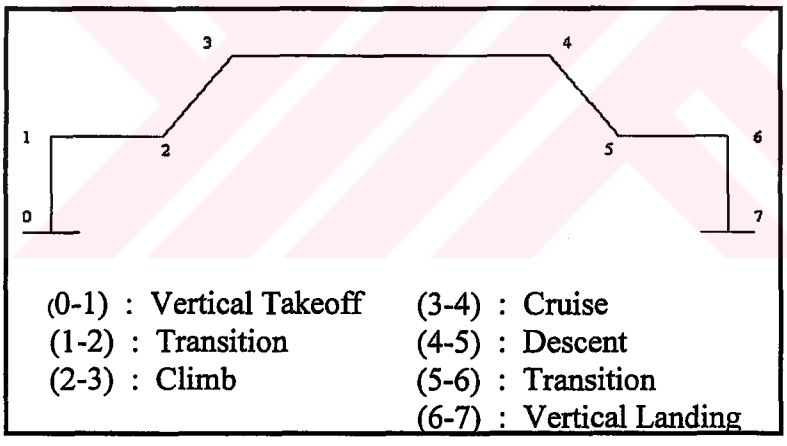

Figure 2.2 Mission Profile for the design VTOL UAV

2.5 Airfoil and Geometry Selection

At this level, initial estimations of aircraft takeoff weight, fuel and empty weights; payload and range trade-off studies are conducted. Then, airfoils, wing and tail geometry are selected, which yield a starting point for further calculations.

Airfoil is one of the most important parts of the airplane. It affects the cruise speed and overall aerodynamic efficiency during all phases of the flight. Airfoil selections are made from Eppler Series [12]. E-583 for the wing and E-521 for both horizontal and vertical tail are selected. The performance graphics and airfoil plots are given in Figure 2.3 and Figure 2.4.

Some performance parameters of E-583 and E-521 airfoils are listed in Table 2.2.

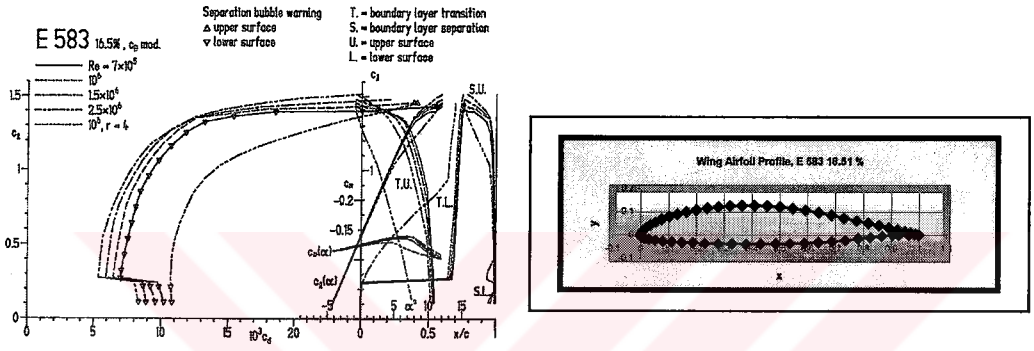

Figure 2.3 Performance plots and airfoil profile of E-583 [12]

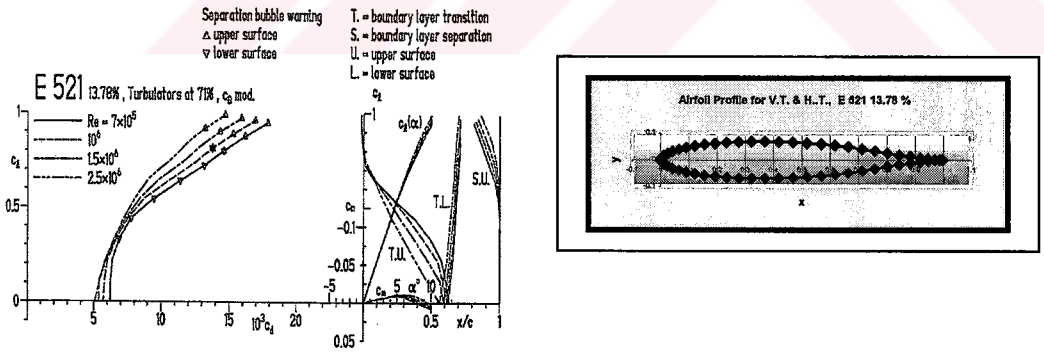

Figure 2.4 Performance plots and airfoil profile of E-521 [12]

Table 2.2 Some Performance Parameters of Selected Airfoils.

Parameter	$C_{\ell\alpha}$ (rad^{-1})	$C_{\ell_{max}}$	$\alpha_{C_{l,max}}$ (deg)	$C_{d_{min}}$	$\left(\frac{L}{D}\right)_{max,\ell}$	t/c
E 583	6.36 rad^{-1}	1.45	11^0	0.0053	125	16.5%
E 521	6.36 rad^{-1}	1.0	10^0	0.0058	62.5	13.78%

The main characteristics of the wing and tail geometry are also determined at this stage. Easy production goal played an important role in making decisions. High wing configuration is used. There is no dihedral and twist. The wing and tail geometry selections performed under this topic are presented in Table 2.3.

Table 2.3 Wing and Tail Geometry Parameters.

Parameter	Wing	Horizontal Tail	Vertical Tail
Aspect Ratio (AR)	6	4	1.6
Taper Ratio (λ)	1	0.5	0.5
Sweep Angle (Λ_{LE})	0	17^0	30^0

2.6 Horsepower-To-Weight Ratio and Wing Loading Selection

Horsepower-to-weight ratio (hp/W) and the wing loading (W/S) are the two most important parameters affecting the aircraft performance. As these parameters are selected, many related aircraft performance parameters are also evaluated accordingly.

The procedure followed in this section begins with the selection of the engine as in the first step. Then the aircraft performance parameters will depend on the properties of this engine. For this purpose, a market search is conducted. The required properties of the engine were to be piston-prop, small, efficient, cheap and

reliable. Limbach L-275-E and Limbach L-90-E are selected to drive main propellers and the aft propeller, respectively. The detailed information is given in the next section.

The wing loading selection is made according to the mission requirements and competitor aircraft. The selected *hp/W* and *W/S* are given in Table 2.4.

Table 2.4 *hp/W* and *W/S* Selections.

hp/W (hp/N)	0.0476
W/S (N/m^2)	574

After selection of the hp/W and W/S and the main geometric parameters, some of the aircraft performance parameters are evaluated by using given methods in [9]. Some of the results are tabulated in Table 2.5.

Table 2.5 *hp/W* and *W/S* – Performance Parameters.

C_{Do}	0.056
L/D_{max}	10.72
$V_{Best\ Range}$ (m/s)	34.7
V_{max} (m/s)	88.4
V_c (m/s)	45

2.7 Propulsion and Fuel System Integration

In this section, size, location and other geometric properties of the propeller are determined. The engine is installed, the fuel system is designed and the wing fuel tank volume is calculated and checked if sufficient volume is available for a fuel tank.

Two, two-blade main propellers with individual engines are used. They are directly connected, housed in ducts, attached to the tips of the wings with a tilt mechanism. Tilt mechanism is achieved via a central shaft, driven with a single actuator. Electric generation is made by through a generator, attached to the aft engine.

A four-blade aft propeller, with inlet and exit guide vanes is installed at the aft of the fuselage. Guide vanes are closed during cruise flight mode. Exit guide vanes are used to obtain thrust vectoring, as shown in Figure 2.6.

Three, two-cylinder, horizontally opposed, two stroke, air cooled piston engines are used in total. Two Limbach L-275-E, horizontally opposed-piston engine, 24 hp @ 7300 rpm, with a mass of 7.5 kg and one Limbach L-90-E, horizontally opposed-piston engine, 4.0 hp @ 7000 rpm with a mass of 4 kg are used.

Some parameters evaluated at this design level are given in Table 2.6.

Table 2.6 Propulsion and Fuel System Integration Results

Main Propeller Diameter	1.2 m
Aft Propeller Diameter	0.44 m
Available Wing Fuel Volume	63.4 cm^3

Limbach Flugmotoren GmbH, German company, manufactures four-stroke and two-stroke piston engines for very light aeroplanes and powered gliders and UAV's.

Limbach L 275 E, shown in Figure 2.5 is intended for low cost propulsion of UAVs and micro-light aircraft. The main characteristics are tabulated in Table 2.7.

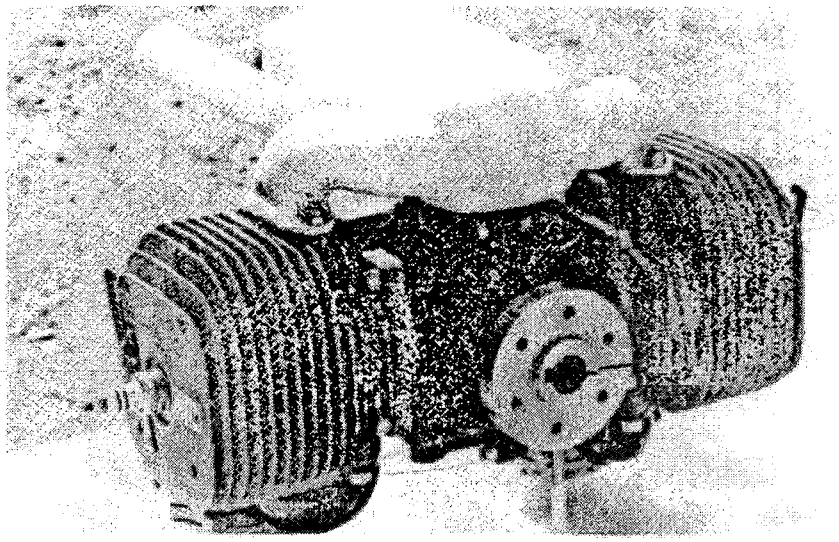

Figure 2.5 Limbach L 275E [13]

In order to determine the thrust obtained by propellers and calculate the maximum takeoff weight, the software developed by Şen and Telçeker is used [14]. This code, written in Fortran, uses design conditions such as blade number, tip radius, hub radius, engine speed, cruise speed, airfoil section, rpm, design lift coefficient, and free stream conditions (density, kinematic viscosity). By using this code, the thrust and related parameter maximum takeoff weight are calculated.

Table 2.7 The main characteristics of Limbach L 275E [15]

Type	Two-cylinder horizontally opposed two stroke air-cooled piston engine
Cylinders	Cast aluminum alloy with Nicasil Liner. Bore 66 mm. Stroke 40 mm. Capacity 274 cc
Induction	Two all-attitude-diaphragm carburettors
Fuel Grade	90 octane, mixed 25:1 with two-stroke oil
Ignition	12 V Bosch transistored, one Bosch WK 175T6 plug per cylinder
Accessories	Leistritz type turbo silencer (muffler)
Dimensions	Length overall : 226 mm , Width overall : 390 mm , Height overall : 187 mm
Weight (with silencer)	7.5 kg
Performance rating	18 Kw (24 hp) at 7300 rpm

2.8 Initial Sizing

Geometry sizing is performed to estimate aircraft geometric parameters such as, wing and tail surface areas, spans and chord, etc. These results are tabulated in Table 2.8, Table 2.9 and Table 2.10.

Table 2.8 Initial Sizing Section Results – Weights

Maximum Takeoff Weight, W_0 (N)	1008
Empty Weight, W_e (N)	674
Payload Weight+Fuel Weight, W_p+ W_f (N)	334

Table 2.9 Initial Sizing Section Results – Performance Parameters

# of Set	W_p (N)	W_f (N)	V_c (m/s)	Range (km)
Set 1	98	236	45	1400
Set 2	134	201	45	1034
Set 3	178	156	45	591

Table 2. 10 Initial Sizing Results – Geometric Parameters

Wing Span (m)	3.243
Wing Chord (m)	0.541
Fuselage Length (m)	3.713
Fuselage Diameter (m)	0.65
Wing Area (m^2)	1.754
Horizontal Tail Area (m^2)	0.631
Horizontal Tail Area (m^2)	0.255

2.9 Configuration Layout

The initial drawings of the conceptual design are developed at this step. Wing, tails and fuselage wetted areas, mean aerodynamic chord locations; etc. are also evaluated at this level.

The three-view drawings of the design VTOL UAV are available in two modes, hover and forward flight, respectively, in Figure 2.6 through Figure 2.11. These following drawings are made by Ms. Armutcuoğlu.

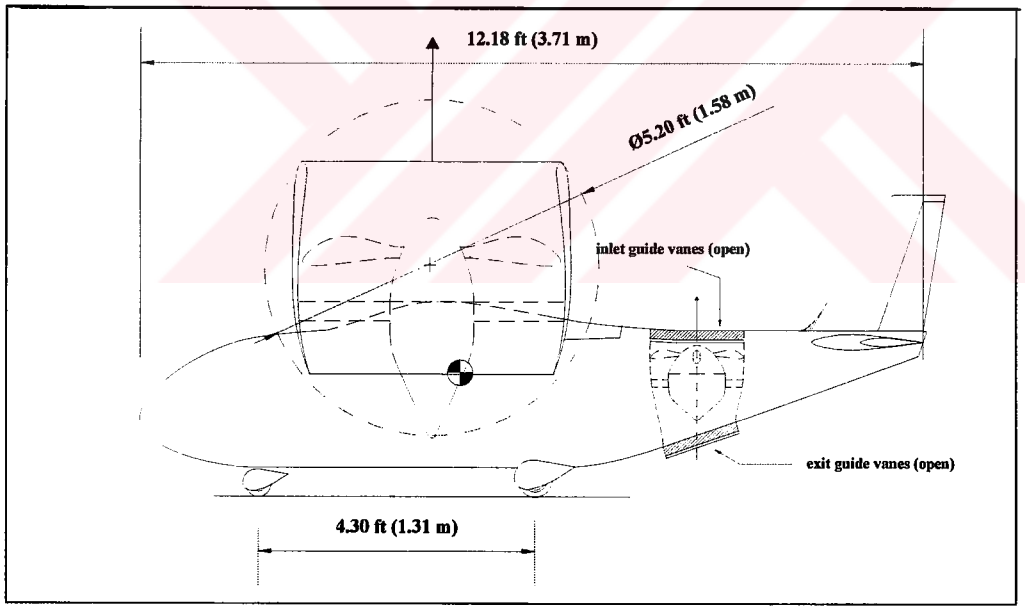

Figure 2.6 Side view of tilt-duct VTOL UAV in hover flight mode

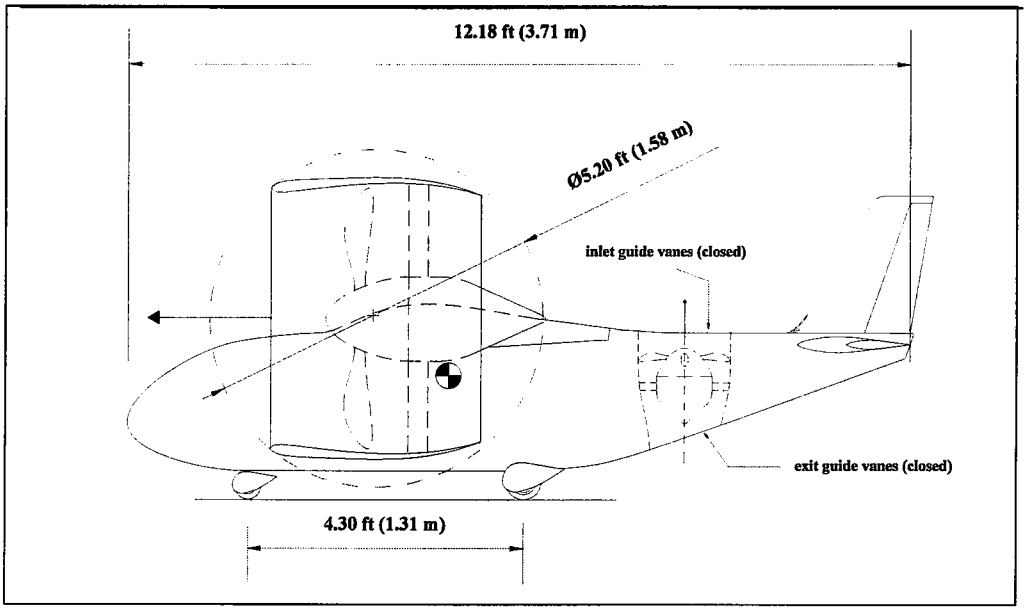

Figure 2.7 Side view of tilt-duct VTOL UAV in forward flight mode

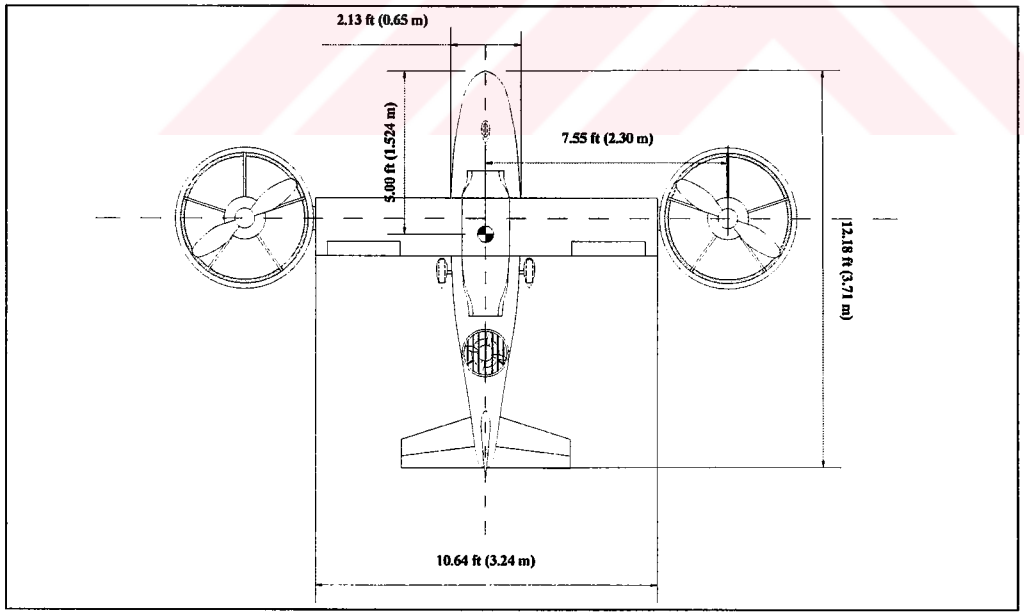

Figure 2.8 Top view of tilt-duct VTOL UAV in hover flight mode

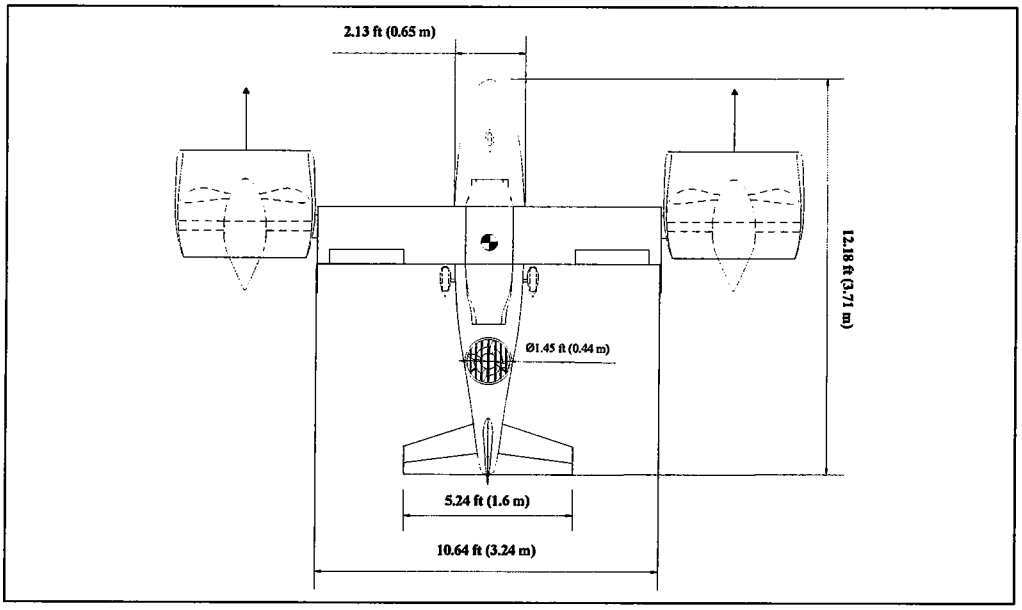

Figure 2.9 Top view of tilt-duct VTOL UAV in forward flight mode

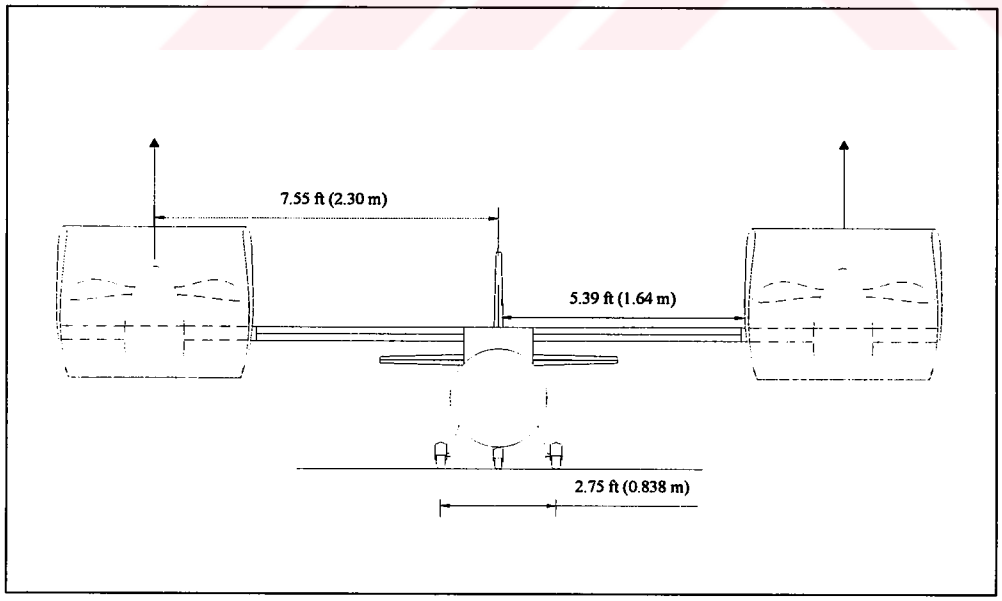

Figure 2.10 Front view of the tilt-duct VTOL UAV in hover flight mode

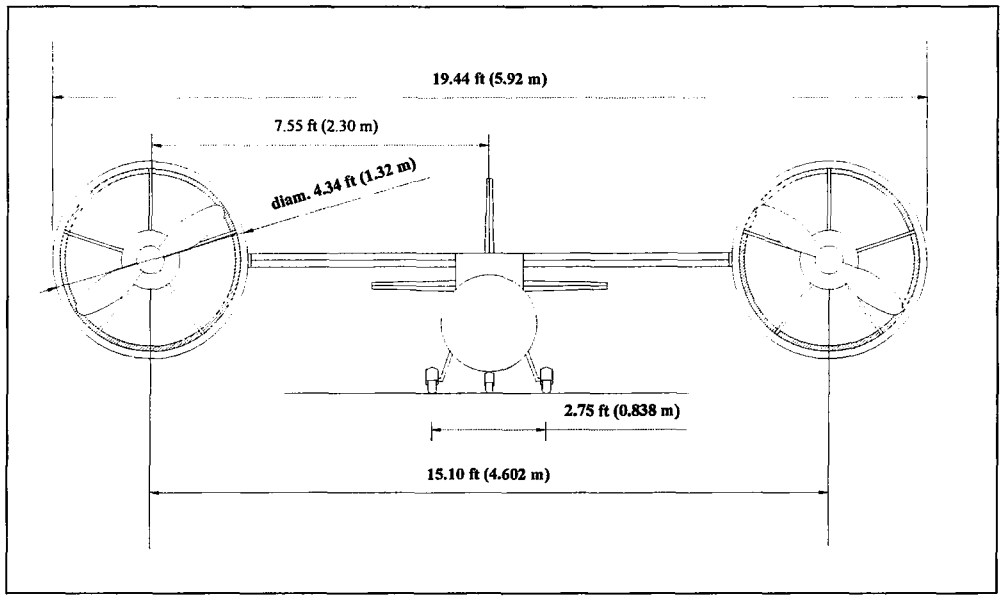

Figure 2.11 Front view of the tilt-duct VTOL UAV in forward flight mode

2.10 Landing Gear and Subsystems

The decisions on landing gear arrangement and subsystems are made at this level. Non-retractable, tricycle type of landing gears are used, i.e. one nose and two main gears. Oleo pneumatic shock absorbers are used on each unit [9].

Tire selections are also performed and aerodynamic caps are used on each tires in order to minimize drag. Tire properties are listed in Table 2.11.

Table 2.11 Landing Gear-Tire Properties [9]

Tire Data	Main Tire	Nose Tire
Max. Loading (N)	2890	2000
Unloaded Infl. Pressure (psi)	45	55
Max. Diameter (cm)	25.4	20
Max. Width (cm)	10.4	7.6
Max. Wheel Diameter (cm)	8.1	7.3
Rolling radius (cm)	8.25	7.25
Weight (N)	13.35	6.68
Tip back angle: 35.5^0		Overturn Angle: 58^0

Additionally, electrical subsystem, duct tilting subsystem, control actuation subsystems for inlet and exit guide vanes, control surfaces, and throttle, navigation subsystem, flight control subsystem, and other subsystems are needed and require detail design.

Main structure is made of composite material. Also aluminium alloys are used. Circular cross section is used.

2.11 Weights and Balance

Aircraft component weights are obtained using well-known methods [9] and are given in Table 2.12.

Table 2.12 Approximate Component Weights and C.G. Locations.

Item	Weight (N)	Location (Xcg / mac^*)
Wing	57.5	2.703
Horizontal Tail	9.2	6.144
Vertical Tail	5.1	6.587
Fuselage	131.4	3.253
Main Landing Gear	86.7	3.486
Nose Landing Gear	21	1.056
Main Engines	304.4	2.491
Aft engine	85.2	4.83
Camera	78.5	$\cong 0$
Aircraft Estimated cg location		2.82

$^*mac$ = 0.541 m. Datum is aircraft's nose..

2.12 Control Policy

There are two main engines and propellers in ducts located at the tips of the wing as shown in Figure 2.8. Another engine and propeller mechanism is integrated to the fuselage at the aft, as shown in Figure 2.7. This aft engine is used to control pitch by controlling throttle in hover and transition flight modes. It also contributes to lift. Additional pitch control as well as yaw control is realized through exit guide vanes by controlling two halves of these vanes separately. Roll control is achieved by differential thrust realized at the main engines. Engine throttles and exit guide vanes are separately controlled.

As the ducts are tilted forward, the aircraft accelerates. The wings generate lift as speed increases. This is the transition mode. At the beginning of transition, hover mode is dominant. Transition flight mode is a mixture of the hover and forward flight modes until the intended mode becomes dominant. As the aircraft gains speed, control is gradually switched to aerodynamic control surfaces.

When the ducts become horizontal, the aircraft operates as a conventional propeller driven airplane. The wings provide necessary lift. Conventional, rudder, aileron, elevator control surfaces are used. All of the guide vanes (i.e., inlet and exit) are closed during forward flight. Aft section engine is used only to obtain electricity in this mode and disconnected from the aft propeller through and electromagnetic clutch. Flaps are not used.

The most forward c.g. location is determined from 'takeoff rotation' criteria by taking moment with respect to main landing gears. The most aft c.g. location, is so called neutral point of the aircraft is calculated by the methods given in [9, 16]. Stability derivatives are calculated by using Advanced Airplane Analysis software [17].

A detailed flight mechanics and stability analysis of the tilt-duct VTOL UAV are given in the following chapters.

Table 2.13 Some Stability and Control Parameters

Most forward c.g location wrt mac, $\overline{X}_{cg_f}$	0.5114
Most aft c.g location wrt mac, $\overline{X}_{cg}$	0.621
Neutral point location wrt mac, , $\overline{X}_{NP}$	0.813
Static Margin	0.192

CHAPTER 3

FLIGHT MECHANICS ANALYSIS

3.1 Introduction

The flight mechanics equations of the tilt-duct VTOL UAV are developed in this chapter. Parts of the work given in this chapter were presented in the international conference [18].

Modeling VSTOL type aircraft has important difficulties when compared with related work done for conventional type aircraft. The important key features can be listed in the following three sections.

3.2 Basic Principles of VSTOL Aircraft

VSTOL aerodynamics is concerned with the production of lift and drag throughout the VSTOL aircraft flight regime. At low speeds, in the powered flight regime the term "lift" in a general sense refers to the vertical force that sustains the aircraft in flight. This may be a combination of engine thrust and the wing lift. At higher speeds in the aerodynamic flight regime, the aerodynamic forces and moments are produced in a more or less conventional manner and the techniques used to determine aerodynamic forces on conventional aircraft generally apply. We

can calculate power required (conventional) and power required (hover) by using the principles told above [2].

3.3 Non dimensional Parameters and Data Correlation

It is extremely difficult to measure the forces and moments acting on a VSTOL aircraft. Existing techniques for presenting forces and moments in use for conventional aircraft are often inadequate for VSTOL aircraft study. Data correlation and wind tunnel tests for VSTOL aircraft are very important. [2]

Data correlation for VSTOL aircraft is extremely difficult, because external forces and moments are the sum of conventional aerodynamic effects, engine thrust and induced aerodynamic effects. Unfortunately, each of these individual effects is a function of different variables and selecting valid non-dimensional correlating parameters is a matter of concern for the VSTOL designer. It is essential that a valid parameter be used. Data on VSTOL aircraft are scarce. Extrapolation and interpolation of this limited data will only be as accurate as the correlating parameter.

Downwash velocity, augmentation, power required in transition, effect of span, effect of spanwise load distribution, induced aerodynamic effects and induced aerodynamic interference effects are important properties for VSTOL aerodynamics [2].

3.4 Ground Proximity Effects

Aircraft possessing VSTOL capability typically operate in close proximity to the surface for relatively long periods of the time in comparison with other aircraft. Under these conditions, the downwash or exhaust generated by the aircraft in producing lift can affect the environment including personnel, facilities, equipment and the operation of the aircraft itself. The effects can be favorable or

adverse, the characteristics depending largely on the design configuration of the aircraft. Ground proximity effects can be considered in three categories [2]:

a) Aircraft performance effects : When operating in the vicinity of the ground, the aircraft downwash creates changes in the pressure and temperature patterns of the air surrounding the aircraft. These changes can affect aircraft performance by altering the lift generated at power levels or by reducing the power or thrust developed by the engine(s). Lift and power effects can be listed in this category.

b) Aircraft Stability and Control Effects : The stability and control of VSTOL aircraft can be significantly affected while operating in the influence of downwash deflected by the ground environment. This condition affects attitude and height stability and control in addition to creating random disturbances in order which increase the pilot or autopilot workload in the hover flight.

c) Operational effects : The operation of VSTOL aircraft in the proximity to the ground generates various effects on the environment, personnel or the aircraft itself which can interfere with mission accomplishment.

3.5 Equations of Motion

To analyze the dynamics of an aircraft, it is first necessary to obtain its equations of motion. The equations of motion are derived by applying Newton's Laws of Motion which relate the summation of the external forces and moments to the linear and angular accelerations of the system or body. To explain the motion of the aircraft, a suitable axis (coordinate) system is necessary. In the aircraft problems, two type of axis systems, i.e. inertial axis system and body fixed axis system, are widely used.

3.5.1 Axis Systems

There are several types of axis systems in order to use in analysing the aircraft motion [19].

a) Inertial (earth) axis system : It can be thought as fixed to the earth and assumed to be non moving (inertial) in the analyses for the aircraft motion. A set of axes commonly used are; x_e, is chosen to point north, y_e then pointing east with the orthogonal triad being completed when the axis, z_e down.

b) Body (aircraft) fixed axis system : By definition, the center of the axis system is located at the c.g. of the aircraft. In general the axis system is fixed to the aircraft and rotates with it.

The axis is taken with Ox_b forward, Oy_b out the right wing and Oz_b downward as seen by the pilot to form a right handed axis system.

Forces, moments and velocities (linear and angular) are also defined in this reference frame. By using a system of axes fixed in the aircraft the inertia terms, which appear in the equations of motion, may be considered as constant. Furthermore, the aerodynamic forces and moments depend only upon the angles, α and β, which orient the total velocity vector, $\vec{V}_T$, in relation to the axis, x_b. The angular orientation of the body axis system with respect to the inertial axis system depends strictly upon the orientation sequence. This is known as Euler angles transformation. This sequence of rotations is customarily taken as follows [20]:

1- Rotate the earth axes, x_e, y_e, z_e through some azimuthal angle φ about axis z_e to reach some intermediate axes x_1, y_1 and z_1.

2- Rotate these intermediate axes x_1, y_1 and z_1, through some angle of elevation, θ about the axis y_1 to reach a second intermediate set of axes x_2, y_2 and z_2.

3- Rotate the second intermediate axes, x_2, y_2 and z_2 through an angle of bank, ϕ about the axis x_2 to reach the body axis system.

These rotations are shown in Figure 3.1. Taking unit vectors related to these axes systems gives;

$$\begin{bmatrix} i_b \\ j_b \\ k_b \end{bmatrix} = \mathbf{T}_\phi \mathbf{T}_\theta \mathbf{T}_\varphi \begin{bmatrix} i_e \\ j_e \\ k_e \end{bmatrix} \tag{3.5.1}$$

where

$$\mathbf{T}_\varphi = \begin{bmatrix} \cos\varphi & \sin\varphi & 0 \\ -\sin\varphi & \cos\varphi & 0 \\ 0 & 0 & 1 \end{bmatrix} ; \mathbf{T}_\theta = \begin{bmatrix} \cos\theta & 0 & -\sin\theta \\ 0 & 1 & 0 \\ \sin\theta & 0 & \cos\theta \end{bmatrix} ; \mathbf{T}_\phi = \begin{bmatrix} 1 & 0 & 0 \\ 0 & \cos\phi & \sin\phi \\ 0 & -\sin\phi & \cos\phi \end{bmatrix} \tag{3.5.2}$$

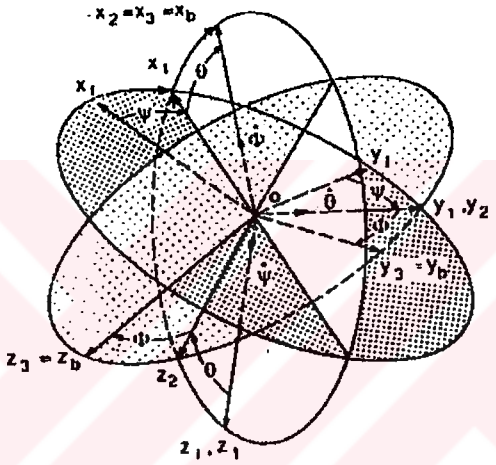

Figure 3.1 Relation between inertial frame and body axes frame [20]

c) Stability axis system : The axis x_s is chosen to coincide with the velocity vector, V at the start of the motion. Therefore, between the x_s and x_b, there is a angle of attack, α. The equations of motion are derived by using the axis systems are a special subset of the set derived by using body axis system. Here, the rotation takes place through the angle of attack, α about the axis y_b.

The relation between stability axis and body reference axis can be given as follows by the help of the unit vectors of related coordinate systems:

$$\begin{bmatrix} i_s \\ j_s \\ k_s \end{bmatrix} = \begin{bmatrix} \cos\alpha & 0 & \sin\alpha \\ 0 & 1 & 0 \\ -\sin\alpha & 0 & \cos\alpha \end{bmatrix} \begin{bmatrix} i_b \\ j_b \\ k_b \end{bmatrix} \tag{3.5.3}$$

In the compact form,

$$\mathbf{I}_s = \mathbf{T}_\alpha \mathbf{I}_b \tag{3.5.4}$$

d) Wind Axis System : Because this system is oriented with respect to the aircraft's flight path, time varying terms which correspond to the moments and cross products of inertia appear in the equations of motion. Such terms considerably complicate the analysis of aircraft motion.

The rotation takes place through angle of sideslip, β about the axis, z_s. Then the relation can be given as follows in the similar manner;

$$\mathbf{I}_w = \mathbf{T}_\beta \mathbf{I}_s \tag{3.5.5}$$

where

$$\mathbf{T}_\beta = \begin{bmatrix} \cos\beta & \sin\beta & 0 \\ -\sin\beta & \cos\beta & 0 \\ 0 & 0 & 1 \end{bmatrix} \tag{3.5.6}$$

Also,

$$\mathbf{I}_w = \mathbf{T}_\beta \mathbf{T}_\alpha \mathbf{I}_b \tag{3.5.7}$$

e) Sensor Signals: Because an AFCS (Automatic Flight Control Systems) uses feedback signals from motion sensors, it is important to remember that such signals are relative to the axis system of the aircraft. This simple fact can sometimes cause the performance obtained from an AFCS to be modified and in certain flight tasks may have to be taken into account. However in straight and level flight at cruise, it is insignificant.

During the flight, forces that are exerted on the aircraft can be separated into aerodynamic, propulsive, gravitational and other. Definitions of the forces,

moments and velocity components in the body fixed coordinate system are given in Figure 3.2.

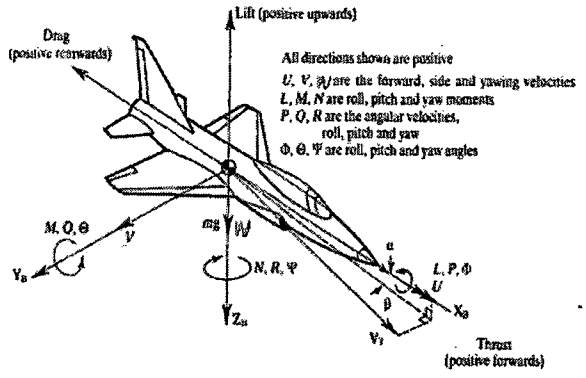

Figure 3.2 Components of force, moment and velocity in the body fixed axis[19]

The definitions in Table 3.1 will be used for body reference axis at the rest of the thesis. Otherwise, the axis system will be shown by the help of the superscript or subscript.

Table 3.1 Components of related expressions in the body reference frame.

	Roll axis x_b	Pitch axis y_b	Yaw axis z_b
Angular rates	p	q	r
Velocity components	u	v	w
Force components	X	Y	Z
Moment components	L	M	N
Moment of inertia about,	I_{xx}	I_{yy}	I_{zz}
Products of inertia	I_{yz}	I_{xz}	I_{xy}

3.5.2 Usual Equations of Motion

Usual non-linear equations of motion of rigid aircraft in body fixed axis system, are given as follows; [20]

Force (translational) equations:

$$
\begin{aligned}
X &= m(\dot{u} + qw - rv) \\
Y &= m(\dot{v} + ru - pw) \\
Z &= m(\dot{w} + pv - qu)
\end{aligned}
\tag{3.5.8}
$$

Moment (rotational) Equations:

$$
\begin{aligned}
L &= \dot{p}I_{xx} + qr(I_{zz} - I_{yy}) - (\dot{r} + pq)I_{xz} \\
M &= \dot{q}I_{yy} - pr(I_{zz} - I_{xx}) + (p^2 - r^2)I_{xz} \\
N &= \dot{r}I_{zz} + pq(I_{yy} - I_{xx}) + (qr - \dot{p})I_{xz}
\end{aligned}
\tag{3.5.9}
$$

where

$$
\begin{aligned}
X &= X_a + X_T + X_g + X_{other} & L &= L_a + L_T + L_{other} \\
Y &= Y_a + Y_T + Y_g + Y_{other} & M &= M_a + M_T + M_{other} \\
Z &= Z_a + Z_T + Z_g + Z_{other} & N &= N + N_T + N_{other}
\end{aligned}
\tag{3.5.10}
$$

where, subscript *a, T, g,* and *other* represents aerodynamic, thrust, gravitational and other externally applied forces, respectively.

The equation set Eqn. (3.5.9) is for an aircraft with rotating component effect neglected. However, in a tilt-duct aircraft such as this VTOL UAV, the right hand side of Eqn. (3.5.9) must be modified for this new aircraft.

3.5.3 Modification of Rotational Equations of Motion

For a tilt-duct VTOL UAV, where some components have considerable inertia, such as ducts, and propellers; the usual rotational equations of motion must be modified. Inertia matrices must be transferred to body fixed coordinate system. For this purpose the five additional axis systems must be defined. These are three propeller fixed axis system for left, right and aft propellers and two ducts fixed axis systems for right and left ducts. The relevant transformation matrices are defined as follows:

• *Duct fixed axis system to body fixed axis system*: The ducts make angle, μ with the x_b axis shown in Fig. 3.3. Transformation matrix, $\mathbf{T}_{d/b}$ are given as follows;

$$\mathbf{T}_{d/b} = \begin{bmatrix} \cos\mu & 0 & \sin\mu \\ 0 & 1 & 0 \\ -\sin\mu & 0 & \cos\mu \end{bmatrix} \tag{3.5.11}$$

This transformation will be the same for both left and right ducts assuming that the duct tilt angles are the same. Two ducts are taken account as one component and the transformation is then achieved.

• *Main propellers to ducts*

There are counter rotating main propellers. Due to this reason, two different transformation matrices must be written as follows:

Left main propeller to duct: The angular velocity of the left main propeller is,

$$\vec{\omega}_{pl} = \omega_1 \vec{i}_{pl} = \omega_1 \vec{i}_d \tag{3.5.12}$$

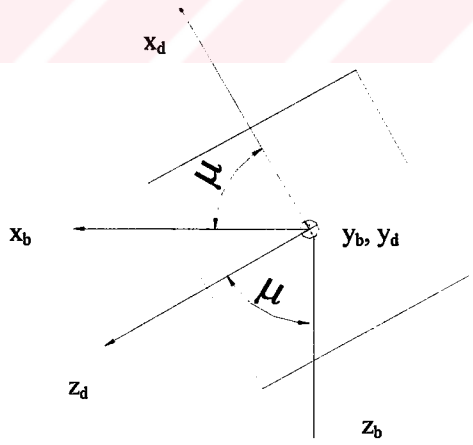

Figure 3.3 Duct angle, μ ; duct fixed, and body fixed coordinate frames

where $\vec{i}_{pl}$ and $\vec{i}_d$ are the unit vectors for x-axis of the left propeller fixed axis system and duct fixed axis system, respectively. The propeller axis system is shown in Figure 3.4 Then,

$$\boldsymbol{T}_{pl/d} = \begin{bmatrix} 1 & 0 & 0 \\ 0 & \cos\omega_1 t & -\sin\omega_1 t \\ 0 & \sin\omega_1 t & \cos\omega_1 t \end{bmatrix} \tag{3.5.13}$$

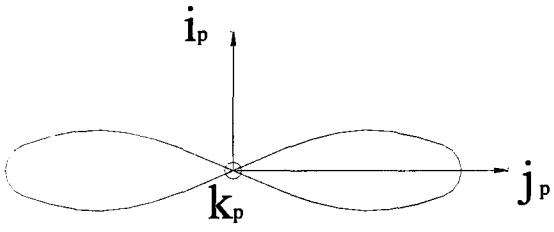

Figure 3.4 Propeller fixed axis system

Right main propeller to duct: Similarly the angular velocity of the right main propeller is given as,

$$\vec{\omega}_{pr} = \omega_2 \vec{i}_{pr} = \omega_2 \vec{i}_d \tag{3.5.14}$$

where $\vec{i}_{pr}$ and $\vec{i}_d$ are the unit vectors for x-axis of the right propeller fixed axis system and duct fixed axis system, respectively. Then,

$$\boldsymbol{T}_{pr/d} = \begin{bmatrix} 1 & 0 & 0 \\ 0 & \cos\omega_2 t & -\sin\omega_2 t \\ 0 & \sin\omega_2 t & \cos\omega_2 t \end{bmatrix} \tag{3.5.15}$$

- *Aft propeller to body*

  The angular velocity of the aft propeller is given as:

$$\vec{\omega}_{pa} = \omega_3 \vec{k}_{pa} = \omega_3 \vec{k} \tag{3.5.16}$$

where $\vec{k}_{pa}$ and $\vec{k}$ are the unit vectors of z-axis of the aft fixed axis system and body fixed axis system, respectively. Then,

$$T_{pa/b} = \begin{bmatrix} \cos\omega_3 t & -\sin\omega_3 t & 0 \\ \sin\omega_3 t & \cos\omega_3 t & 0 \\ 0 & 0 & 1 \end{bmatrix} \tag{3.5.17}$$

The total inertia tensor for this aircraft will have contributions from propeller and ducts.

$$[\mathbf{I}_t] = [\mathbf{I}_{body}] + [\mathbf{I}_{d/b}] + [\mathbf{I}_{pl/b}] + [\mathbf{I}_{pr/b}] + [\mathbf{I}_{pa/b}] \tag{3.5.18}$$

where

$$\begin{aligned} [\mathbf{I}_{d/b}] &= \mathbf{T}_{d/b}[\mathbf{I}_d]\mathbf{T}_{d/b}^T \\ [\mathbf{I}_{pl/b}] &= \mathbf{T}_{d/b}\mathbf{T}_{pl/d}[\mathbf{I}_{pl}]\mathbf{T}_{pl/d}^T\mathbf{T}_{d/b}^T \\ [\mathbf{I}_{pr/b}] &= \mathbf{T}_{d/b}\mathbf{T}_{pr/d}[\mathbf{I}_{pr}]\mathbf{T}_{pr/d}^T\mathbf{T}_{d/b}^T \\ [\mathbf{I}_{pa/b}] &= \mathbf{T}_{pa/b}[\mathbf{I}_{pa}]\mathbf{T}_{pa/b}^T \end{aligned} \tag{3.5.19}$$

The final statements for the expressions given in Eqn. (3.5.19) can be written as following;

$$[\mathbf{I}_{d/b}] = \begin{bmatrix} I_{dxx}\cos^2\mu & 0 & -I_{dxz}\sin^2\mu \\ 0 & I_{dyy} & 0 \\ -I_{dzx}\sin^2\mu & 0 & I_{dzz}\cos^2\mu \end{bmatrix} \tag{3.5.20}$$

$$[\mathbf{I}_{pl/b}] = \begin{bmatrix} I_{plxx}\cos^2\mu & 0 & 0 \\ 0 & \cos^2(\omega_1 t)I_{plyy} & 0 \\ 0 & 0 & I_{plzz}\cos^2\mu\cos^2(\omega_1 t) \end{bmatrix} \tag{3.5.21}$$

$$[\mathbf{I}_{pr/b}] = \begin{bmatrix} I_{prxx}\cos^2\mu & 0 & 0 \\ 0 & \cos^2(\omega_2 t)I_{pryy} & 0 \\ 0 & 0 & I_{przz}\cos^2\mu\cos^2(\omega_2 t) \end{bmatrix} \tag{3.5.22}$$

$$[\mathbf{I}_{pa/b}]=\begin{bmatrix} I_{paxx}\cos^2(\omega_3 t) & -I_{paxy}\sin^2(\omega_3 t) & 0 \\ -I_{payx}\sin^2(\omega_3 t) & I_{payy}\cos^2(\omega_3 t) & 0 \\ 0 & 0 & I_{pazz} \end{bmatrix} \tag{3.5.23}$$

The inertia tensor of the aircraft with taking into consideration that the aircraft is a rigid body can be written as follows,

$$[\mathbf{I}_{body}]=\begin{bmatrix} I_{xx} & I_{xy} & I_{xz} \\ I_{yx} & I_{yy} & I_{yz} \\ I_{zx} & I_{zy} & I_{zz} \end{bmatrix} \tag{3.5.24}$$

Substituting Eqn. (3.5.21) through Eqn. (3.5.24) into Eqn. (3.5.18) gives the total inertia tensor as follows;

$$[\mathbf{I}_t]=\begin{bmatrix} I_{xx}+\cos^2\mu\left[I_{plxx}+I_{prxx}+I_{dxx}\right]+ & I_{xy}-I_{paxy}\sin^2(\omega_3 t) & I_{xz}-I_{dxz}\sin^2\mu \\ I_{paxx}\cos^2(\omega_3 t) & & \\ & I_{yy}+\cos^2(\omega_1 t)I_{plyy}+ & \\ I_{yx}-I_{payx}\sin^2(\omega_3 t) & \cos^2(\omega_2 t)I_{pryy}+ & I_{yz} \\ & \cos^2(\omega_3 t)I_{payy}+I_{dyy} & \\ & & I_{zz}+I_{pazz}+ \\ I_{zx}-I_{dzx}\sin^2\mu & I_{zy} & \cos^2\mu\begin{bmatrix} I_{dzz}+I_{plzz}\cos^2(\omega_1 t) \\ I_{przz}\cos^2(\omega_2 t) \end{bmatrix} \end{bmatrix} \tag{3.5.25}$$

The total angular momentum of the aircraft in the body fixed axis system is given as,

$$\vec{H}=\left(pI_{txx}-qI_{txy}-rI_{txz}\right)\vec{i}+\left(-pI_{txy}+qI_{tyy}-rI_{tyz}\right)\vec{j}+\left(-pI_{txz}-qI_{tyz}+rI_{tzz}\right)\vec{k} \tag{3.5.26}$$

where I_{tij} are the components of the total inertia tensor given in Eqn. (3.5.25) and the angular velocity of the aircraft is,

$$\vec{\omega}=p\vec{i}+q\vec{j}+r\vec{k} \tag{3.5.27}$$

Then, the angular momentum of this aircraft can be written as:

$$\vec{H}=\vec{i}\left\{\begin{matrix}p\left[I_{xx}+\cos^2\mu\left(I_{plxx}+I_{prxx}+I_{dxx}\right)+I_{paxx}\cos^2(\omega_3 t)\right]-q\left[I_{xy}-I_{paxy}\sin^2(\omega_3 t)\right]-\\ r\left[I_{xz}-I_{dxz}\sin^2\mu\right]\end{matrix}\right\}+$$
$$\vec{j}\left\{\begin{matrix}-p\left[I_{yx}-I_{payx}\sin^2(\omega_3 t)\right]+\\ q\left[I_{yy}+\cos^2(\omega_1 t)I_{plyy}+\cos^2(\omega_2 t)I_{pryy}+\cos^2(w_3 t)I_{payy}+I_{dyy}\right]-rI_{yz}\end{matrix}\right\}+$$
$$\vec{k}\left\{\begin{matrix}-p\left[I_{zx}-I_{dzx}\sin^2\mu\right]-qI_{zy}+\\ r\left[I_{zz}+I_{pazz}+\cos^2\mu\left(I_{dzz}+I_{plzz}\cos^2(\omega_1 t)+I_{przz}\cos^2(w_2 t)\right)\right]\end{matrix}\right\}$$

(3.5.28)

Having written the angular momentum, the rotational equations are obtained as follows;

$$\frac{d\vec{H}}{dt}=L\vec{i}+M\vec{j}+N\vec{k} \tag{3.5.29}$$

The time derivative of the angular momentum vector shall be taken in the usual fashion, i.e.,

$$\frac{d\vec{H}}{dt}=\dot{\vec{H}}\Big|_{Body}+\vec{\omega}\times\vec{H} \tag{3.5.30}$$

To simplify the derivation, while taking the derivatives in the body fixed frame, propeller angular rates, $\omega_1,\omega_2,\omega_3$ may be taken constant. Even with this assumption, the resulting equations are quite complicated as shown in Eqn. (3.5.31) and Eqn. (3.5.32).

$$\dot{\vec{H}}\Big|_{Body}=\vec{i}\left\{\begin{matrix}\dot{p}I_{xx}+\left(\dot{p}\cos^2\mu-\sin(2\mu)\dot{\mu}p\right)\left(I_{plxx}+I_{prxx}+I_{dxx}\right)+\dot{p}\cos^2(\omega_3 t)I_{paxx}-\sin(2\omega_3 t)\omega_3 pI_{paxx}\\ -\dot{q}I_{xy}+\dot{q}\sin^2(\omega_3 t)I_{paxy}+\sin(2\omega_3 t)\omega_3 qI_{paxy}-\dot{r}I_{xz}+\dot{r}\sin\mu I_{dxz}+\sin(2\mu)\dot{\mu}rI_{dxz}\end{matrix}\right\}+$$
$$\vec{j}\left\{\begin{matrix}-\dot{p}I_{yx}+\dot{p}\sin^2(\omega_3 t)I_{payx}+\sin(2\omega_3 t)\omega_3 pI_{payx}+\dot{q}I_{yy}+\dot{q}\cos^2(\omega_1 t)I_{plyy}-\\ \sin(2\omega_1 t)\omega_1 qI_{plyy}+\dot{q}\cos^2(\omega_2 t)I_{pryy}-\sin(2\omega_2 t)\omega_2 qI_{pryy}+\dot{q}I_{dyy}-\dot{r}I_{yz}\end{matrix}\right\}+$$
$$\vec{k}\left\{\begin{matrix}-\dot{p}I_{zx}+\dot{p}\sin^2\mu I_{dzx}+\sin(2\mu)\dot{\mu}pI_{dzx}-\dot{q}I_{zy}+\dot{r}I_{zz}+\dot{r}I_{pazz}+\dot{r}\cos^2\mu I_{dzz}-r\sin(2\mu)\dot{\mu}rI_{dzz}\\ \dot{r}\cos^2\mu\cos^2(\omega_1 t)I_{plzz}-r\dot{\mu}\sin(2\mu)\cos^2(\omega_1 t)I_{plzz}-r\cos^2\mu\sin(2\omega_1 t)\omega_1 I_{plzz}\\ +\dot{r}\cos^2\mu\cos^2(\omega_2 t)I_{przz}-r\dot{\mu}\sin(2\mu)\cos^2(\omega_2 t)I_{przz}-r\cos^2\mu\sin(2\omega_2 t)\omega_2 I_{przz}\end{matrix}\right\}$$

(3.5.31)

$$\vec{\omega}\times\vec{H}=\vec{i}\left\{\begin{bmatrix}-qp\left(I_{zx}-I_{dzx}\sin^2\mu\right)-q^2I_{zy}+qr\left(I_{zz}+I_{pazz}+\cos^2\mu\begin{bmatrix}I_{dzz}+I_{plzz}\cos^2(\omega_1t)+\\I_{przz}\cos^2(\omega_2t)\end{bmatrix}\right)\end{bmatrix}+\right.$$
$$\left.\begin{bmatrix}pr\left(I_{yx}-I_{payx}\sin^2(\omega_3t)\right)-rq\begin{pmatrix}I_{yy}+\cos^2(\omega_1t)I_{plyy}+\cos^2(\omega_2t)I_{pryy}+\\\cos^2(\omega_3t)I_{payy}+I_{dyy}\end{pmatrix}+r^2I_{yz}\end{bmatrix}\right\}+$$
$$\vec{j}\left\{\begin{bmatrix}pr\left(I_{xx}+\cos^2\mu\left[I_{plxx}+I_{prxx}+I_{dxx}\right]+\cos^2(\omega_3t)I_{paxx}\right)-rq\left(I_{xy}-I_{paxy}\sin^2(\omega_3t)\right)-\\r^2\left(I_{xz}-I_{dxz}\sin^2\mu\right)\end{bmatrix}+\right.$$
$$\left.\left[p^2\left(I_{zx}-I_{dzx}\sin^2\mu\right)+pqI_{zy}-pr\left(I_{zz}+I_{pazz}+\cos^2\mu\left[I_{dzz}+I_{plzz}\cos^2(\omega_1t)+I_{przz}\cos^2(\omega_2t)\right]\right)\right]\right\}$$
$$+\vec{k}\left\{\begin{bmatrix}-p^2\left(I_{yx}-I_{payx}\sin^2(\omega_3t)\right)+pq\begin{pmatrix}I_{yy}+\cos^2(\omega_1t)I_{plyy}+\cos^2(\omega_2t)I_{pryy}+\\\cos^2(\omega_3t)I_{payy}+I_{dyy}\end{pmatrix}-prI_{yz}\end{bmatrix}+\right.$$
$$\left.\begin{bmatrix}-pq\left(I_{xx}+\cos^2\mu\left[I_{plxx}+I_{prxx}+I_{dxx}\right]+I_{paxx}\cos^2(\omega_3t)\right)+q^2\left(I_{xy}-I_{paxy}\sin^2(\omega_3t)\right)+\\qr\left(I_{xz}-I_{dxz}\sin^2\mu\right)\end{bmatrix}\right\}$$

(3.5.32)

Substituting Eqn. (3.5.31) and Eqn. (3.5.32) into Eqn. (3.5.30) gives the final statement for $\frac{d\vec{H}}{dt}$ that can be written in terms of externally applied moments in the aircraft as follows;

$$L=\begin{Bmatrix}\dot{p}I_{xx}+\left(\dot{p}\cos^2\mu-\sin(2\mu)\dot{\mu}p\right)\left(I_{plxx}+I_{prxx}+I_{dxx}\right)+\dot{p}\cos^2(\omega_3t)I_{paxx}-\sin(2\omega_3t)\omega_3pI_{paxx}\\-\dot{q}I_{xy}+\dot{q}\sin^2(\omega_3t)I_{paxy}+\sin(2\omega_3t)\omega_3qI_{paxy}-\dot{r}I_{xz}+\dot{r}\sin\mu I_{dxz}+\sin(2\mu)\dot{\mu}rI_{dxz}\end{Bmatrix}+$$
$$\left\{\begin{bmatrix}-qp\left(I_{zx}-I_{dzx}\sin^2\mu\right)-q^2I_{zy}+qr\left(I_{zz}+I_{pazz}+\cos^2\mu\begin{bmatrix}I_{dzz}+I_{plzz}\cos^2(\omega_1t)+\\I_{przz}\cos^2(\omega_2t)\end{bmatrix}\right)\end{bmatrix}+\right.$$
$$\left.\begin{bmatrix}pr\left(I_{yx}-I_{payx}\sin^2(\omega_3t)\right)-rq\begin{pmatrix}I_{yy}+\cos^2(\omega_1t)I_{plyy}+\cos^2(\omega_2t)I_{pryy}+\\\cos^2(\omega_3t)I_{payy}+I_{dyy}\end{pmatrix}+r^2I_{yz}\end{bmatrix}\right\}$$

(3.5.33)

$$M=\begin{Bmatrix}-\dot{p}I_{yx}+\dot{p}\sin^2(\omega_3t)I_{payx}+\sin(2\omega_3t)\omega_3pI_{payx}+\dot{q}I_{yy}+\dot{q}\cos^2(\omega_1t)I_{plyy}-\\\sin(2\omega_1t)\omega_1qI_{plyy}+\dot{q}\cos^2(\omega_2t)I_{pryy}-\sin(2\omega_2t)\omega_2qI_{pryy}+\dot{q}I_{dyy}-\dot{r}I_{yz}\end{Bmatrix}+$$

$$\left\{\begin{bmatrix} pr\left(I_{xx}+\cos^2\mu\left[I_{plxx}+I_{prxx}+I_{dxx}\right]+\cos^2(\omega_3 t)I_{paxx}\right)-rq\left(I_{xy}-I_{paxy}\sin^2(\omega_3 t)\right)- \\ r^2\left(I_{xz}-I_{dxz}\sin^2\mu\right) \end{bmatrix}+ \\ \left[p^2\left(I_{zx}-I_{dzx}\sin^2\mu\right)+pqI_{zy}-pr\left(I_{zz}+I_{pazz}+\cos^2\mu\left[I_{dzz}+I_{plzz}\cos^2(\omega_1 t)+I_{przz}\cos^2(\omega_2 t)\right]\right)\right]\end{bmatrix}\right\}$$

(3.5.34)

$$N=\left\{\begin{matrix} -\dot{p}I_{zx}+\dot{p}\sin^2\mu I_{dzx}+\sin(2\mu)\dot{\mu}pI_{dzx}-\dot{q}I_{zy}+\dot{r}I_{zz}+\dot{r}I_{pazz}+\dot{r}\cos^2\mu I_{dzz}-r\sin(2\mu)\dot{\mu}rI_{dzz} \\ \dot{r}\cos^2\mu\cos^2(\omega_1 t)I_{plzz}-r\dot{\mu}\sin(2\mu)\cos^2(\omega_1 t)I_{plzz}-r\cos^2\mu\sin(2\omega_1 t)\omega_1 I_{plzz} \\ +\dot{r}\cos^2\mu\cos^2(\omega_2 t)I_{przz}-r\dot{\mu}\sin(2\mu)\cos^2(\omega_2 t)I_{przz}-r\cos^2\mu\sin(2\omega_2 t)\omega_2 I_{przz} \end{matrix}\right\}+$$

$$\left\{\begin{bmatrix} -p^2\left(I_{yx}-I_{payx}\sin^2(\omega_3 t)\right)+pq\begin{pmatrix} I_{yy}+\cos^2(\omega_1 t)I_{plyy}+\cos^2(\omega_2 t)I_{pryy}+ \\ \cos^2(\omega_3 t)I_{payy}+I_{dyy} \end{pmatrix}-prI_{yz} \end{bmatrix}+ \\ \begin{bmatrix} -pq\left(I_{xx}+\cos^2\mu\left[I_{plxx}+I_{prxx}+I_{dxx}\right]+I_{paxx}\cos^2(\omega_3 t)\right)+q^2\left(I_{xy}-I_{paxy}\sin^2(\omega_3 t)\right)+ \\ qr\left(I_{xz}-I_{dxz}\sin^2\mu\right) \end{bmatrix}\end{bmatrix}\right\}$$

(3.5.35)

Using Eqn. (3.5.33) through Eqn. (3.5.35) modified version for equation set Eqn. (3.5.9) is obtained.

3.5.4 Externally Applied Forces and Moments

The externally applied force and moment components are classified in Eqn. (3.5.10). In this section, expressions for these components are presented in general. With necessary assumptions and simplifications, they can be written for hover, transition and forward flight modes, separately.

Gravitational forces may be written as follows [21];

$$\begin{bmatrix} X_g \\ Y_g \\ Z_g \end{bmatrix}=\begin{bmatrix} -mg\sin\theta \\ mg\cos\theta\sin\phi \\ mg\cos\theta\cos\phi \end{bmatrix} \qquad (3.5.36)$$

where m, g, θ, and ϕ represents the total mass of the aircraft, gravitational acceleration, pitch attitude and roll attitude, respectively.

Thrust forces and related moments due to power plants and propellers should be resolved into body axis frame.

$$\begin{aligned} X_T &= (T_1 + T_2)\cos\mu \\ Y_T &= T_3 \cos\eta \\ Z_T &= -(T_1 + T_2)\cos\mu - T_3 \sin\eta \end{aligned} \tag{3.5.37}$$

and,

$$\begin{aligned} L_T &= (T_1 - T_2)\sin\mu l_4 \\ M_T &= (T_1 + T_2)\sin\mu l_1 - T_3 \sin\eta l_2 - (T_1 + T_2)\cos\mu l_3 \\ N_T &= T_3 \cos\eta l_2 + (T_1 - T_2)\cos\mu l_4 \end{aligned} \tag{3.5.38}$$

In the above equations, T_1, T_2, T_3 are the thrust of the left, right and aft propellers, μ, and η are the duct angle of the main propellers, and the resultant exit guide vane angle of the aft propeller, as shown in Figure 3.3 and Figure 3.5 l_1, l_2 ,l_3, l_4 are the proper moment arms for the thrust vectors respectively.

In order to calculate the aerodynamic forces and moments, aerodynamic stability derivatives for cruise and transition flight mode are obtained from the Advanced Airplane Analysis (AAA) program [17]. These stability derivatives are presented in Appendix A. However, since the aircraft is not a conventional type, it requires detailed wind tunnel tests, especially for transition flight modes.

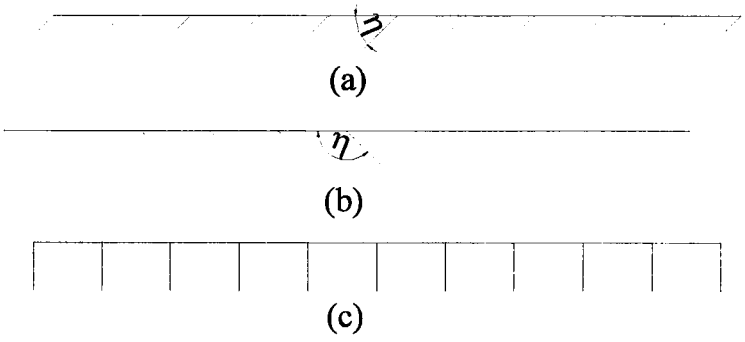

Figure 3.5 Exit guide vane configurations in order to obtain pitch and yaw control during hover and transition flight mode
a) For positive yaw b) For negative yaw c) Neutral (only pitch)

CHAPTER 4

LONGITUDINAL STABILITY ANALYSIS

4.1 Introduction

In this chapter, first trimmed flight conditions of the tilt-duct VTOL UAV for straight, wings level flight are presented. Only longitudinal motion is considered. Thus, equilibrium equations corresponding to axial force, vertical force and pitching moment are sufficient for the analysis. Three flight modes of the aircraft are investigated; hover, transition and cruise flight mode. Then, solution method, employed to find necessary trim conditions, is presented. Trim conditions obtained are tabulated. Then, longitudinal stability analysis is carried out at these trim conditions.

Trim in flight mechanics means steady flight conditions. Thus, the derivatives of the translational velocities must be zero. This means that the resultant force acting on the aircraft is zero. Additionally, derivatives of the rotational rates must also be zero. This means that the resultant moment acting on the aircraft is zero.

4.2 Longitudinal Trim Flight Equations

4.2.1 Hover mode

During hover, there will not be any aerodynamic forces acting on the lifting and control surfaces. Main forces acting on the system are due to gravity and thrust force generated by the propellers. Assuming that roll and yaw moments as well as side forces are already balanced; longitudinal accelerations must be equal to zero.

In this mode, the duct angle and exit guide vane angle, in the absence of yawing moments, will be 90^0, and the pitch attitude will be 0^0. The trim flight condition is achieved simply, by adjusting the throttle settings to keep the aircraft in hover mode. These equilibrium equations may be written as follows,

$$\begin{aligned} X &= (T_1 + T_2)\cos\mu - mg\sin\theta = 0 \\ Z &= -(T_1 + T_2)\sin\mu - T_3\sin\eta + mg\cos\theta = -(T_1 + T_2 + T_3) + mg \\ M &= (T_1 + T_2)l_1\sin\mu - T_3 l_2\sin\eta - (T_1 + T_2)l_3\cos\mu = (T_1 + T_2)l_1 - T_3 l_2 \end{aligned} \tag{4.2.1}$$

4.2.2 Cruise mode

In this mode, aerodynamic forces and moments are present. These forces are usually in the stability axis system. Consequently, this axis system is used. Then, the following equilibrium equations may be written.

$$\begin{aligned} X_s &= T^m \delta_T^m \cos\alpha - mg\sin(\theta - \alpha) - QSC_D \\ Z_s &= -T^m \delta_T^m \sin\alpha + mg\cos(\theta - \alpha) - QSC_L \\ M &= -T^m \delta_T^m l_3 + QScC_M \end{aligned} \tag{4.2.2}$$

where, α, is the angle of attack, T^m, is the total static thrust, δ_T^m is the throttle setting of the main propellers, Q is the dynamic pressure, S is the wing area, c is the chord length, C_D, C_L and C_M, are aerodynamic drag coefficient, lift coefficient and pitching moment coefficient, respectively. These aerodynamic coefficients are calculated as follows: [22]

$$
\begin{aligned}
C_D &= C_{D_0} + kC_L^2 \\
C_L &= C_{L_0} + C_{L_\alpha}\alpha \\
C_M &= C_{m_0} + C_{m_\alpha}\alpha + C_{m_{\delta_e}}\delta_e + \frac{c}{2V}(C_{m_q}q + C_{m_{\dot{\alpha}}}\dot{\alpha})
\end{aligned}
\tag{4.2.3}
$$

In these equations, V is the total velocity, δ_e is the elevator deflection. These coefficients are obtained from the Advanced Airplane Analysis (AAA) program [17]. However, since straight flight condition is assumed, contributions from dynamic derivatives will be zero in the lift coefficient, C_L, and in the pitching moment coefficient, C_M (i.e. $q = 0, \quad \dot{\alpha} = 0$). For straight wings-level flight at constant altitude, flight path angle will be zero.

The total thrust is the combined thrust forces generated by the left and right propellers. Additionally, the magnitude of the thrust force generated by the propellers depends on the speed of the aircraft. For this, following formulation is used.

$$
T^m = (T_1 + T_2)_{\max} - U\lambda \tag{4.2.4}
$$

where, U is the usual airplane velocity along x_b axis, and $\lambda = \frac{\partial T}{\partial U}$, is a constant indicating the reduction of thrust from its static value in forward flight. In trimmed flight, the resultant forces and pitching moment, X_s, Z_s, M shall be zero.

4.2.3 Transition mode

Transition mode is a mixture of the cruise flight and hover modes. Thus the following force and moment equations may be written.

$$
\begin{aligned}
X_s &= T^m\delta_T^m \cos(\mu+\alpha) - mg\sin(\theta-\alpha) - T^a\delta_T^a \sin\eta\sin\alpha - QSC_{D1} \\
Z_s &= -T^m\delta_T^m \sin(\mu+\alpha) - T^a\delta_T^a \sin\eta\cos\alpha + mg\cos(\theta-\alpha) - QSC_L \\
M &= T^m\delta_T^m\, l_1 \sin\mu - T^a\delta_T^a\, l_2 \sin\eta - T^m\delta_T^m\, l_3 \cos\mu + QScC_M
\end{aligned}
\tag{4.2.5}
$$

where,

$$T_t^m = (T_1 + T_2)_{\max} - \lambda U \cos\mu$$
$$T_t^a = (T_3)_{\max} \tag{4.2.6}$$

and, δ_T^m, and δ_T^a, represent the throttle setting of the main and aft propellers, respectively.

In this case, aerodynamic coefficients will be different than those calculated for the cruise mode. However, the main difference would be in the drag coefficient, C_{D1}. This is due to the tilting duct system. A simplified model is employed. Thus, the value of drag coefficient is interpolated between the duct full up position and cruise flight position. Duct full up position is simply calculated using a component build up approach by adding the drag of a cylinder to the aircraft drag of the cruise flight by using κ value.

$$C_{D1} = C_D + \kappa \sin\mu \tag{4.2.7}$$

Again for trimmed flight, components of the resultant forces in the stability axis system, X_s, Z_s, and pitching moment M must be zero.

4.3 Method of Solution

As discussed in Section 4.2, solution of a trimmed flight problem requires the solution of a set of non-linear equations containing quite number of variables, with physical constraints on them. Such problems are usually solved by using optimization techniques [23]. A similar approach is taken here. In all cases the following cost function is used:

$$f(\mathbf{x}) = X^2 + Z^2 + M^2 \tag{4.3.1}$$

where, X, Z represent the resultant axial, vertical forces, respectively and M represents the resultant pitching moment. Then, the optimization problem is posed as follows,

$$\begin{aligned} &\text{find } \mathbf{x} \text{ such that} \\ &\mathbf{min}\ f(\mathbf{x}) \\ &g(\mathbf{x}) < 0 \\ &h(\mathbf{x}) = 0 \end{aligned} \tag{4.3.2}$$

The vector of optimization parameters, **x**, are throttle settings, duct and exit guide vane angles, aircraft velocity, pitch attitude, elevator deflection, angle of attack, etc. Bounds on all these optimization parameters may be specified. Especially for cruise flight and transition flight modes, equality constraint on total velocity, altitude, etc., may be employed.

All the programming is done in the Matlab environment [24]. A constrained optimization routine, from Matlab Optimization Toolbox is used. The Matlab subroutine, "constr", is a quasi Newtonian gradient type algorithm, and it is possible to specify upper and lower bounds on selected optimization parameters, as well as to specify equality constraints [25].

A different cost function may also be used to obtain the trimmed flight conditions, as following.

$$f(\boldsymbol{x}) = \dot{V}^2 + 100\dot{\alpha}^2 + 10\dot{q}^2 \tag{4.3.3}$$

where the coefficients are selected in order to balance the relative magnitude of each component in the cost function. The related non-linear longitudinal flight mechanics equations for the cruise mode are given below.

$$\begin{aligned} \dot{V} &= \frac{T^m \delta_T^m \cos\alpha - QSC_D}{m} - g\sin(\theta - \alpha) \\ \dot{\alpha} &= \frac{-T^m \delta_T^m \sin\alpha - QSC_L + m(Vq + g\cos(\theta - \alpha))}{mV + QSC_{L\dot{\alpha}} \frac{c}{2V}} \\ \dot{q} &= \frac{QScC_M - T^m \delta_T^m l_3}{I_{yy}} \\ \dot{\theta} &= q \end{aligned} \tag{4.3.4}$$

Similar non-linear equations for the transition mode which includes aft throttle effect and modified drag force due to the tilt mechanism are,

$$\dot{V} = \frac{\{T^m \delta_T^m \cos(\mu+\alpha) - T^a \delta_T^a \sin\eta \sin\alpha - QSC_{D1}\}}{m} - g\sin(\theta-\alpha)$$

$$\dot{\alpha} = \frac{\{-T^m \delta_T^m \sin(\mu+\alpha) - T^a \delta_T^a \sin\eta\cos\alpha - QSC_L + m(Vq + g\cos(\theta-\alpha))\}}{mV + QSC_{L\dot{\alpha}} \frac{c}{2V}} \tag{4.3.5}$$

$$\dot{q} = \frac{\{T^m \delta_T^m l_1 \sin\mu - T^m \delta_T^m l_3 \cos\mu - T^a \delta_T^a l_2 \sin\eta + QScC_M\}}{I_{yy}}$$

$$\dot{\theta} = q$$

4.4 Linearized Longitudinal Equations

In this section, longitudinal stability of the aircraft is analyzed using linearized equations. Since trim conditions imply equilibrium, in each case corresponding trim flight conditions are used for linearization [23].

The equation sets, Eqn. (4.3.4) and Eqn (4.3.5) are linearized by using small variations from steady flight conditions. Thus, all the variables in the nonlinear equations of motion are replaced by an equilibrium value plus a disturbance or perturbance,

$$V = V_e + \tilde{V}, \qquad \alpha = \alpha_e + \tilde{\alpha}, \qquad \theta = \theta_e + \tilde{\theta}, \qquad q = q_e + \tilde{q}$$
$$\delta_T^m = \delta_{Te}^m + \tilde{\delta}_T^m, \qquad \delta_T^a = \delta_{Te}^a + \tilde{\delta}_T^a, \qquad \delta_e = \delta_{ee} + \tilde{\delta}_e \tag{4.4.1}$$

where the subscript e implies equilibrium value and "~" implies variation from equilibrium. Then, the linearized equations in cruise flight mode are,

$$\dot{\tilde{V}} = \left.\frac{\partial f_V}{\partial V}\right|_e \tilde{V} + \left.\frac{\partial f_V}{\partial \alpha}\right|_e \tilde{\alpha} + \left.\frac{\partial f_V}{\partial \theta}\right|_e \tilde{\theta} + \left.\frac{\partial f_V}{\partial \delta_T^m}\right|_e \tilde{\delta}_T^m + \frac{\partial f_V}{\partial \delta_T^a}\tilde{\delta}_T^a$$

$$\dot{\tilde{\alpha}} = \left.\frac{\partial f_\alpha}{\partial V}\right|_e \tilde{V} + \left.\frac{\partial f_\alpha}{\partial \alpha}\right|_e \tilde{\alpha} + \left.\frac{\delta f_\alpha}{\partial q}\right|_e \tilde{q} + \left.\frac{\partial f_\alpha}{\partial \theta}\right|_e \tilde{\theta} + \frac{\partial f_\alpha}{\partial \delta_T^m}\tilde{\delta}_T^m + \frac{\partial f_\alpha}{\partial \delta_T^a}\tilde{\delta}_T^a$$

$$\dot{\tilde{q}} = \left.\frac{\partial f_q}{\partial V}\right|_e \tilde{V} + \left.\frac{\partial f_q}{\partial \alpha}\right|_e \tilde{\alpha} + \left.\frac{\delta f_q}{\partial q}\right|_e \tilde{q} + \left.\frac{\partial f_q}{\partial \delta_e}\right|_e \tilde{\delta}_e + \frac{\partial f_q}{\partial \delta_T^m}\tilde{\delta}_T^m + \frac{\partial f_q}{\partial \delta_T^a}\tilde{\delta}_T^a$$

$$\dot{\tilde{\theta}} = \tilde{q}$$

(4.4.2)

where f_V, f_α, f_q indicates the right hand side of the first three equations, given in Eqn. (4.3.5).

Since the obtained linearized equations are quite lengthy, they are not presented. The linearized longitudinal equations for the cruise mode may also derived in the similar manner by using the equations given in Eqn. (4.3.4).

4.5 Results and Discussion

4.5.1 Hover mode

From Eqn. (4.2.1), and using cost function given in Eqn. (4.3.1) in the trim program developed, the following trim flight conditions for the hover mode are obtained:

$$\delta_{T0}^m = 0.696,\ \delta_{T0}^a = 0.7306,\ \mu_0 = 90^0,\ \eta_0 = 90^0,\ \theta_0 = 0^0$$

Hover mode takes place under the effect of thrust forces generated by the propellers. Since the thrust forces from main and aft propellers have a fixed direction with respect to the aircraft, we have a follower force problem. Thus, if the aircraft is disturbed for example in a pitch up manner, the disturbance can not

be restored. For this reason, this mode is unstable. A stability augmentation system is needed. All three engine throttles shall be controlled during the hover mode.

4.5.2 Cruise Mode

Using Eqn. (4.2.2) and cost function given in Eqn. (4.3.1), trimmed flight conditions are obtained. In the program, flight altitude is specified. In this flight mode, duct angle, μ is equal to 0^0. Exit and inlet guide vanes are closed. Cruise flight velocity is imposed as an equality constraint. The trim program calculates remaining trim flight parameters. The following nominal cruise flight conditions are specified as follows,

$$V_0 = 45 \text{ m/s}, \; h = 2000 \text{ m}$$

where V_0 is the nominal cruising velocity of the aircraft. Corresponding trim flight parameters are found,

$$\alpha_0 = 3^0, \; \theta_0 = 3^0, \; \delta_{e_0} = -0.09^0, \; \delta_{T_0} = 0.263$$

Using Eqn. (4.2.2) and cost function given in Eqn. (4.3.3) gives approximately same trim flight conditions.

The nonlinear cruise flight equations, Eqn. (4.3.4) are linearized by using the equations given in Eqn. (4.4.2) about the above trim conditions to obtain state space representation of the system as follows,

$$\begin{bmatrix} \dot{\tilde{V}} \\ \dot{\tilde{\alpha}} \\ \dot{\tilde{q}} \\ \dot{\tilde{\theta}} \end{bmatrix} = \begin{bmatrix} -0.1011 & 3.8038 & 0 & -9.81 \\ -0.0095 & -1.7936 & 0.992 & 0 \\ 0.0249 & -5.4654 & -1.9242 & 0 \\ 0 & 0 & 1 & 0 \end{bmatrix} \begin{bmatrix} \tilde{V} \\ \tilde{\alpha} \\ \tilde{q} \\ \tilde{\theta} \end{bmatrix} + \begin{bmatrix} 0 & 5.3008 \\ 0 & -0.062 \\ -24.764 & -2.4985 \\ 0 & 0 \end{bmatrix} \begin{bmatrix} \tilde{\delta}_e \\ \tilde{\delta}_T \end{bmatrix}$$

From these linearized equations, the following eigenvalues are calculated,

$\lambda_{1,2} = -1.869 + 2.3209i$ Short Period Mode

$\lambda_{3,4} = -0.040462 + 0.32418i$ Long Period (Phugoid) Mode

The undamped natural frequency, ω_n; damping ratio, ζ; period, T; time and number of cycles to half-amplitude are tabulated in Table 4.1.

Table 4.1 Longitudinal characteristics for specified eigenvalues

Type of mode	ω_n (rad/s)	ζ	T (s)	Time (s)	# of cycles
Short Period	2.98	0.627	2.707	0.37	0.137
Phugoid	0.327	0.124	19.38	17.05	0.88

Other trimmed flight conditions are also specified and related trimmed flight parameters given in Table 4.2 are found. Corresponding eigenvalues are listed in Table 4.3.

Table 4.2 Trimmed flight parameters for various conditions

# of set	V_0 (m/s)	h_0(m)	α_0 (deg)	θ_0 (deg)	δ_{T_0}	δ_{e_0}(deg)
Set 1	38	1500	5.33	5.33	0.195	-0.8
Set 2	35	1200	6.62	6.62	0.177	-1.23
Set 3	32	1000	8.42	8.42	0.165	-1.84

Table 4.3 Eigenvalues calculated from linearized equations at trimmed flight conditions given in Table 4.2.

# of set	Short Period Mode	Long Period (Phugoid) Mode
Set 1	$-1.6684 \pm 1.9984i$	$-0.0313 + 0.3658i$
Set 2	$-1.5891 \pm 1.865i$	$-0.0276 + 0.3912i$
Set 3	$-1.4918 \pm 1.713i$	$-0.0238 + 0.4226i$

It can be seen from the above eigenvalues, the linearized longitudinal equations are stable. The tilt-duct VTOL UAV behaves in a classical manner with easily observable short period and phugoid modes.

4.5.3 Transition Mode

Using Eqn. (4.2.5) together with cost function given in Eqn. (4.3.1), various transition mode trimmed flight conditions are obtained at different forward velocities. In the following, flight conditions are listed. Flight altitude, exit guide vane angle, are all taken the same. Flight altitude, h_0 is taken as 1000 m and exit guide vane angle, η_0 is taken as 90^0. Here, transition is taken account as tilting ducts from 90^0 (hover flight mode) to 0^0 (cruise flight mode). Aircraft velocities from 0.1 m/s to 31 m/s, are specified as equality constraints and remaining parameters are calculated by the program written in Matlab.

Since there are many parameters to optimize, it is decided to impose some constraints on certain variables. For this purpose, two cases are proposed. Case 1 considers a linear variation of the duct angle with aircraft velocity. On the other hand, Case 2 proposes a constraint between the main throttle setting and the aircraft velocity. These cases are presented under separate headings below.

- Case 1

The linear constraint on the duct angle as a function of aircraft velocity, shown in Figure 4.1 is imposed and the corresponding trim data is obtained and given in Table 4.4.

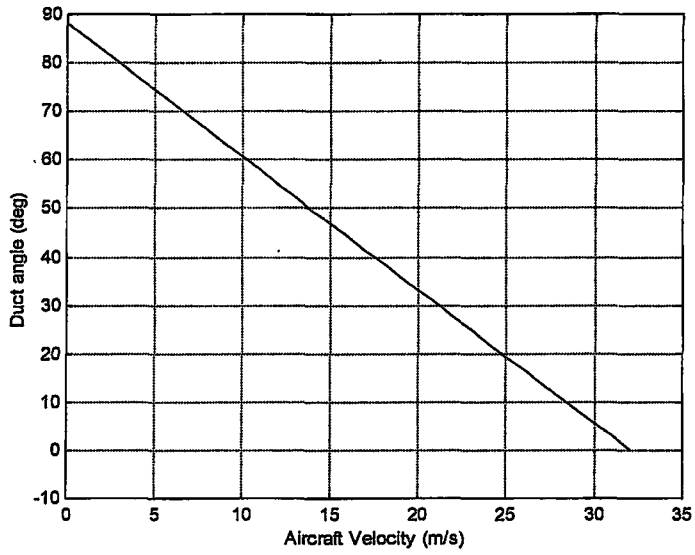

Figure 4.1 Linear constraint imposed on duct angle

Table 4.4 Trim data found together with the linear constraint imposed on the duct angle given in Figure 4.1

V_0 (m/s)	δ_{T0}^m	δ_{T0}^a	μ_0 (deg)	α_0 (deg)	θ_0 (deg)	δ_{e_0} (deg)
0.1	0.701	0.689	88	1.781	1.781	-1.7
1	0.708	0.64	85.52	3.84	3.84	-5
2	0.716	0.573	82.76	6.51	6.51	-1.42
3	0.722	0.511	80	9	9	-5
4	0.727	0.416	77.24	11.46	11.46	-4.4
5	0.728	0.375	74.48	14	14	-5.73
6	0.727	0.279	71.72	16.37	16.37	-2.2
7	0.717	0.225	69	18.26	18.26	-5.8
8	0.706	0.118	66.2	20.6	20.6	-3.5
9	0.68	0.1	63.5	22.5	22.5	-7.5
10	0.65	0.048	60.7	23.76	23.76	-8.2
11	0.6	0.099	57.9	25.7	25.7	-13

Table 4.4 Trim data found together with the linear constraint imposed on the duct angle given in Figure 4.1 (cont'd)

12	0.57	0.005	55.2	26	26	-10.2
13	0.526	0.005	52.4	27.3	27.3	-11
14	0.48	0.03	49.7	27.2	27.2	-11.5
15	0.438	0.005	46.7	27.1	27.1	-10.5
16	0.398	0.095	44.2	25.4	25.4	-12
17	0.361	0.045	41.4	24.6	24.6	-10.2
18	0.335	0.07	38.6	22.9	22.9	-9.75
19	0.31	0.005	35.7	22.2	22.2	-8
20	0.289	0.058	33.1	20.5	20.5	-8
21	0.272	0.062	30.3	19.2	19.2	-7.3
22	0.258	0.036	27.6	17.8	17.8	-6.3
23	0.246	0.062	24.8	16	16	-5.7
24	0.235	0.015	22	15.5	15.5	-5
25	0.225	0.054	19.3	14.2	14.2	-4.9
26	0.217	0.028	16.5	13.3	13.3	-4.1
27	0.209	0	13.8	12.4	12.4	-3.5
28	0.201	0	11	11.5	11.5	-3.15
29	0.193	0	8.8	10.6	10.6	-2.8
30	0.185	0	5.5	9.7	9.7	-2.5
31	0.174	0	2.75	9.5	9.5	-2.11
32	0.165	0	0	8.42	8.42	-1.84

The trim flight parameters calculated above indicate that main throttle setting initially increases with increasing speed. Then it drops as given in Figure 4.2, since aerodynamic forces and moments start to play an important role. As the forward flight velocity is increased, the angle of attack attains large values (i.e. trim flight condition for V_0= 12, 13,14 and 15 m/s). As the speed is increased further, the angle of attack and elevator deflection are reduced towards the values of cruise trim flight condition as shown in Figure 4.4 and Figure 4.5

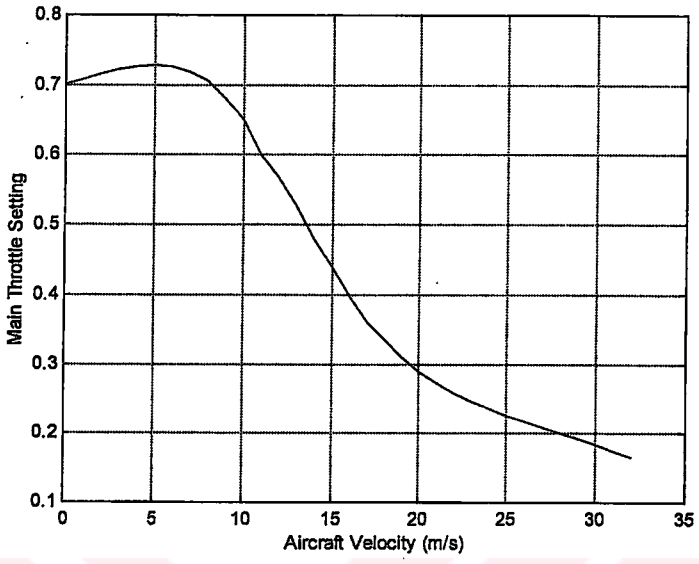

Figure 4.2 Main Throttle Setting vs. Aircraft Velocity (Case 1)

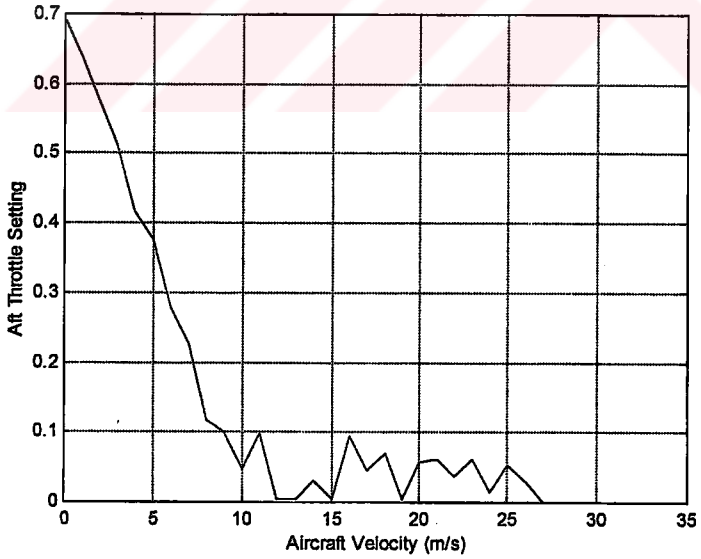

Figure 4.3 Aft Throttle Setting vs. Aircraft Velocity (Case 1)

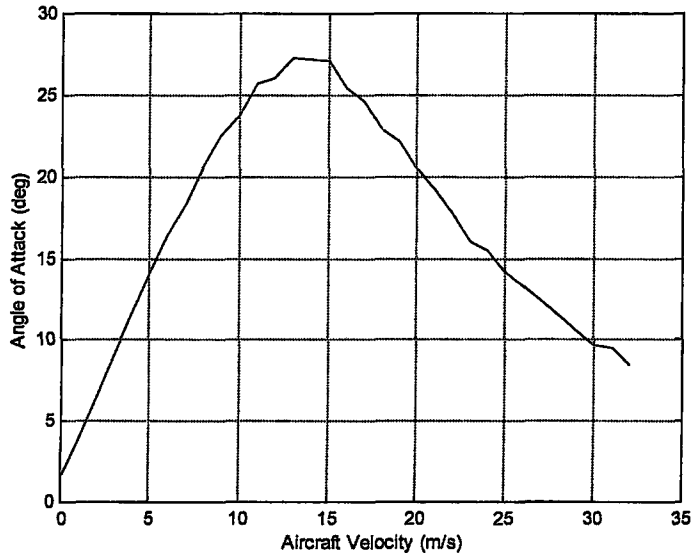

Figure 4.4 Angle of Attack vs. Aircraft Velocity (Case 1)

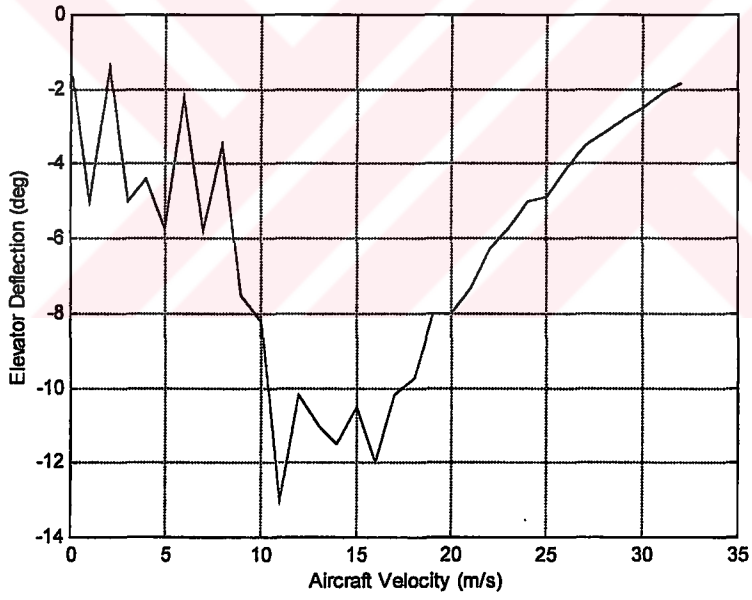

Figure 4.5 Elevator Deflection vs. Aircraft Velocity (Case 1)

The set of non-linear transition flight equations, Eqn. (4.3.5) are linearized at the trim flight conditions tabulated in Table 4.4. The eigenvalues are calculated to investigate the longitudinal stability during the transition. These eigenvalues, (i.e root locus diagram) are plotted in Figure 4.6 where the longitudinal velocity is taken as the parameter.

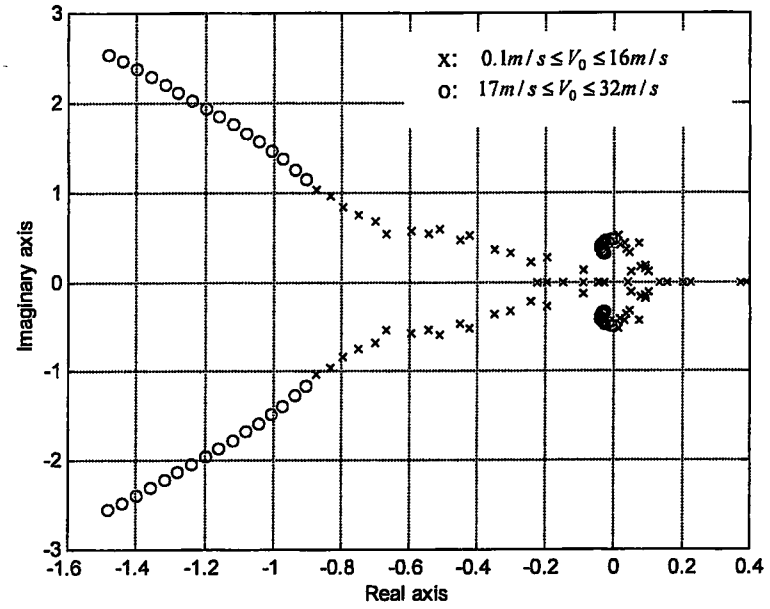

Figure 4.6 Root locus diagram built by using eigenvalues (Case 1)

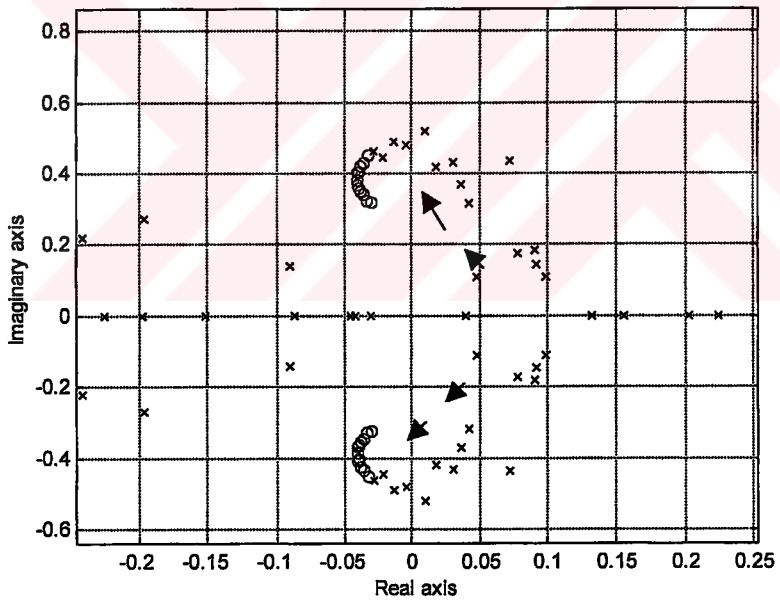

Figure 4.7 Root locus diagram built by using eigenvalues (Case 1) (close-up)

The root locus diagram indicates that the tilt-duct VTOL UAV is unstable in the velocity interval of 0.1-16 m/s of the transition mode. When the aircraft velocity reaches to 17 m/s, aircraft's eigenvalues pass to the stable region. The eigenvalues move smoothly towards the cruise flight values

It should be stressed that trim flight equations are very nonlinear in all cases. The optimization routine used is a gradient type local algorithm. Consequently, it can not be concluded that for a given flight condition, the obtained parameters are the only ones that satisfy the corresponding trim condition. However, since bounds on optimization parameters are imposed, and calculated parameters are physically reasonable, these results may be claimed to be acceptable.

- Case 2

As a next step, instead of a constraint on duct angle, constraints on the aircraft main throttle settings as shown in Figures 4.8 and 4.9 are imposed. However, with these constraints trim conditions could not be obtained since imposed values for main throttle setting are not large enough to achieve trimmed flight at the velocities in question.

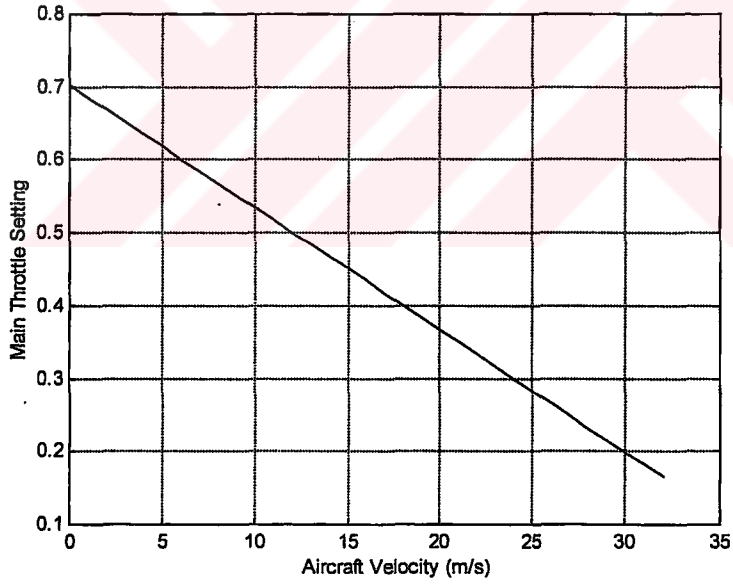

Figure 4.8 Main Throttle Setting vs. Aircraft Velocity, initial value=0.701

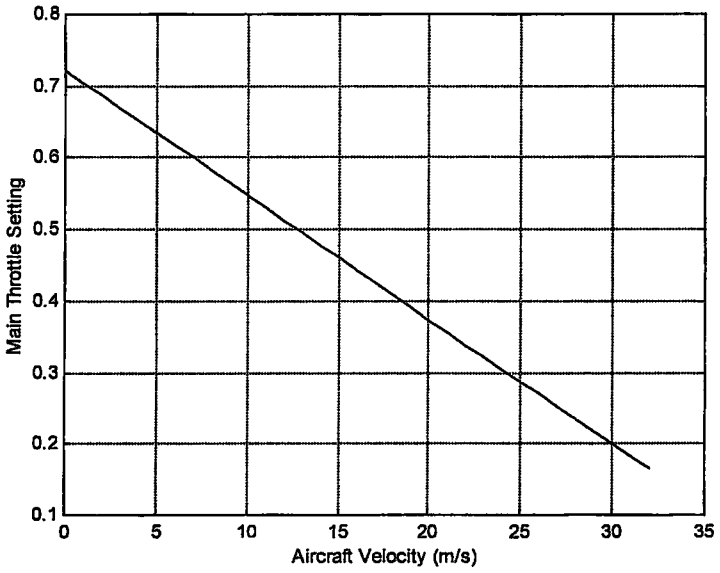

Figure 4.9 Main Throttle Setting vs. Aircraft Velocity, initial value=0.72

Then, a piecewise continuous constraints on the main throttle setting, shown in Figure 4.10, is imposed and the corresponding trim data, given in Table 4.5, is obtained.

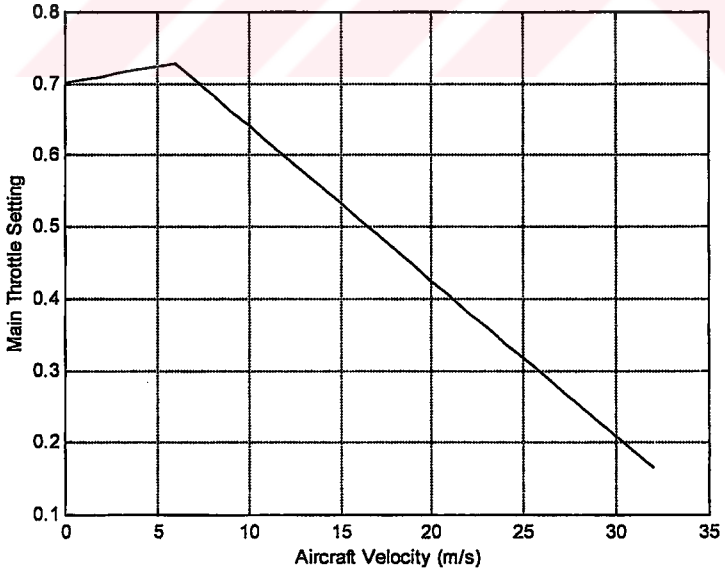

Figure 4.10 Main Throttle Setting vs. Aircraft Velocity (Case 2)

Table 4.5 Trim data obtained together with piecewise continuous linear constraint imposed on throttle setting, given in Figure 4.10.

V_0 (m/s)	δ_{T0}^m	δ_{T0}^a	μ_0 (deg)	α_0 (deg)	θ_0 (deg)	δ_{e_0} (deg)
0.1	0.701	0.692	88.1	1.67	1.67	-5
1	0.706	0.654	86.3	3.27	3.27	-3.5
2	0.710	0.618	84.7	4.74	4.74	-4.6
3	0.715	0.566	82.4	6.78	6.78	-4.3
4	0.720	0.498	79.5	9.35	9.35	-4.4
5	0.724	0.409	76	12.5	12.5	-4.6
6	0.728	0.264	70.5	17.6	17.6	-4.2
7	0.706	0.409	76	11.9	11.9	-4.25
8	0.684	0.553	79	8.6	8.6	-10
9	0.663	0.704	81.5	6	6	-14.7
10	0.641	0.767	79.5	7.1	7.1	-19.34
11	0.62	0.21	63	21.2	21.2	-11.9
12	0.598	0.177	62.9	20.5	20.5	-9.3
13	0.576	0.158	63	19.5	19.5	-7.6
14	0.554	0.505	67.5	14.1	14.1	-13.2
15	0.533	0.655	68.7	12	12	-14.5
16	0.511	0.781	69	10.5	10.5	-15.35
17	0.489	0.15	62	15.4	15.4	-5.2
18	0.468	0.489	63.5	12.32	12.32	-9.6
19	0.446	0.399	61.2	12.43	12.43	-8
20	0.425	0.516	60	11.35	11.35	-9
21	0.403	0.653	58.4	10.17	10.17	-10
22	0.381	0.15	53.1	12.38	12.38	-4.7
23	0.36	0.243	50.1	11.57	11.57	-5.5
24	0.338	0.174	46	11.46	11.46	-4.8
25	0.316	0.244	41.2	11	11	-5.25
26	0.295	0.685	36.8	9.34	9.34	-8.3

Table 4.5 Trim data obtained together with piecewise linear constraint imposed on throttle setting, given in Figure 4.10 (cont'd)

27	0.273	0.549	30	9.46	9.46	-7
28	0.252	0.392	23.5	9.57	9.57	-5.5
29	0.23	0.15	16.8	9.74	9.74	-3.6
30	0.208	0.031	10.7	9.5	9.5	-2.7
31	0.187	0.02	5.2	8.67	8.67	-2.3
32	0.165	0	0	8.4	8.4	-1.84

The trim flight parameters calculated above indicate that duct angle changes in a nonlinear fashion with increasing aircraft velocity, as shown in Figure 4.11. Additional nonlinearities on the aft throttle setting, angle of attack and elevator deflection are observable from Figures 4.12-4.14. It is very difficult to operate the aircraft in such a nonlinear transition mode.

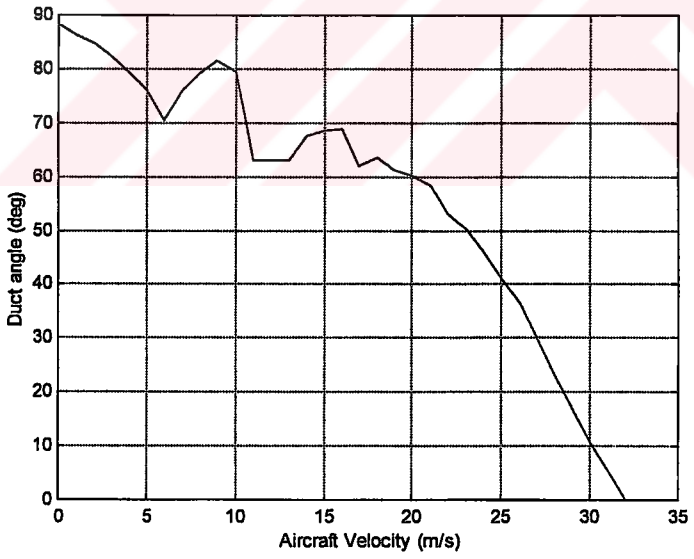

Figure 4.11 Duct angle vs. Aircraft Velocity (Case 2)

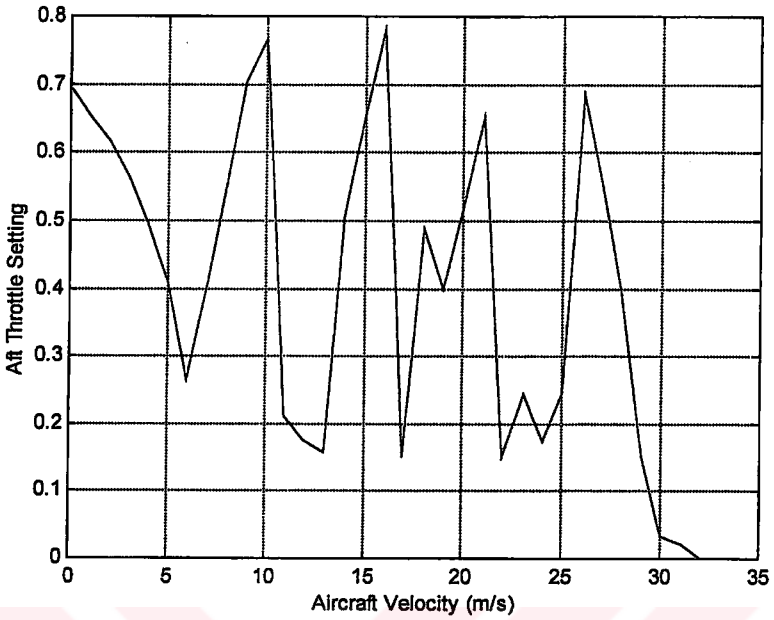

Figure 4.12 Aft Throttle Setting vs. Aircraft Velocity (Case 2)

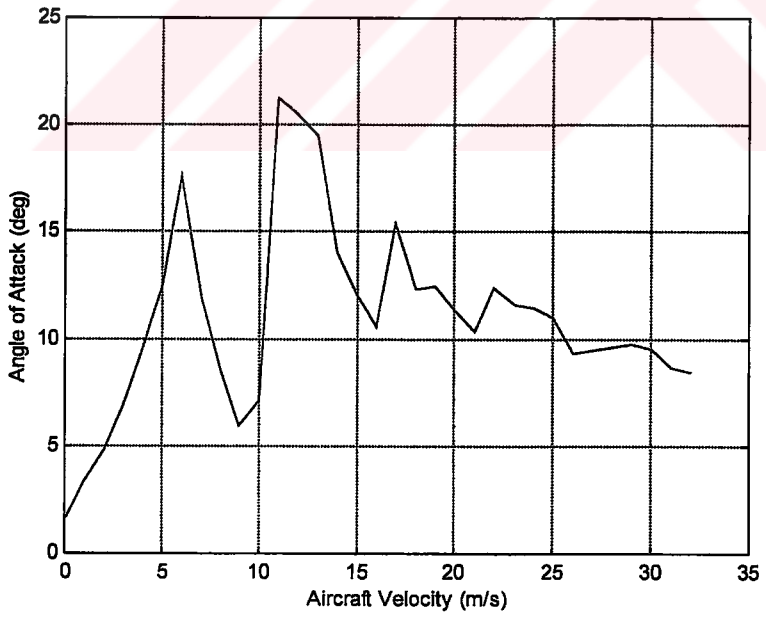

Figure 4.13 Angle of Attack vs. Aircraft Velocity (Case 2)

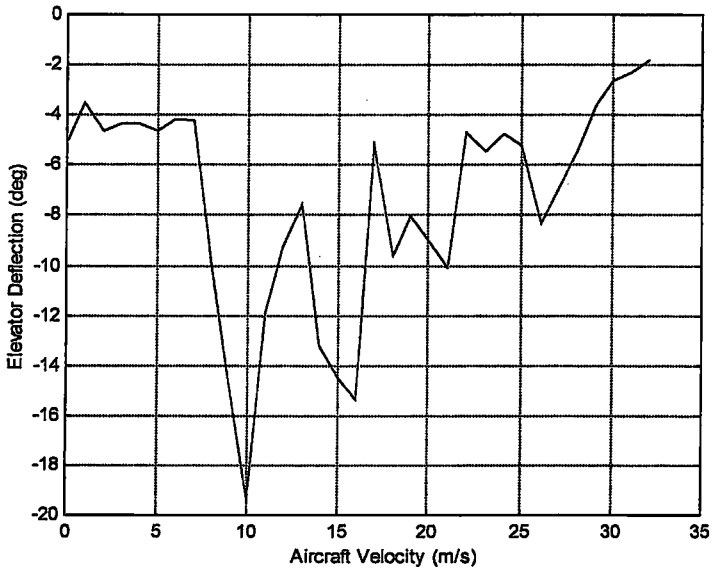

Figure 4.14 Elevator Deflection vs. Aircraft Velocity (Case 2)

However, the set of non-linear transition flight equations, Eqn. (4.3.5) are linearized at the various trim flight conditions given in Table 4.5. The eigenvalues are obtained to investigate the longitudinal stability during the transition trim flight. These eigenvalues, (i.e root locus diagram), are shown in Figure 4.15.

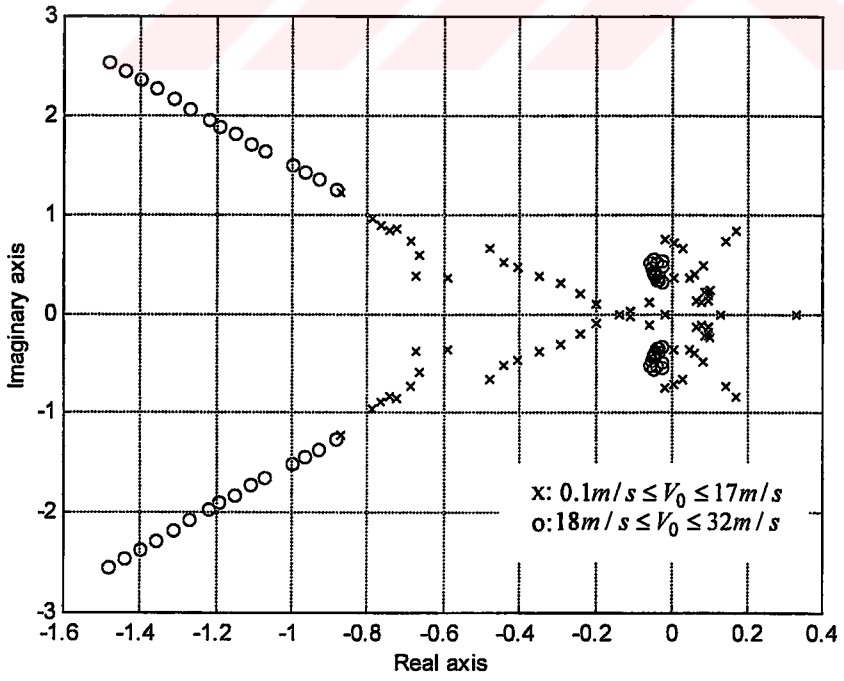

Figure 4.15 Root locus diagram built by using eigenvalues (Case 2)

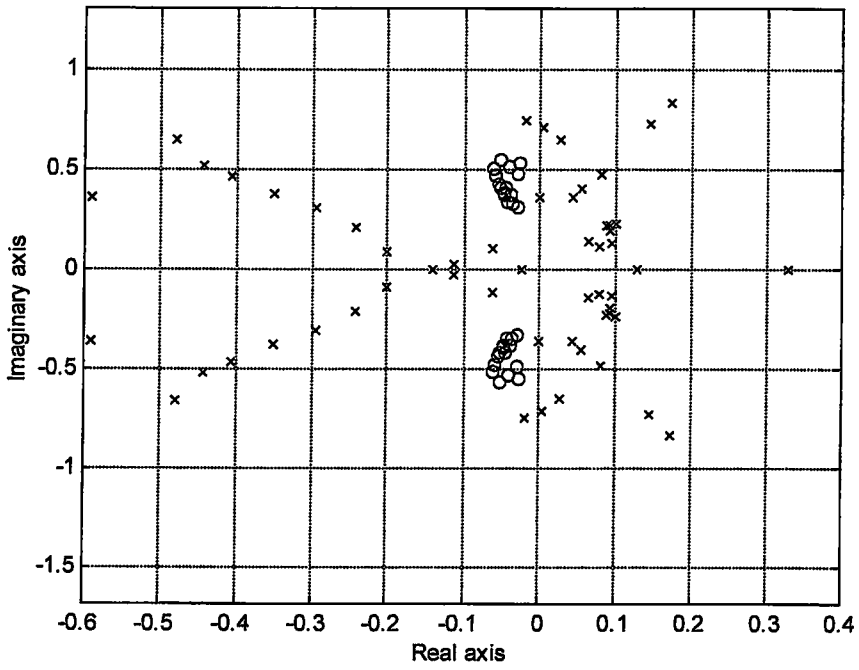

Figure 4.16 Root locus diagram built by using eigenvalues (Case 2) (close-up)

The root locus diagram indicates that the tilt-duct VTOL UAV is unstable in the velocity interval of 0.1-17 m/s of the transition mode. When the aircraft velocity reaches to 18 m/s, the aircraft's eigenvalues pass to the stable region. The eigenvalues move smoothly towards the cruise flight values as can be observed from the plot.

CHAPTER 5

AUTOMATIC FLIGHT CONTROL SYSTEM

5.1 Introduction

The evolution of modern aircraft created a need for power driven aerodynamic control surfaces and automatic control systems. In addition, the widening performance envelope created a need to augment the stability of the aircraft dynamics over some parts of the envelope. In general, aircraft envelope covers a very wide range of dynamic pressure. For example, in the landing phase the dynamic pressure may have low values where as at higher speeds it has higher values. Large variations in the dynamic pressure cause correspondingly large variations in the coefficients of the dynamic equations. Other factors also contribute to changes in the aircraft dynamics. These factors involve Mach number, aerodynamic angles and changing mass properties due to different payloads and fuel loads [23].

Because of the large changes in aircraft dynamics, a dynamic mode that is stable and adequately damped in one flight condition may become unstable or at least inadequately damped, in an another flight condition. A lightly damped oscillatory mode makes it difficult for the pilot to control the trajectory precisely. These problems are overcome by using feedback control to modify the aircraft

dynamics. The aircraft motion variables are sensed and used to generate signals that can be fed into the aircraft control-surface actuators, thus modifying the dynamic behaviour. This feedback must be adjusted according to the flight condition. This adjustment process is called "gain scheduling". In its simplest forms, it involves only changing the amount of feedback according to a predetermined schedule [23].

A main problem in the design of systems with gain scheduling is to find suitable scheduling variables. This is normally done by taking knowledge about the physics of the system as a base for the operation. The concept of gain scheduling originated in connection with the development of flight control systems. In flight control system applications, generally the Mach number and the dynamic pressure are measured by air data sensors and used as scheduling variables. Figure 5.1 shows the gain scheduling scheme.

In the case of low-performance aircraft with relatively narrow envelopes and control surfaces that are not power driven, an unsatisfactory dynamic mode must be corrected by modifying the basic design. As in the case of the high performance aircraft, this requires an understanding of the dynamic modes and their dependence on the aerodynamic coefficients and stability derivatives [23].

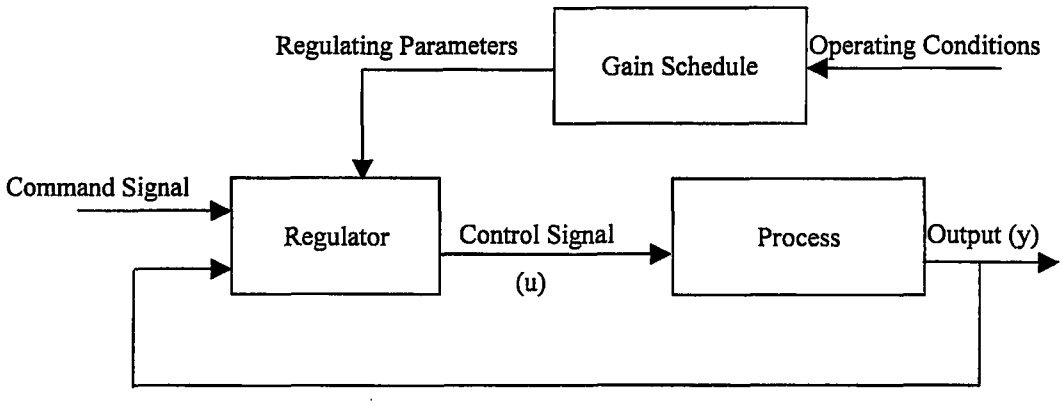

Figure 5.1 Gain Scheduling Scheme [26].

5.2 The Functions of Automatic Flight Control Systems

The description and analyses carried out on aircraft modes, which are given in the literature show that they can be divided into two different categories.

First category contains modes that involve mainly the rotational degrees of freedom, such as the short period, roll subsidence and dutch-roll modes. Second category contains the modes that involve flight path changes such as phugoid (long period) and spiral modes [21].

The frequencies of the modes belonging to the first category tend to be sufficiently high that a pilot would find it difficult or impossible to control the aircraft if the modes are lightly damped or unstable. Thus, it is necessary to provide automatic control systems to give these modes suitable damping and natural frequencies. Such control systems are called as "stability augmentation systems" (SAS). The inherent stability of an airplane depends upon the aerodynamic stability derivatives. The magnitude of them affects both the damping and frequency of the longitudinal and lateral-directional motions. The stability derivatives are the function of the aircraft's aerodynamic and geometric characteristics. For a particular flight regime it would be possible to design an aircraft to possess desirable flying qualities. If the augmentation system is intended to control the mode and to provide the pilot with a particular type of response to the control inputs, it is called as "control augmentation system" (CAS) [21,23].

There is another class of flight control systems called "autopilots". The autopilots are used for establishing and maintaining desired flight conditions. Once the autopilot is engaged, it continues to hold these flight conditions without further intervention from the pilot. Autopilots are commonly used for maintaining pitch attitude, altitude, Mach number, altitude, prescribed glide slope during approach and landing, etc. The principal element of an autopilot is sensing element called gyroscope (gyro). It may be positional gyro or a rate gyro. Whenever, there is a

deviation from the preselected condition, the gyro senses the change and generates electrical signals, which are amplified and are used to drive the servo devices that move the appropriate control surfaces in the desired manner [21,23].

The common types of SAS, CAS and the autopilot functions are tabulated in Table 5.1.

Table 5.1 The common types of SAS, CAS and autopilot functions [23]

SAS	CAS	Autopilots
Pitch Damper	Pitch Rate	Pitch Attitude (Displacement) hold
Yaw Damper	Normal acceleration	Altitude hold, Mach hold
Roll Damper	Roll Rate	Automatic landing, Bank angle hold
	Lateral-directional	Turn coordination, heading hold/VOR hold

5.3 The Flying Quality Requirements

The control system design can only be performed satisfactorily if a set of design requirements or performance criteria is available. In the case of control systems for piloted aircraft generally applicable quantitative design criteria are very difficult to obtain. The reason for this is that the ultimate evaluation of a human operator control system is necessarily subjective and, with aircraft, the pilot evaluates the aircraft in different ways depending on the type of the aircraft and phase of flight [20,21,23].

Also, pilot opinion is influenced by such factors like weather conditions, stick force gradients, visibility, design and layout of cockpit controls, physical and emotional condition of the pilot, etc. In view of such widely varying factors that can affect pilot's opinion, it is usual to conduct several tests over many flights and many pilots and take an average of all the test results.

The Cooper-Harper scale is a systematic method of quantifying these test results. It assigns three levels to describe the flying qualities of an airplane as follows [21].

- Level 1: Flying qualities adequate to accomplish the mission flight phase.
- Level 2: Flying qualities adequate to accomplish the mission flight phase when some increase in pilot workload or degradation in mission effectiveness exists or both.
- Level 3: Flying qualities such that the mission can be controlled safely, but pilot workload is excessive or mission effectiveness is inadequate or both.

The flight phases is divided as follows, where Category A flight phases can be terminated safely, and Category B and C flight phases can be completed.

- Category A: Nonterminal flight phases that require rapid maneuvering, precision tracking, or precise flight path control. Air-to-air combat, ground attack, weapon delivery and launch, aerial recovery, in flight refuelling (receiver), terrain following, close formation flying are included in this category.
- Category B: Nonterminal flight phases that are normally accomplished using gradual manoeuvres and without precision tracking, although accurate flight path control may be required. Climb, cruise, loiter, in flight refuelling (tanker), descent, aerial delivery, emergency deceleration and etc are included in this category.
- Category C: Terminal flight phases are normally accomplished using gradual manoeuvres and usually require accurate flight path control. Takeoff, catapult takeoff, approach, landing are included in this category.

The aircraft are classified as follows.

- Class I: Small, light aircraft, such as light utility, primary trainer and light observation aircraft.
- Class II: Medium-weight, low-to-medium maneuverability airplane, such as heavy utility/search and rescue, light or medium transport/cargo/tanker, reconnaissance, tactical bomber
- Class III: Large, heavy, low-to-medium maneuverability aircraft such as heavy transport/cargo/tanker, heavy bomber.
- Class IV: High maneuverability aircraft, such as fighter/interceptor, attack, tactical reconnaissance.

Extensive research and development activities have been conducted by various government agencies and the civil and military aviation authorities to relate the Cooper-Harper flying qualities to physical parameters like the frequency and damping ratio of the oscillatory motions of the aircraft. The military specifications MIL-F-8785C, used also for civilian aircraft are as follows and used in this analysis. Only, the longitudinal flying qualities are presented.

- **Phugoid Mode Specifications**

Level I=$\zeta \succ 0.04$, Level II=$\zeta \succ 0$, Level III=$T_2 \succ 55s$

In the Level III, the aircraft is assumed to have an unstable (divergent) phugoid mode, and T_2 denotes the time required for the amplitude to double the initial value [21].

- **Short Period Mode Specifications**

The damping ratios of the short period mode for various levels of flying qualities for Category A, B and C flight phases are given in Table 5.2.

Table 5.2 Damping ratios for short period mode [21]

	Cat. A and C $\zeta_{sp,\min}$	Cat. A and C $\zeta_{sp,\max}$	Cat. B $\zeta_{sp,\min}$	Cat. B $\zeta_{sp,\max}$
Level I	0.35	1.3	0.3	2
Level II	0.25	2	0.2	2
Level III	0.15	No limit	0.15	No limit

The requirements on the natural frequencies of the short period mode for category A, B, and C flight phases according to MIL-F-8785C should lie within the limits as given in Table 5.3.

Table 5.3 Limits on $\omega_{n,sp}^2/(n/\alpha)$ [21]

	Cat. A min	Cat. A max	Cat. B min	Cat. B max	Cat. C Min	Cat. C max
Level I	0.28	3.6	0.085	3.6	0.16	3.6
Level II	0.16	10	0.038	10	0.096	10
Level III	0.16	No limit	0.038	No limit	0.096	No limit

Where n is the load factor as given by,

$$n = \frac{L}{W} = \frac{1/2\rho V^2 S C_L}{W} \tag{5.3.1}$$

For linear range of angle of attack,

$$\frac{n}{\alpha} = \left(\frac{1}{2W}\right)\rho V^2 S C_{L_\alpha} \tag{5.3.2}$$

Thus, the ratio of Eqn. (5.3.2) depends on the flight velocity and flight altitude.

5.4 Automatic Flight Control System Design for VTOL UAV Longitudinal Dynamics

5.4.1 Hover Flight Mode Stability Augmentation System Design

In general, in the case of some aircraft, it is desired to increase the damping of the short period oscillation with satisfactory natural frequency or make the mode stable. For this purpose, the pitch stability augmentation systems are used.

First, a pitch stability augmentation system is designed for the hover mode of the tilt-duct VTOL UAV. The dynamic equations are written with the help of the hover mode static equations of (4.2.1).

$$\begin{aligned} m\dot{u} &= -mg\sin\theta \\ m\dot{w} &= -T^m\delta_T^m - T^a\delta_T^a + mg\cos\theta \\ I_{yy}\dot{q} &= T^m\delta_T^m l_1 - T^a\delta_T^a l_2 \\ \dot{\theta} &= q \end{aligned} \tag{5.4.1}$$

Then, these non-linear equations are linearized using the trim conditions presented in Section 4.5.1. Thus, the following state space model is obtained.

$$\begin{bmatrix} \dot{\tilde{u}} \\ \dot{\tilde{w}} \\ \dot{\tilde{q}} \\ \dot{\tilde{\theta}} \end{bmatrix} = \begin{bmatrix} 0 & 0 & 0 & -9.81 \\ 0 & 0 & 0 & 0 \\ 0 & 0 & 0 & 0 \\ 0 & 0 & 1 & 0 \end{bmatrix} \begin{bmatrix} \tilde{u} \\ \tilde{w} \\ \tilde{q} \\ \tilde{\theta} \end{bmatrix} + \begin{bmatrix} 0 & 0 \\ -12.4586 & -1.5573 \\ -1.381 & -1.3156 \\ 0 & 0 \end{bmatrix} \begin{bmatrix} \tilde{\delta}_T^m \\ \tilde{\delta}_T^a \end{bmatrix} \tag{5.4.2}$$

Then, transfer function between pitch rate and aft throttle setting is found,

$$\frac{\tilde{q}(s)}{\tilde{\delta}_T^a(s)} = \frac{-1.3156}{s} \tag{5.4.3}$$

The eigenvalues of (5.4.2) show that there is quadruple pole at the origin and the system is unstable. The block diagram shown in Figure 5.2 is used in the analysis.

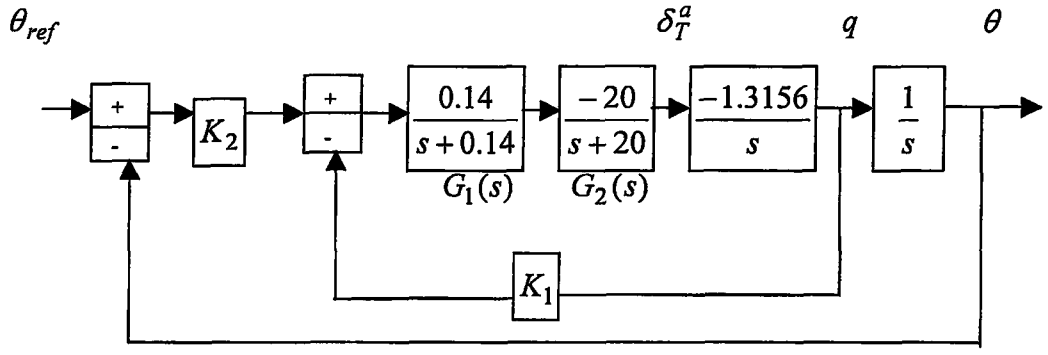

Figure 5.2 Block diagram for the pitch stabilization system for hover mode

where $G_1(s)$ and $G_2(s)$ represent transfer functions for engine time lag and aft throttle servo, respectively. Here, the time constant for the aft engine is taken as 7 s to model the engine response time. In order to select the gain, K_1, the root locus diagram, shown in Figure 5.3 is constructed for the inner loop.

It is calculated from root locus diagram that, the inner loop is stable for the following interval,

$$0 \prec K_1 \prec 13.9483$$

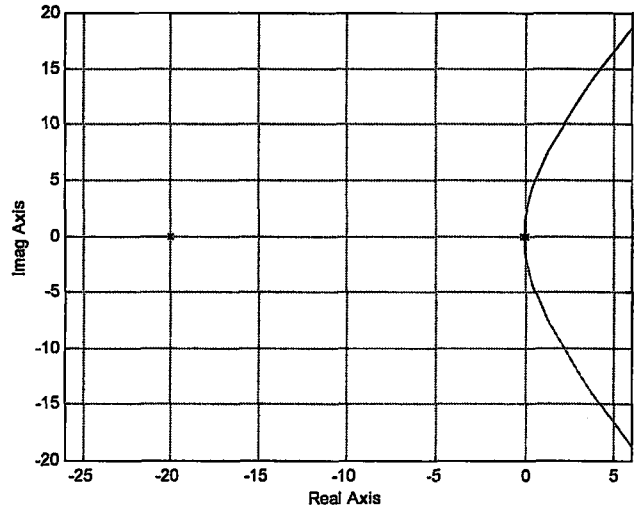

Figure 5.3 Root locus diagram for inner loop

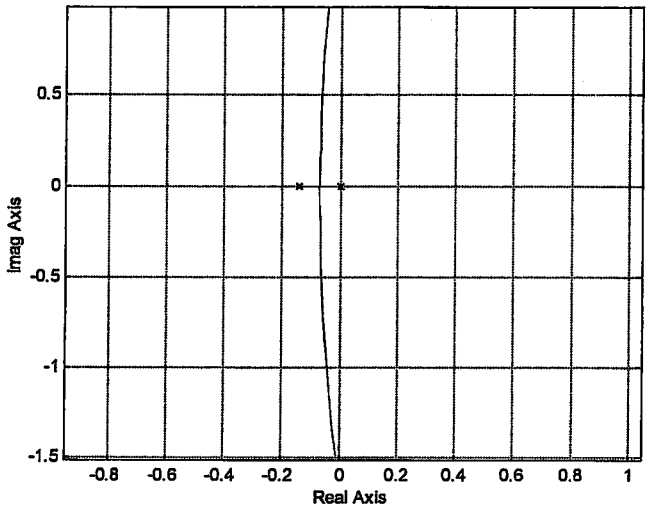

Figure 5.4 Root locus diagram for inner loop (close-up)

There are two opportunities to select the gain, K_1. These are selecting K_1 to get conjugate pair of complex roots or a pair of real roots. These two cases are investigated below.

- Case 1

In first case, K_1 is selected as 1.4046 to get the following inner closed loop roots.

$$p_1 = -20.013, \quad p_2 = -0.0635 + 0.5045i, \quad p_3 = -0.0635 - 0.5045i$$

After obtaining the closed loop transfer function of the inner loop, then the root locus diagram, shown in Figure 5.5 is obtained. Finally, the gain, K_2 is selected to get good flying characteristics. The stability condition on K_2 is given as follows;

$$0 \prec K_2 \prec 0.194$$

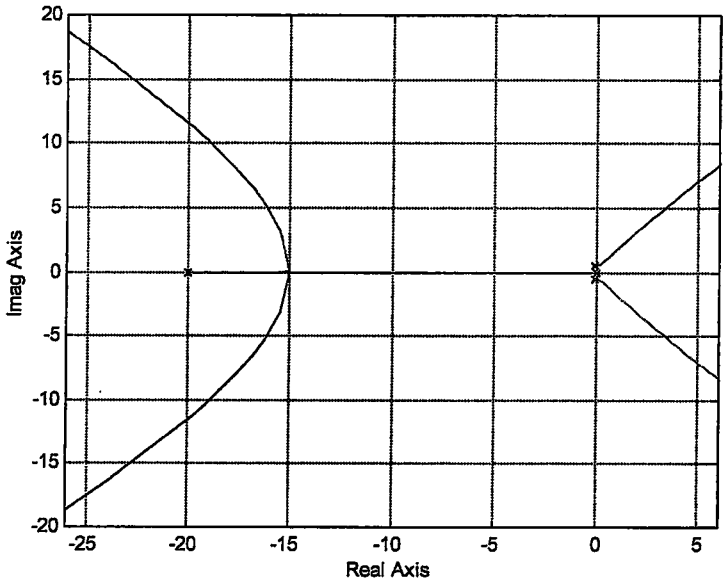

Figure 5.5 The root locus diagram for the outer loop (Case 1)

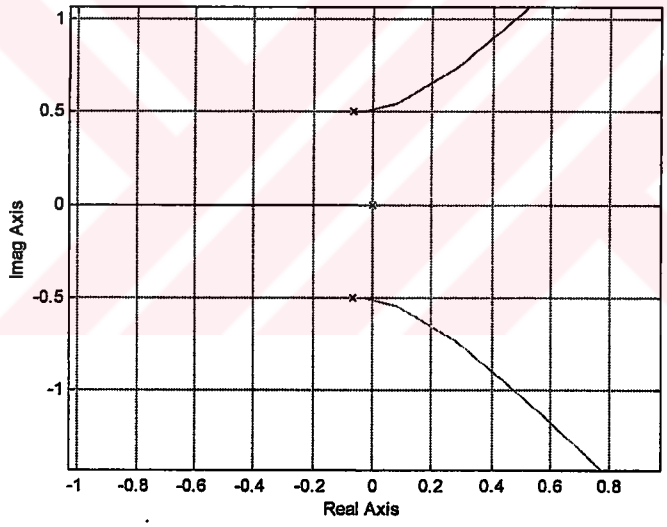

Figure 5.6 The root locus diagram for the outer loop (close-up)

The gain, K_2, is selected as 0.0991 and the following transfer function is obtained,

$$\frac{\theta(s)}{\theta_{ref}(s)} = \frac{0.36505}{s^4 + 20.14s^3 + 2.8s^2 + 5.1741s + 0.36505} \tag{5.4.4}$$

where the roots of the characteristic equation, i.e., the denominator of the closed loop transfer function of (5.4.4) are stable and given as following.

$p_1 = -20.013$, $p_2 = -0.0719$, $p_3 = -0.0276 + 0.5029i$, $p_4 = -0.0276 - 0.5029i$

The unit-step response of the system, shown in Figure 5.7 is satisfactory.

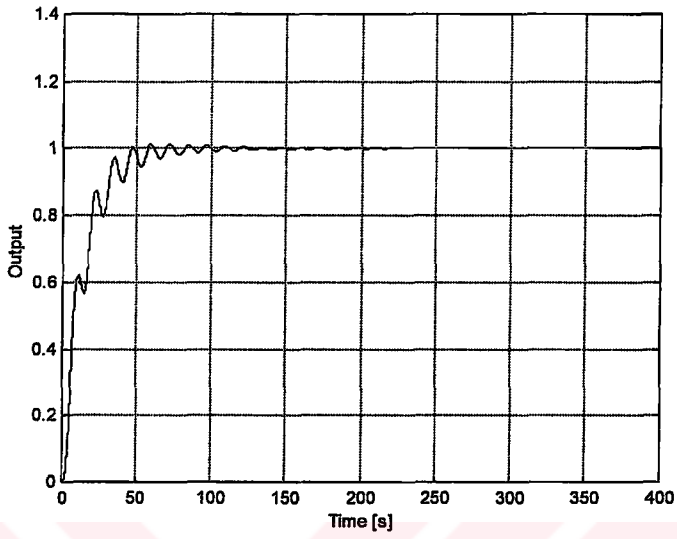

Figure 5.7 The unit-step response of the system (Case 1)

Then, the linear simulation is performed in Matlab-Simulink environment. The model is given in Figure 5.8. There is an initial 0.2 rad/s disturbance on pitch rate given to the system. It means, there is a disturbance of this magnitude on the pitch rate trim value. Also saturation limits, +0.25~-0.25 is imposed on aft throttle signal.

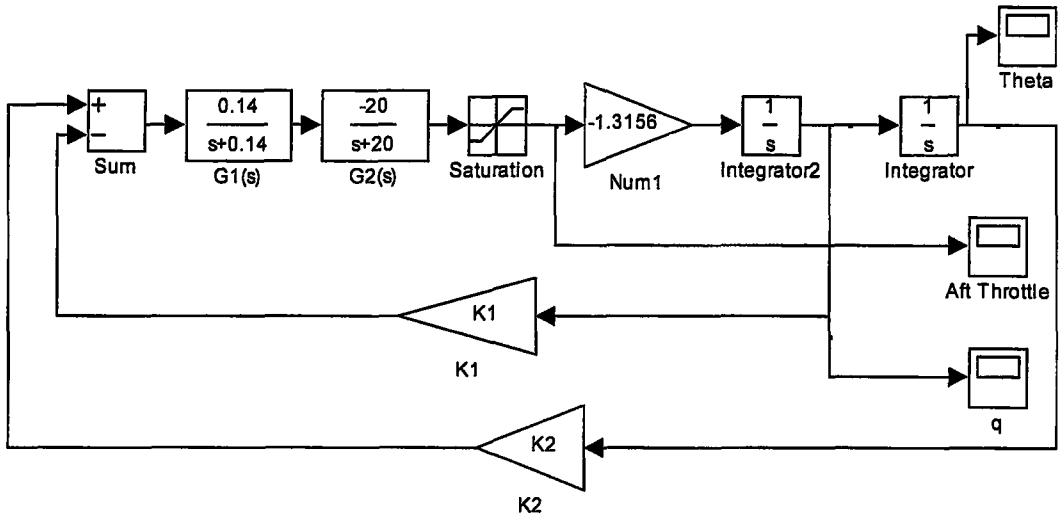

Figure 5.8 Linear simulation model for hover mode

The graphics obtained for pitch attitude and pitch rate are given in Figure 5.9.

Since the system is a lightly damped, ($\zeta = 0.055$), oscillations are observed in the graphics. This effect is mainly due to the sluggish behaviour of the aft engine. The peak values are reasonable and the variables converge.

- Case 2

In the second case, K_1 is selected to have real double root at $p = -0.07$ ($K_1 = 0.0265$). This gain led a large stability interval for K_2 which may be observed from Figure 5.10 and Figure 5.11.

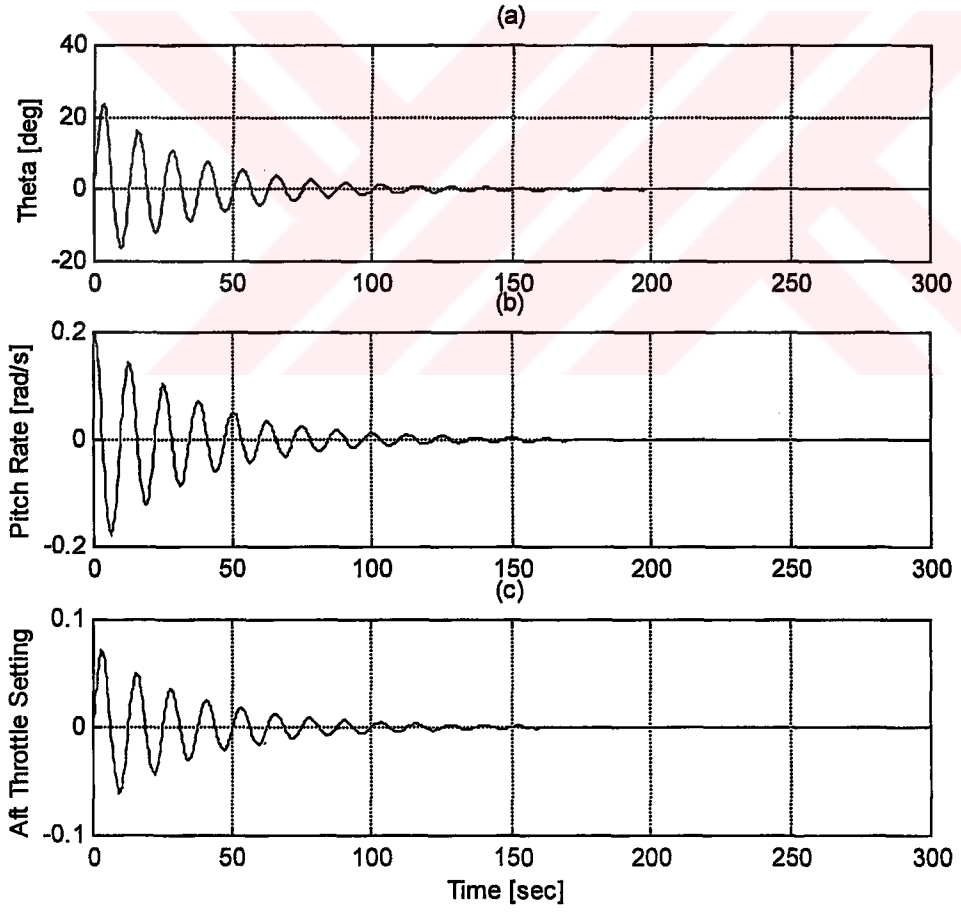

Figure 5.9 Response of the system to an initial 0.2 rad/s pitch rate disturbance
(Case 1 $K_1 = 1.4046$, $K_2 = 0.0991$)
a) Pitch Attitude b) Pitch Rate c) Aft Throttle Setting

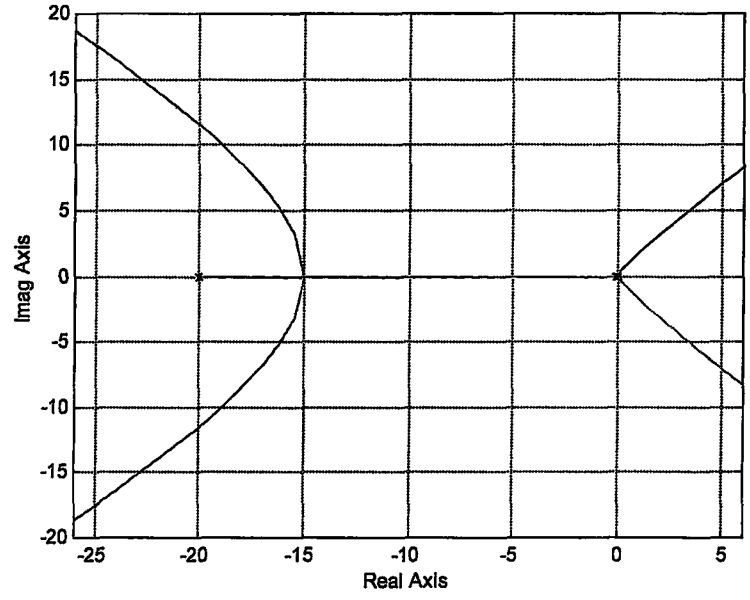

Figure 5.10 The root locus diagram for the outer loop (Case 2)

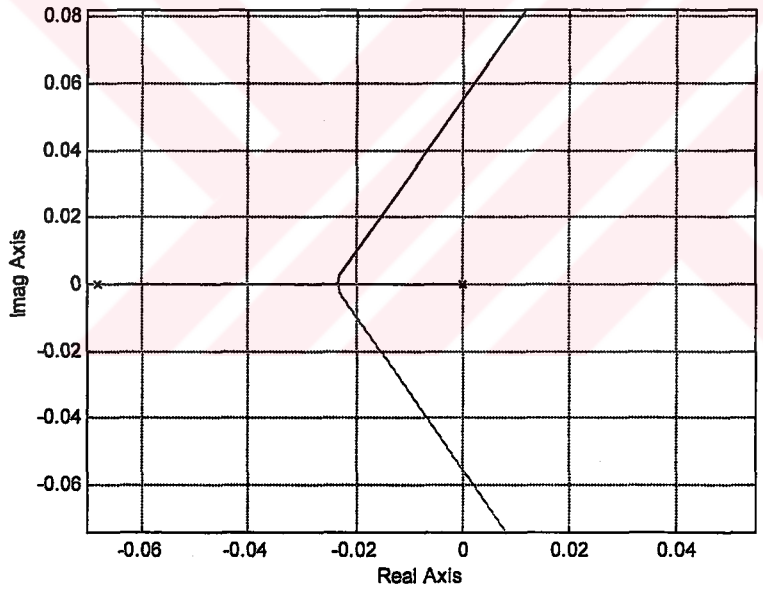

Figure 5.11 The root locus diagram for the outer loop (close-up) (Case 2)

The second gain, K_2, is selected as 0.0005525. Then, the damping coefficient of the overall closed loop system becomes 0.6 and, the following transfer function is obtained,

$$\frac{\theta(s)}{\theta_{ref}(s)} = \frac{0.00203}{s^4 + 20.14s^3 + 2.8s^2 + 0.097618s + 0.00203} \qquad (5.4.5)$$

where the roots of the characteristic equation, i.e., the denominator of the closed loop transfer function of (5.4.5) are stable and given as following.

$$p_1 = -20.0002,\ p_2 = -0.1016,\ p_3 = -0.0191 + 0.0253i,\ p_4 = -0.0191 - 0.0253i$$

The unit-step response of the system, shown in Figure 5.12 is satisfactory.

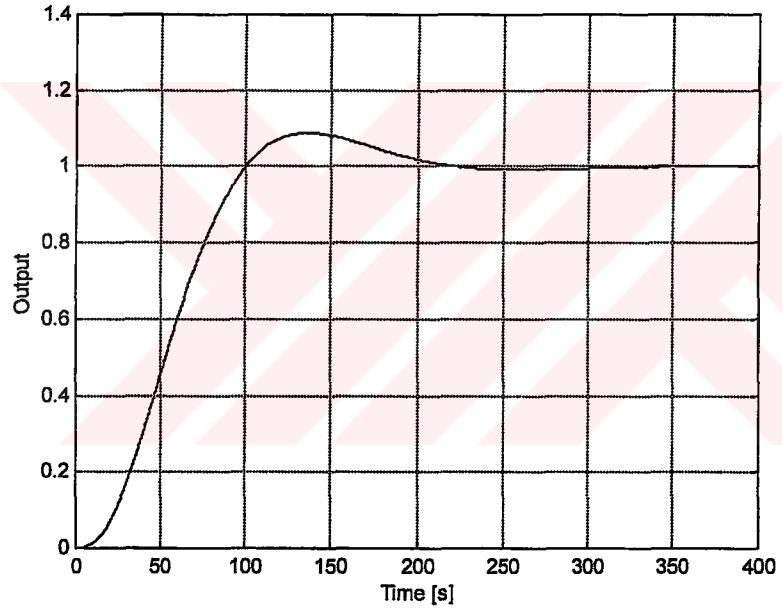

Figure 5.12 The unit step response of the system
(Case 2, $K_1 = 0.0265$, $K_2 = 0.0005525$)

Finally, by using the same model, given in Figure 5.8, but changing the feedback gains, the graphics, given in Figure 5.13 are obtained.

From this simulation, it may be observed that, the pitch attitude attains unfeasible values as shown in Figure 5.13 (a). Thus the design is not acceptable.

Then, the second gain, K_2 is selected to obtain overall closed loop system having relatively low damping ratio. K_2 is found to be equal to 0.0017 where the damping ratio is equal to approximately 0.2. The following closed loop poles are obtained and the unit step response of the system is given in Figure 5.14.

$$p_1 = -20,\ p_2 = -0.1209,\ p_3 = -0.0094 + 0.05i,\ p_4 = -0.0094 - 0.05i$$

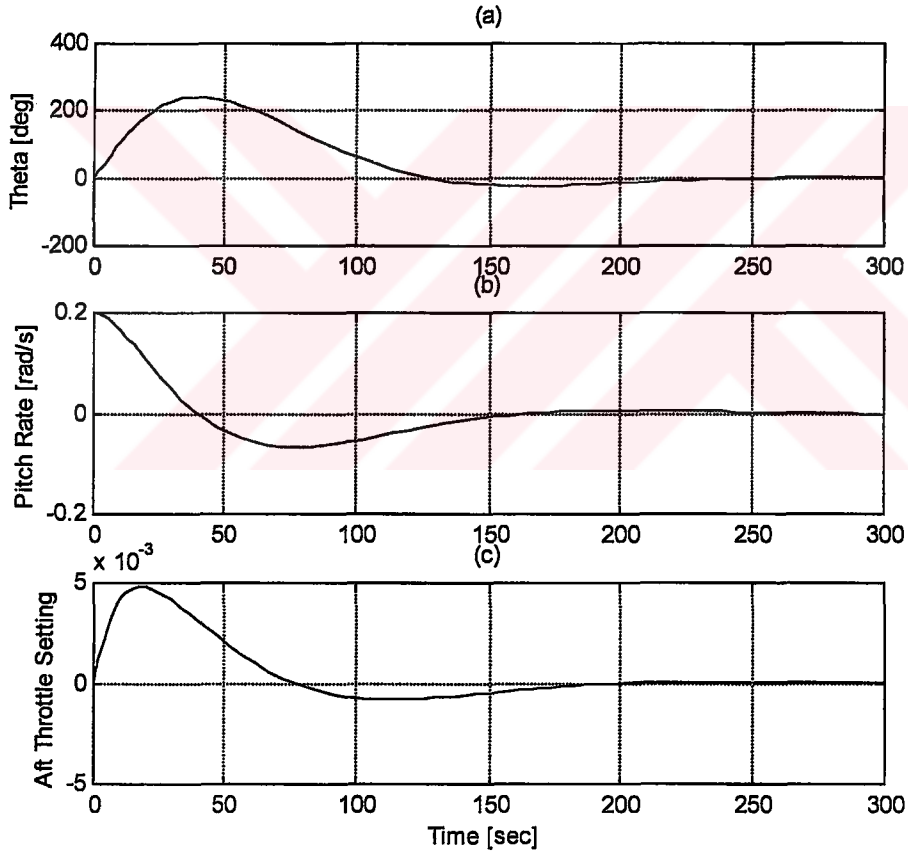

Figure 5.13 Response of the system to an initial 0.2 rad/s pitch rate disturbance
(Case 2 $K_1 = 0.0265$, $K_2 = 0.0005525$)
a) Pitch Attitude b) Pitch Rate c) Aft Throttle Setting

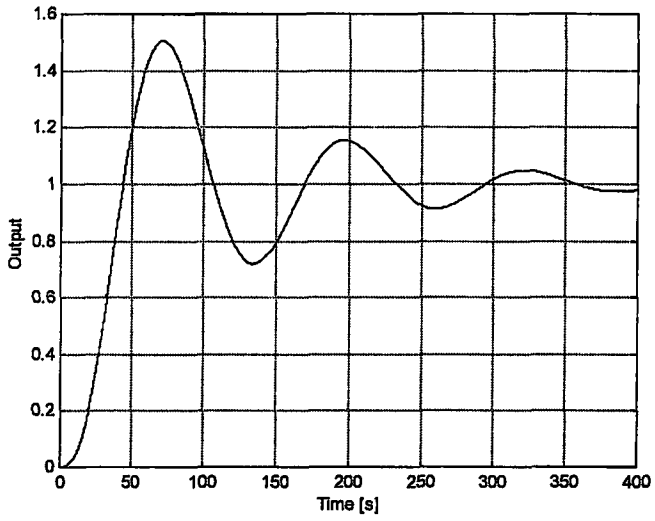

Figure 5.14 The unit step response of the system
(Case 2, Low damping, $K_1 = 0.0265$, $K_2 = 0.0017$)

Using these new feedback gains, ($K_1 = 0.0265$, $K_2 = 0.0017$), linear simulation with the same conditions mentioned before is performed. However, the simulation results again showed very large values for pitch attitude.

5.4.2 Transition Flight Mode Stability Augmentation System Design

The transition flight regime covers aircraft velocities from 0.1 m/s to 32 m/s where the duct angle changes from full up to full forward position gradually as described in the previous chapter. During this time the aircraft performance is quite unsatisfactory. For example, from 0.1 m/s to 16 m/s the aircraft is unstable. Above this velocity the aircraft is poorly damped. At low forward velocities, the pitching moment created by the elevator is not sufficient. Thus, aft propeller shall be used. On the other hand, at high velocities the elevator shall be the main instrument to control the longitudinal dynamics. Thus, the control authority shall pass from aft engine control to elevator control as the forward velocity increases. Similarly, the reverse shall happen in the landing phase of this tilt-duct VTOL UAV.

A pitch stability augmentation system, shown in Figure 5.15 is initially proposed. The system requires the measurement of angle of attack, pitch rate and pitch attitude. The angle of attack sensor is small wind vane mounted on the side of the aircraft forebody. The signal from this kind of a sensor is often noisy and the noise filter is needed to reduce noise strength. In the second inner loop, the pitch rate is measured by a rate gyro. Finally pitch attitude measurement requires an integrating gyro.

To design the stability augmentation system for the transition flight regime, the structure given in Figure 5.15 is used. For each velocity, related transfer function is used and root locus analysis with sequential loop closing is performed to obtain corresponding feedback gains. This analysis did not yield satisfactory results. Thus, a full-state variable feedback design is used.

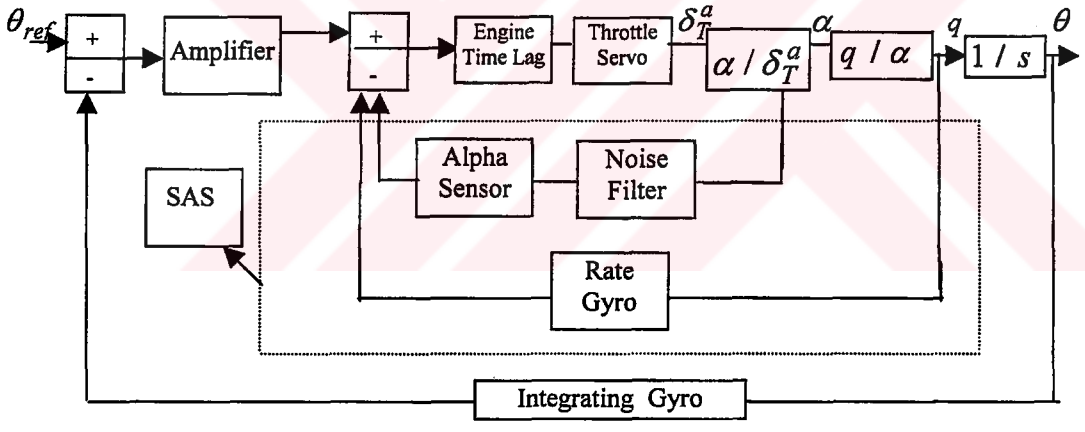

Figure 5.15 Block diagram of pitch stability augmentation system (SAS) for transition mode

For state variable feedback design, all four longitudinal states, aircraft velocity, angle of attack, pitch rate and pitch attitude must be available. The air-velocity is usually measured by a pitot-static sensor, pitch rate and attitude are measured by rate and integrating gyro, respectively, and the angle of attack is measured by a vane-type angle of attack sensor.

Using the states mentioned full state variable feedback with eigenvalue assignment technique is applied. For this purpose, the following eigenvalues that yield good handling qualities (Section 5.3) are selected for short period mode.

$$\lambda_{1,2} = -3.2 \pm 2.4i \tag{5.4.6}$$

These roots have a damping ratio of 0.8 and a natural frequency of 4 rad/s for the short period mode corresponding to Category B-Level I short-period flying qualities. For the phugoid mode,

$$\lambda_{3,4} = -0.0181 \pm 0.1196i \tag{5.4.7}$$

are selected. These roots have a damping ratio of 0.15 and a natural frequency of 0.121 rad/s, giving good Category B-Level I phugoid flying qualities. With these short period and phugoid roots, the following characteristic equation may be constructed,

$$s^4 + 6.4362s^3 + 16.2463s^2 + 0.6728s + 0.2341 \tag{5.4.8}$$

In full-state feedback design, the closed loop poles are assigned to the desired poles. The system, given in the state space form,

$$\dot{x} = Ax + Bu, \qquad x \in R^k \quad , \quad u \in R^n \tag{5.4.9}$$
$$y = Cx, \qquad y \in R^m$$

where $x = \begin{bmatrix} V & \alpha & q & \theta \end{bmatrix}$ and $u = \begin{bmatrix} \delta_e & \delta_T^a \end{bmatrix}$. In the velocity interval of 0.1 m/s to 15 m/s, the most effective input is aft throttle setting. Over this velocity, elevator input shall be preferred. For each discrete velocity, A and B matrices are obtained. For example, the following A and B matrices are written for V = 0.1 m/s,

$$A=\begin{bmatrix} -0.0006 & 0.0044 & 0 & -9.81 \\ -0.409 & -0.0022 & 0.9919 & 0 \\ -0.0004 & -0.0000385 & -0.00472 & 0 \\ 0 & 0 & 1 & 0 \end{bmatrix} \tag{5.4.10}$$

$$B=\begin{bmatrix} 0 & -0.0484 \\ 0 & -15.44 \\ -0.0001 & -1.2973 \\ 0 & 0 \end{bmatrix} \tag{5.4.11}$$

For the purposes of the eigenvalue assignment, we will assume that there is only one controller, i.e. $u=\left[\delta_T^a\right]$ and express the given plant in the phase variable (controllable canonical) form by taking only the second column of B matrix given in Eqn. (5.4.11). The advantage of this transformation is that the elements of the last row of a matrix in phase-variable form are the coefficients of the characteristic equation. Then, the full-state feedback design is done in the transformed space, and finally, an inverse transformation is made to obtain the state feedback law in the original state space [21].

The given plant is expressed in the phase variable form as follows [21],

$$\dot{z}=A_pZ+B_pu \tag{5.4.12}$$

where z is a new state vector and matrices A_p and B_p are in the phase-variable form and are defined as,

$$\begin{aligned} z &= Px \\ A_p &= PAP^{-1} \\ B_p &= PB \end{aligned} \tag{5.4.13}$$

The transformation matrix, P is constructed as follows,

i) Obtain the state-controllability matrix, Q_c given by,

$$Q_c=\begin{bmatrix} B & AB & A^2B & A^3B \end{bmatrix} \tag{5.4.14}$$

ii) Form the matrices, P_1, P_2, P_3 and P_4 as follows,

$$P_1=\begin{bmatrix} 0 & 0 & 0 & 1 \end{bmatrix}Q_c^{-1}$$

$$P_2 = P_1 A,\ P_3 = P_1 A^2,\ P_4 = P_1 A^3 \tag{5.4.15}$$

$$P = \begin{bmatrix} P_1 & P_2 & P_3 & P_4 \end{bmatrix}'$$

Then, the matrices A_p and B_p are found by substituting (5.4.14) and (5.4.15) into (5.4.13).

$$A_p = \begin{bmatrix} 0 & 1 & 0 & 0 \\ 0 & 0 & 1 & 0 \\ 0 & 0 & 0 & 1 \\ -0.000146 & 0.00379 & -0.00187 & -0.0075 \end{bmatrix} \tag{5.4.16}$$

$$B_p = \begin{bmatrix} 0 \\ 0 \\ 0 \\ 1 \end{bmatrix} \tag{5.4.17}$$

The input with full-state feedback in the transformed system is,

$$u = -Kz \tag{5.4.18}$$

where K is given by,

$$K = \begin{bmatrix} k_1 & k_2 & k_3 & k_4 \end{bmatrix} \tag{5.4.19}$$

Then,

$$\dot{z} = \left(A_p - B_p K\right) z \tag{5.4.20}$$

and,

$$\begin{bmatrix} \dot{z}_1 \\ \dot{z}_2 \\ \dot{z}_3 \\ \dot{z}_4 \end{bmatrix} = \begin{bmatrix} 0 & 1 & 0 & 0 \\ 0 & 0 & 1 & 0 \\ 0 & 0 & 0 & 1 \\ -(0.000146+k_1) & -(-0.00379+k_2) & -(0.00187+k_3) & -(0.0075+k_4) \end{bmatrix} \times \begin{bmatrix} z_1 \\ z_2 \\ z_3 \\ z_4 \end{bmatrix} \tag{5.4.21}$$

The characteristic equation of this transformed phase-variable form is,

$$s^4 + (0.0075 + k_4)s^3 + (0.00187 + k_3)s^2 + (-0.00379 + k_2)s + (0.000146 + k_1) = 0 \tag{5.4.22}$$

After equating the coefficients of Eqn. (5.4.8) and Eqn. (5.4.22), the following gains are obtained,

$k1 = 0.23395$ $k2 = 0.6766$ $k3 = 16.2444$ $k4 = 6.4287$

Then, the desired full-state feedback control law is,

$$u = -KPx \tag{5.4.23}$$

This procedure can be repeated for other velocities and necessary feedback gains may be calculated. Then, using the forward velocity as a parameter, the gains required for the flight condition may be interpolated.

The following graphics are obtained for k_1, k_2, k_3, and k_4.

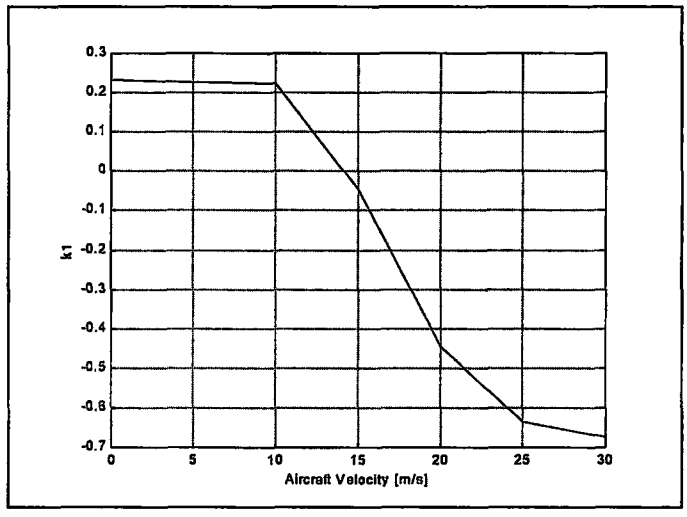

Figure 5.16 k_1 vs. Aircraft Velocity

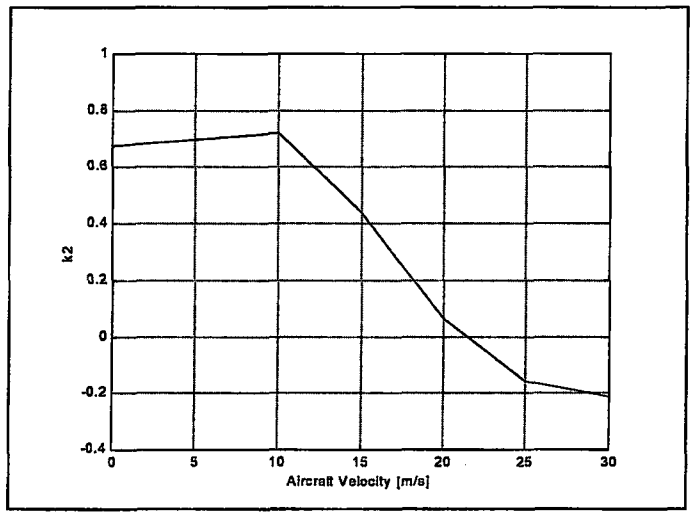

Figure 5.17 k_2 vs. Aircraft Velocity

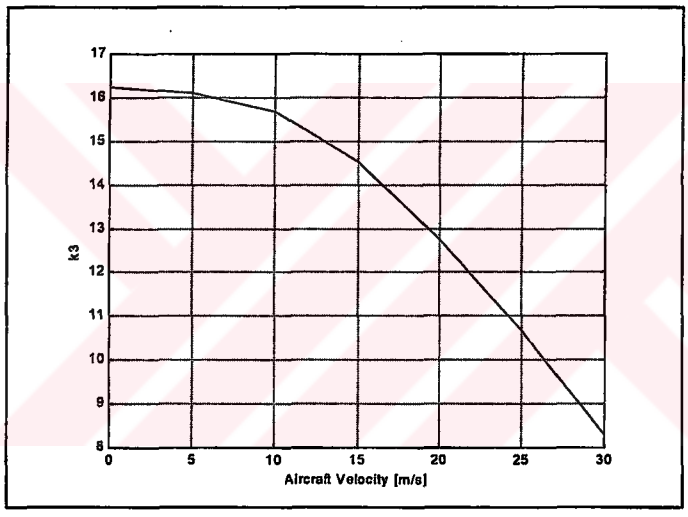

Figure 5.18 k_3 vs. Aircraft Velocity

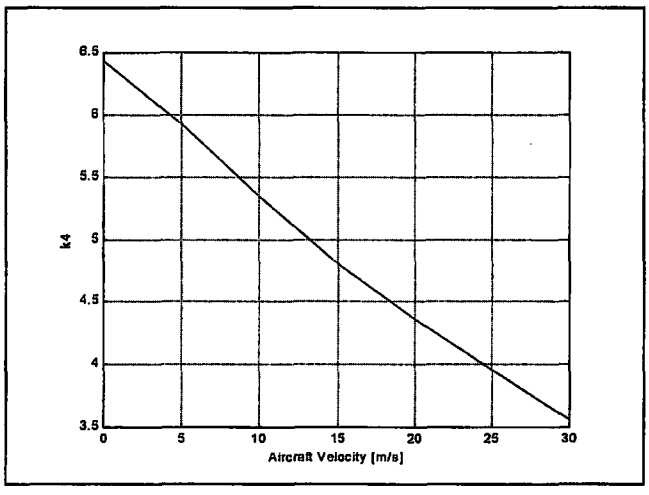

Figure 5.19 k_4 vs. Aircraft Velocity

Note that the transformation matrix depends on the input matrix B, which is different whether elevator or aft engine is used. Furthermore, since the control cannot be switched from aft throttle setting to elevator instantaneously, a blending between these two inputs is necessary especially in the neighbourhood of forward velocity of 15 m/s. In this application, the blending technique is proposed throughout the transition flight regime.

- Blending of Controls

For this purpose, a new input, which is the linear combination of elevator deflection $\tilde{\delta}_e$ and aft throttle setting, $\tilde{\delta}_T^a$. Then,

$$\tilde{\delta}_e = \nabla_1 u_1 \tag{5.4.24}$$

$$\tilde{\delta}_T^a = (1-\nabla_1) u_1 \tag{5.4.25}$$

where, ∇_1 is a blending coefficient defined as follows.

$$\nabla_1 \equiv \begin{cases} \nabla_1 = 0 & 0.1 \le V \le 5 \\ \nabla_1 = -0.003333V^2 + 0.15V - 0.66667 & 6 \le V \le 19 \\ \nabla_1 = 1 & 20 \le V \le 32 \end{cases} \tag{5.4.26}$$

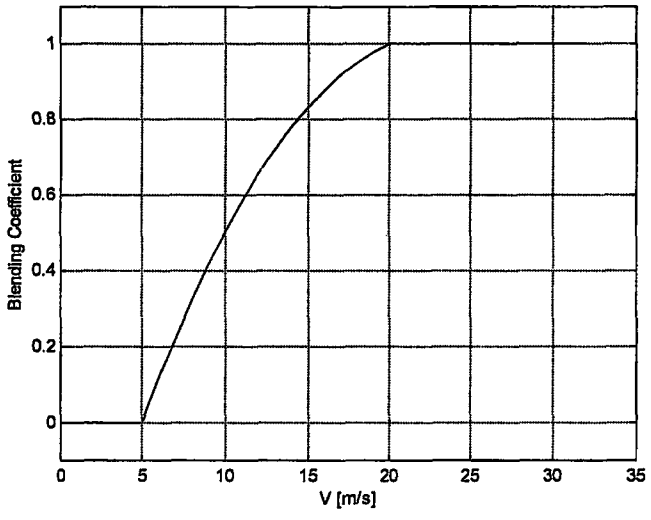

Figure 5.20 Changing of the blending coefficient with aircraft forward velocity

Then, by using Eqn. (5.4.24) and Eqn. (5.4.25), the input matrix becomes,

$$\ldots\ldots+\begin{bmatrix} x_1 & y_1 \\ x_2 & y_2 \\ x_3 & y_3 \\ x_4 & y_4 \end{bmatrix}\begin{bmatrix} \widetilde{\delta}_e \\ \widetilde{\delta}_T^a \end{bmatrix} \tag{5.4.27}$$

$$\ldots\ldots+\begin{bmatrix} x_1 & y_1 \\ x_2 & y_2 \\ x_3 & y_3 \\ x_4 & y_4 \end{bmatrix}\begin{bmatrix} \nabla_1 \\ 1-\nabla_1 \end{bmatrix}[u_1] \tag{5.4.28}$$

For each forward velocity not only column x and y in the above matrix change, but blending coefficient, ∇_1 changes as well. The new input matrix, B is different. But, feedback gains in the transformed domain remain the same (Fig. 5.16-Fig. 5.19). However, the transformation matrix, P depends on the input matrix and is different for each forward velocity.

In order to verify the control system designed by using eigenvalue assignment and blending technique described above, linear simulations are performed. The linear simulation model and general information on used and selected simulation parameters are presented in Appendix B.

The results obtained for $V=5\ m/s$, $V=10\ m/s$, $V=15\ m/s$ and $V=20\ m/s$ are presented in Appendix C. These results indicate that the system responds satisfactorily. The values, which the states attain, are reasonable and no saturation occurs with the actuators. In each case, the saturation limits for aft engine and elevator are taken to be ± 0.1. This corresponds to $\pm\%10$ authority in the aft throttle and $\pm 5.73^0$ authority in the elevator.

Note that, the sluggish aft throttle engine dynamics is not included in these design calculations, although aft throttle is effective for forward velocity interval of $0.1\ m/s \le V \le 19\ m/s$ in proposed blending technique.

When the sluggish aft throttle engine effect is added into the simulation directly, the system did not perform well. Excessive saturation occurred in the actuators. Thus, the design must be modified to take this effect into account. Since the elevator dynamics is quite fast, the blending technique may become unreasonably complicated. Thus, a linear quadratic regulator (LQR) design technique becomes more appropriate.

- Linear Quadratic Regulator (LQR) Design

Linear quadratic regulator (LQR) controller with full-state feedback will be examined. Given a system,

$$\dot{x} = Ax + Bu, \qquad x \in R^k \quad , \quad u \in R^n$$

$$y = Cx, \qquad y \in R^m \tag{5.4.29}$$

The goal of the LQR is to find a controller that minimizes a quadratic performance index,

$$J = \frac{1}{2}\int_0^\infty \left(x^T Q x + u^T R u\right) dt \tag{5.4.30}$$

This gives a state variable feedback controller,

$$u = -Kx \tag{5.4.31}$$

and the optimal feedback gain matrix may be found by solving the algebraic Riccati equation and Kalman gain, [23]

Algebraic Riccati Equation (ARE): $A^T P + PA + Q - PBR^{-1}B^T P = 0$ (5.4.32)

Kalman Gain: $K = R^{-1}B^T P$ (5.4.33)

Then, the optimal cost is given by,

$$J = \frac{1}{2} x^T(0) P x(0) \tag{5.4.34}$$

First, let's define our state and input variables.

$$x = \begin{bmatrix} V & \alpha & q & \theta & \delta_{Tr}^a \end{bmatrix}^T \tag{5.4.35}$$
$$u = \begin{bmatrix} \delta_e & \delta_{Tc}^a \end{bmatrix}^T$$

where δ_{Tr}^a and δ_{Tc}^a denote realized and commanded aft throttle settings, respectively. The dynamics of the aft engine is modelled as a first order system,

$$\dot{\delta}_{Tr}^a = -0.14\delta_{Tr}^a + 0.14\delta_{Tc}^a \tag{5.4.36}$$

Then, A and B matrices are constructed for each forward velocity. The most important aspect of LQR design is the selection of the performance index weighting matrices, Q and R. Here, they are selected as follows,

$$Q = \begin{bmatrix} 1/V^2_{\max} & 0 & 0 & 0 & 0 \\ 0 & 1/\alpha^2_{\max} & 0 & 0 & 0 \\ 0 & 0 & 1/q^2_{\max} & 0 & 0 \\ 0 & 0 & 0 & 1/\theta^2_{\max} & 0 \\ 0 & 0 & 0 & 0 & 1/\delta^2_{Tr\max} \end{bmatrix} \tag{5.4.37}$$

where

$$V_{\max} = 6\,m/s\,,\ \alpha_{\max} = 0.3\,rad\,,\ q_{\max} = 0.3\,rad/s\,,$$
$$\theta_{\max} = 0.3\ rad\,,\ \delta^a_{Tr\max} = 0.1$$

and

$$R = \begin{bmatrix} 1/(\delta_{e\max}\nabla_1)^2 & 0 \\ 0 & 1/(\delta^a_{Tc\max}(1-\nabla_1))^2 \end{bmatrix} \qquad (5.4.38)$$

where

$$\delta_{e\max} = 0.1 rad, \qquad \delta^a_{Tc\max} = 0.1$$

and ∇_1 is the blending coefficient, given in Eqn. (5.4.26).

The design equations, given in Eqn. (5.4.32) and Eqn. (5.4.33) are solved in Matlab environment [24], using Matlab function "lqr". The inputs to the function are A, B, Q and R matrices and the outputs are the optimal gain matrix, K, the solution of the algebraic Riccati equation, P, and the eigenvalues of the matrix [A-BK], corresponding to new system matrix, which is obtained after applying the feedback control law given in Eqn. (5.4.31). The matrices at various flight conditions and corresponding feedback gains are given in Appendix D.

The performance of the design is checked by using a linear simulation model given in Appendix E. Also, the general information on the simulation model is presented in the same appendix. The simulation results obtained for $V = 5\ m/s$, $V = 10\ m/s$, $V = 15\ m/s$ and $V = 20\ m/s$ are presented in Appendix F.

It can be observed from the figures given in Appendix F that at low speeds the aft throttle setting is effective input to the system. As the aircraft gains speed, the elevator becomes more dominant. When the forward velocity reaches the value of $V = 20\ m/s$, it becomes the only input to the system. All of the state variables converge to their trim value without showing any excessive values. The closed loop system designed by linear quadratic regulator (LQR) is highly damped as expected. However, no saturation in the final control elements is encountered. Thus, the designs are acceptable.

To check the gain scheduling, two different forward velocity values are chosen. These velocities are $V = 7 m/s$ and $V = 23 m/s$. The gains for these

forward velocities are obtained by interpolating the necessary gains from the gains at neighbouring forward velocities. It is observed that, the system works properly again. These results are also presented in Appendix D and Appendix F.

During transition flight the most probable mode shall be velocity acquire mode. For this purpose an outer guidance loop shall be constructed around the autopilot to generate necessary commands continuously. The autopilot gains (i.e. the gains of the linear quadratic regulator) shall be continuously updated with forward flight velocities attained. The proposed flight director algortihms shall be designed and verified using nonlinear simulation in the future.

5.4.3 Autopilots Designed for the Cruise Flight Mode

5.4.3.1 Pitch Attitude Autopilot

The simplest form of autopilot, which is the type that first appeared in aircraft and is still being used in some of the older transport aircraft, is the pitch attitude type autopilot. This autopilot is designed to hold the aircraft in straight and level flight with little or no maneuvering capability. A block diagram for such an autopilot is shown in Figure 5.21.

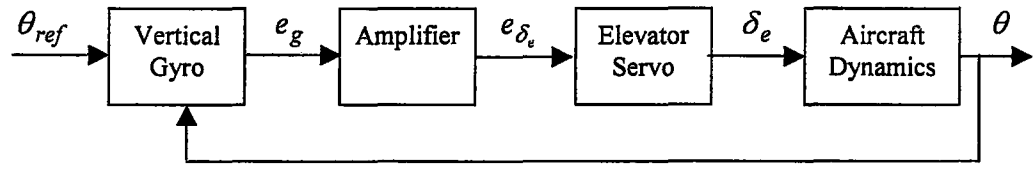

Figure 5.21 Pitch attitude autopilot

For this type of autopilot the aircraft is initially trimmed to straight and level flight, the reference aligned, and then the autopilot engaged. If the pitch attitude varies from the reference, a voltage, e_g is produced by the signal generator on the vertical gyro. This voltage is amplified and fed to the elevator servo. Then,

the servo positions the elevator, causing the aircraft to pitch about y axis and so returning it to the desired pitch attitude. In general, the elevator servo is at least a second order system; but if properly designed, its natural frequency is higher than that of aircraft. If the damping ratio is high enough, the elevator servo can be represented by a sensitivity (gain) multiplied by a first-order to time lag. Representative characteristic times vary from 0.1 to 0.03 s.

There is one disadvantage of this system, from a servo point of view; it is a Type 0 system; i.e., there are no integrations in the forward loop. Thus, if some fixed external moments were applied, resulting from a change in trim, there would have to be an error in θ to generate a voltage to drive the elevator servo. Thus, it produces an elevator deflection to balance the interfering moment. Then, this would require the pilot to make occasional adjustments of the reference to maintain the desired flight path.

As given in Section 4.5.2, cruise flight mode trimmed flight conditions are found for steady state straight, wings level flight. The following state space representation is obtained for the cruise velocity of V_0 = 45 m/s and flight altitude, h_0 = 2000 m.

$$\begin{bmatrix} \dot{\tilde{V}} \\ \dot{\tilde{\alpha}} \\ \dot{\tilde{q}} \\ \dot{\tilde{\theta}} \end{bmatrix} = \begin{bmatrix} -0.1011 & 3.8038 & 0 & -9.81 \\ -0.0095 & -1.7936 & 0.992 & 0 \\ 0.0249 & -5.4654 & -1.9242 & 0 \\ 0 & 0 & 1 & 0 \end{bmatrix} \begin{bmatrix} \tilde{V} \\ \tilde{\alpha} \\ \tilde{q} \\ \tilde{\theta} \end{bmatrix} + \begin{bmatrix} 0 & 5.3008 \\ 0 & -0.062 \\ -24.764 & -2.4985 \\ 0 & 0 \end{bmatrix} \begin{bmatrix} \tilde{\delta}_e \\ \tilde{\delta}_T \end{bmatrix} \tag{5.4.39}$$

Using above state space representation, the following transfer function is calculated.

$$\frac{\tilde{\theta}(s)}{\tilde{\delta}_e(s)} = \frac{-24.764s^2 - 46.291s - 5.386}{s^4 + 3.819s^3 + 9.289s^2 + 1.117s + 0.947} \tag{5.4.40}$$

The amplifier and elevator servo blocks are combined into one block, and the vertical gyro replaced by a sum sign. As the aircraft transfer function is

negative, the sign of the elevator servo transfer function is made negative in order to obtain positive forward transfer function. Block diagram for the VTOL UAV in cruise flight mode is shown in Figure 5.22.

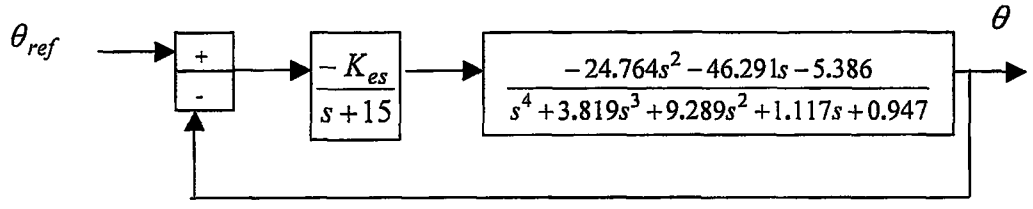

Figure 5.22 Block diagram for the VTOL UAV in cruise flight mode and autopilot

The root locus diagram is given in Figure 5.23. From this figure, it can be seen that if K_{es} is equal to or larger than 23, two loci pass to the instability region. In other words, the stability condition on K_{es} is given as follows,

$$0 \prec K_{es} \prec 23$$

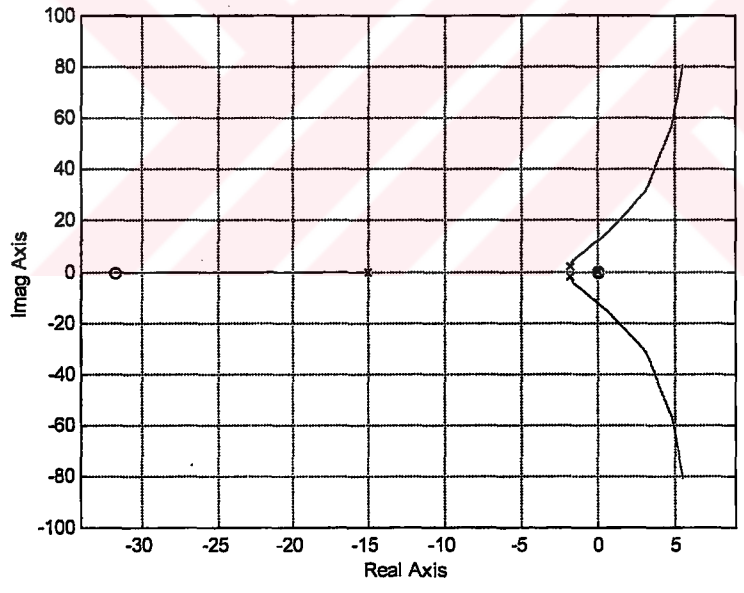

Figure 5.23 Root locus for the VTOL UAV in cruise flight mode and autopilot

To increase the damping ratio of the short period mode an inner feedback loop for pitch rate may be added. The pitch rate is measured by a rate gyro.

5.4.3.2 Altitude-hold autopilot

Altitude-hold autopilots are generally used by commercial airplanes during the cruise flight when the airplane is in the cruise mode. It allows the aircraft to be held at a fixed altitude. The sensed altitude is normally the pressure altitude, that is, altitude computed in the air-data computer from external pressure measurements. Usually, with such a system, the airplane is manually operated during the climb and descent portions of the flight. Once the aircraft has reached the desired cruise altitude, the altitude-hold autopilot is engaged. The autopilot will then maintain that altitude, making whatever corrections necessary when updrafts or downdrafts tend to cause the aircraft to gain or lose altitude [21, 27]. The schematic diagram for the altitude hold autopilot is given in Figure 5.24.

Some autopilots have the feature that enables the pilot to enter a given flight altitude in advance. In this case, the autopilot flies the aircraft, making it climb or descend to attain the desired altitude. On reaching that altitude, the autopilot automatically levels the aircraft and, afterwards, it will maintain that altitude until told to do otherwise.

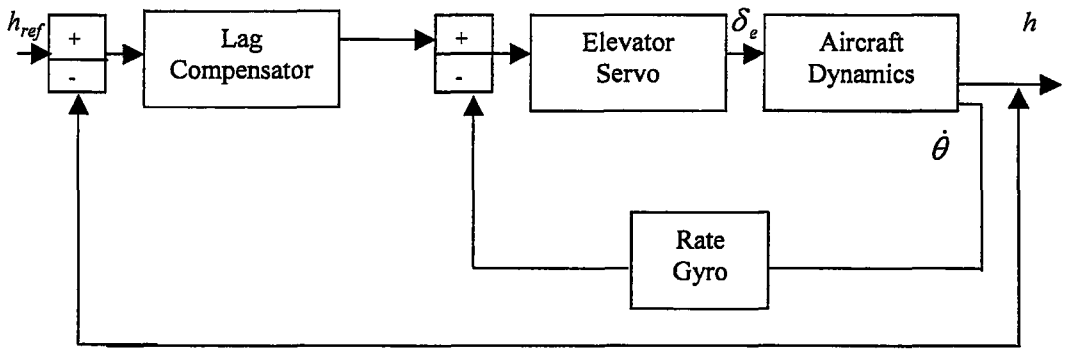

Figure 5.24 Schematic diagram of altitude-hold autopilot

The corresponding block diagram is shown in Figure 5.25. This aircraft dynamics belongs to the steady state, wings level straight flight condition of V_0 = 38 m/s and $h_0 = 1500$ m.

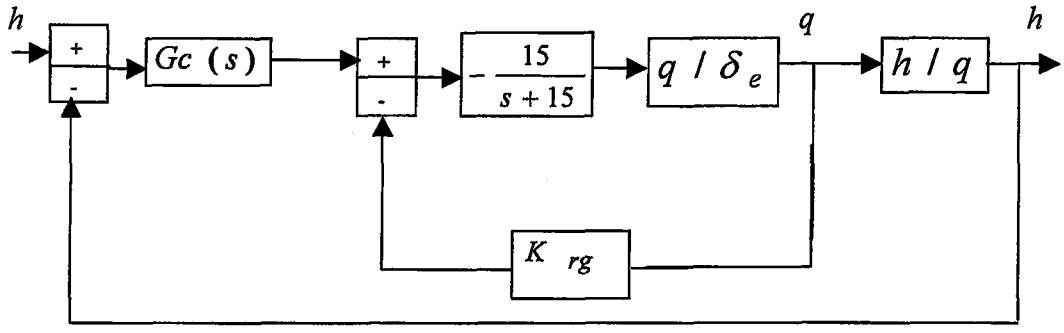

Figure 5.25 Block diagram of altitude-hold autopilot

There is a lag compensator in the forward path, which is required to retain stability on closing the outer loop. The transfer function of the lag compensator is assumed as,

$$G_c(s) = K_{lc}\frac{s+0.8}{s+8} \tag{5.4.41}$$

The transfer function for the altitude-to-elevator input can be obtained as follows,

$$\dot{h} = V_0 \sin(\gamma) \tag{5.4.42}$$

$$\gamma = \theta - \alpha \tag{5.4.43}$$

where V_0 is the flight velocity and γ is the flight path angle. Then, taking Laplace transform yields,

$$\frac{h(s)}{\tilde{\delta}_e(s)} = \frac{V_0}{s}\frac{\left(\tilde{\theta}(s) - \tilde{\alpha}(s)\right)}{\tilde{\delta}_e(s)} \tag{5.4.44}$$

The necessary transfer functions for this flight condition are obtained and given as follows,

$$\frac{\tilde{\theta}(s)}{\tilde{\delta}_e(s)} = \frac{-18.5637s^2 - 31.397s - 3.7324}{s^4 + 3.399s^3 + 7.12s^2 + 0.87312s + 0.9136} \tag{5.4.45}$$

$$\frac{\tilde{\alpha}(s)}{\tilde{\delta}_e(s)} = \frac{-18.421s^2 - 1.74s - 2.4133}{s^4 + 3.399s^3 + 7.12s^2 + 0.87312s + 0.9136} \tag{5.4.46}$$

$$\frac{\tilde{q}(s)}{\tilde{\delta}_e(s)} = \frac{-18.5637s^3 - 31.397s^2 - 3.7324s}{s^4 + 3.399s^3 + 7.12s^2 + 0.87312s + 0.9136} \tag{5.4.47}$$

Then, substituting (5.4.45), (5.4.46) and $V_0 = 38$ m/s into (5.4.44) gives,

$$\frac{h(s)}{\tilde{\delta}_e(s)} = \frac{-5.4226s^2 - 1126.967s - 50.125}{s^5 + 3.399s^4 + 7.12s^3 + 0.87312s^2 + 0.9136s} \tag{5.4.48}$$

The root-locus plot of the inner loop as shown in Figure 5.26 is obtained, and a point on the root-locus corresponding to $\zeta = 0.86$, which gives the gain of rate gyro, K_{rg}=0.1057. This means approximately, %34 improvement in the damping ratio compared to the basic system (open loop) damping of 0.64. This gives good short period flying qualities given in Section 5.3.

The next step is to design the outer loop. First, the closed loop transfer function of the inner loop is obtained for the selected rate gyro gain as above.

$$G(s) = \frac{278.455s^3 + 470.955s^2 + 55.986s}{s^5 + 18.399s^4 + 87.537s^3 + 157.4531s^2 + 19.9281s + 13.704} \tag{5.4.49}$$

The transfer function, $h(s)/\tilde{q}(s)$ is calculated as following,

$$\frac{h(s)}{\tilde{q}(s)} = \frac{h(s)}{\delta_e(s)} \frac{\delta_e(s)}{\tilde{q}(s)} \tag{5.4.50}$$

Then,

$$\frac{h(s)}{\tilde{q}(s)} = \frac{5.4222s^2 + 1126.967s + 50.125}{18.5637s^4 + 31.397s^3 + 3.7324s^2} \tag{5.4.51}$$

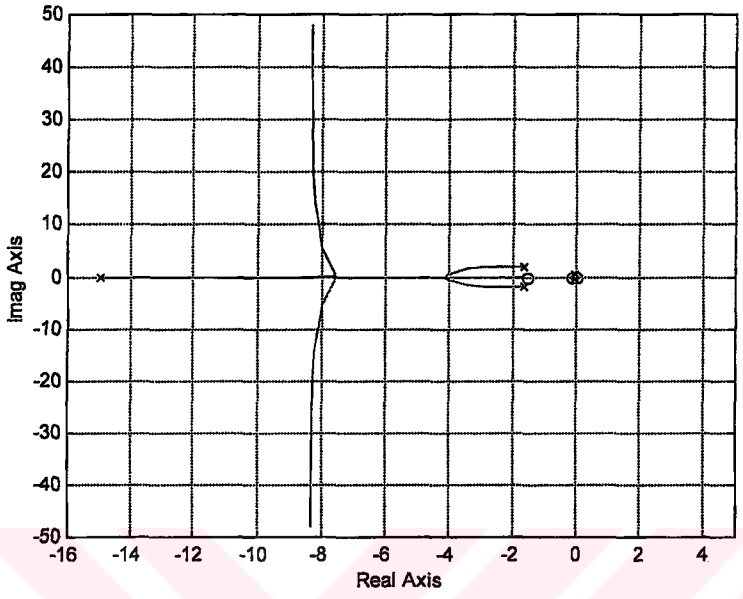

Figure 5.26 The root locus diagram of the inner loop

The lag compensator pole ($s = -8$) is sufficiently away from the origin so that it has very little effect on the short period dynamics. The root-locus diagram of the outer loop is drawn and it is observed that almost low values of the compensator gain, K_{lc} will make the system stable. A higher value of this gain will make the system unstable. The value of $K_{lc} = 0.078$ is selected.

Then, the overall closed loop transfer function is obtained,

$$\frac{h(s)}{h_{ref}(s)} = \frac{118s^5 + 24771s^4 + 62252s^3 + 40771s^2 + 5629s + 175}{19s^9 + 521s^8 + 5190s^7 + 23391s^6 + 51678s^5 + 71360s^4 + 74499s^3 + 44860s^2 + 6038s + 175} \tag{5.4.52}$$

To verify the design, simulation of the response of the system to unit-step input is achieved using Eqn. (5.4.52), as shown in Figure 5.27. The large overshoot is due to the low value of the damping ratio. Except for this, the system performance is satisfactory.

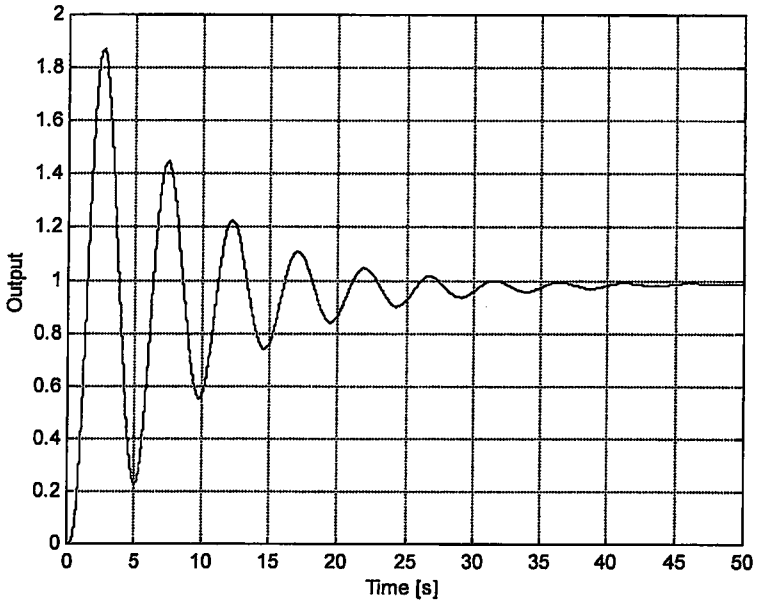

Figure 5.27 Unit-step response of the designed altitude-hold autopilot

In the literature, it is observed that it is impossible to control the flight path angle (γ) without simultaneous control of the velocity. Therefore, the automatic velocity control system concept, shown in Figure 5.28 may be used as following,

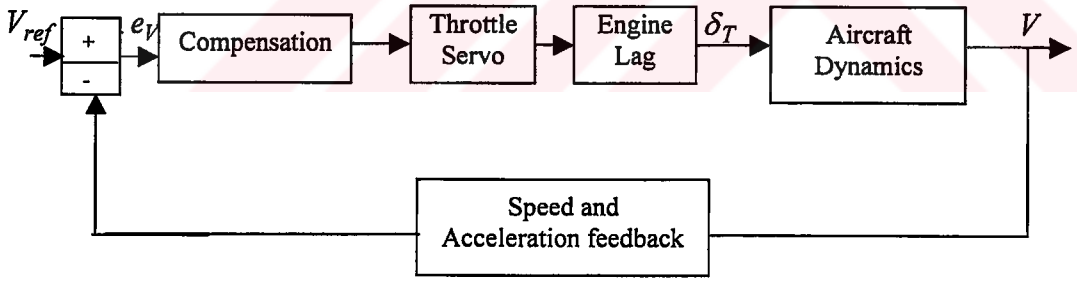

Figure 5.28 Conceptual design for automatic velocity control system

Automatic velocity control system is sometimes called as phugoid damping. The time constant for the main engine used in the tilt-duct VTOL UAV may be taken as 7 s and it is satisfactory. This time lag represents the time required for the thrust the engine to build up after a movement of the throttle. Since V is the change in the air speed, the input to the aircraft dynamics block is the change in the throttle setting value from that required for straight and level, unaccelerated flight.

The first block in the forward loop is a proportional plus integral controller, which makes the system Type 1 and also provides compensation by adding a zero at $s = 0.15$. Velocity and the acceleration are used in the feedback path. Both the velocity error and the acceleration can be supplied by a single instrument. The block diagram, used in this application is shown in Figure 5.29.

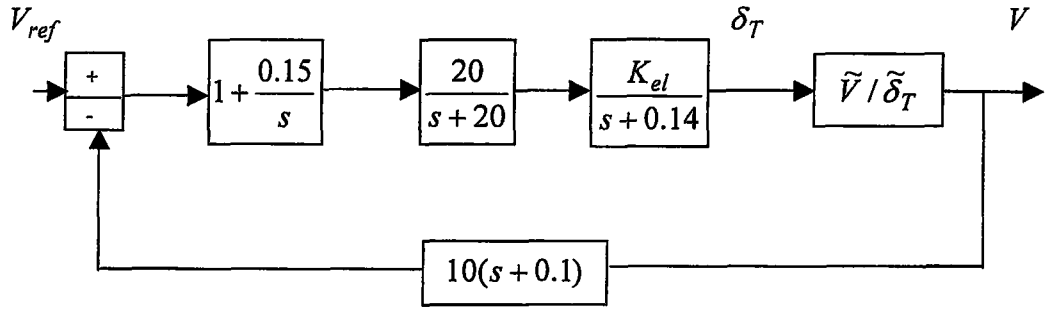

Figure 5.29 Block diagram of the automatic velocity control system

The flight condition is still steady state, wings level straight flight of $V_0 =$ 38 m/s and $h_0 = 1500$ m. Then,

$$\frac{\tilde{V}(s)}{\tilde{\delta}_T(s)} = \frac{6.3928s^3 + 21.0682s^2 + 58.198s + 38.4612}{s^4 + 3.3993s^3 + 7.12^2 + 0.8731s + 0.9136} \qquad (5.4.53)$$

After obtaining the necessary transfer function, root locus diagram will be drawn by using open loop transfer function to select K_{el} value. Then, closed loop transfer function may be calculated.

5.4.3.3 Mach-hold Autopilot

In the Mach-hold autopilot mode, the aircraft is made to fly at a constant Mach number by automatically controlling the flight path angle through the elevators. For this mode of operation the aircraft is first trimmed to fly straight and level and the power adjusted to yield the desired Mach number. The Mach-hold mode of the flight control system is then engaged. Usually, as the aircraft cruises the fuel is used and the total weight of the aircraft decreases. Then, the velocity of

the aircraft tends to increase. The increase in the velocity is sensed by sensors and corrected for by an up-elevator signal coming from the controller, which cause the aircraft to climb. The net result of the operation in Mach-hold mode is that the aircraft is made to climb slowly as fuel is consumed in order to maintain a constant Mach number.

A Mach-hold system could be designed in a very similar to the previous altitude-hold autopilot design example. For the analysis of the Mach hold mode, it is assumed that the altitude variations are small enough to represent the variations in Mach number by the variations in the velocity. Figure 5.30 is a block diagram of the Mach-hold mode of the flight control system.

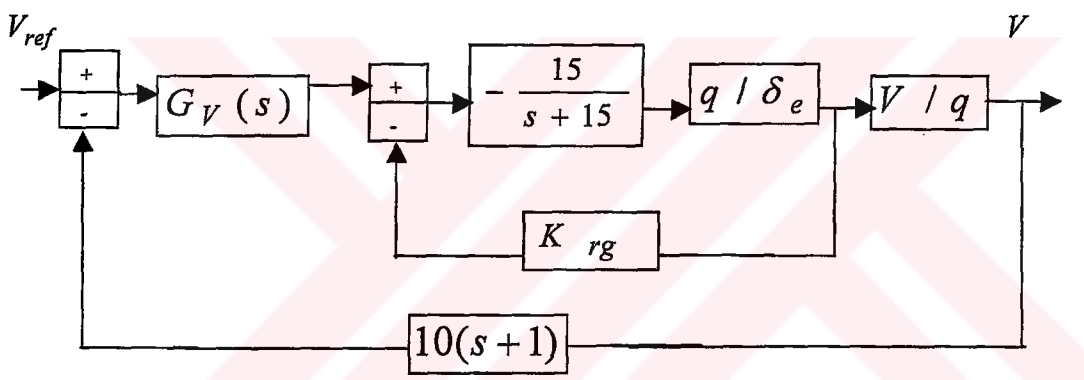

Figure 5.30 Block diagram of Mach-hold Autopilot

where ,

$$G_V(s) = \frac{-K_V(s+0.4)}{s+4} \tag{5.4.54}$$

Flight condition is still same. For the inner loop, the analysis is done in the previous section and the closed loop transfer function of the inner loop is given in Eqn. (5.4.49). As a next step, outer loop analysis is done. First, the following transfer function is obtained.

$$\frac{\tilde{V}(s)}{\tilde{\delta}_e(s)} = \frac{112.3354s + 290.8070}{s^4 + 3.3993s^3 + 7.12s^2 + 0.8731s + 0.9136} \tag{5.4.55}$$

Then,

$$\frac{\tilde{V}(s)}{\tilde{q}(s)} = \frac{\tilde{V}(s)}{\tilde{\delta}_e(s)} \frac{\tilde{\delta}_e(s)}{\tilde{q}(s)} \tag{5.4.56}$$

Substituting (5.4.47) and (5.4.55) into (5.4.56) gives,

$$\frac{\tilde{V}(s)}{\tilde{q}(s)} = \frac{-(112.3354s + 290.8070)}{18.5637s^3 - 31.397s^2 - 3.7324s} \tag{5.4.47}$$

Finally, root locus diagram is drawn for the outer loop to select the gain, K_V as shown in Figure 5.31.

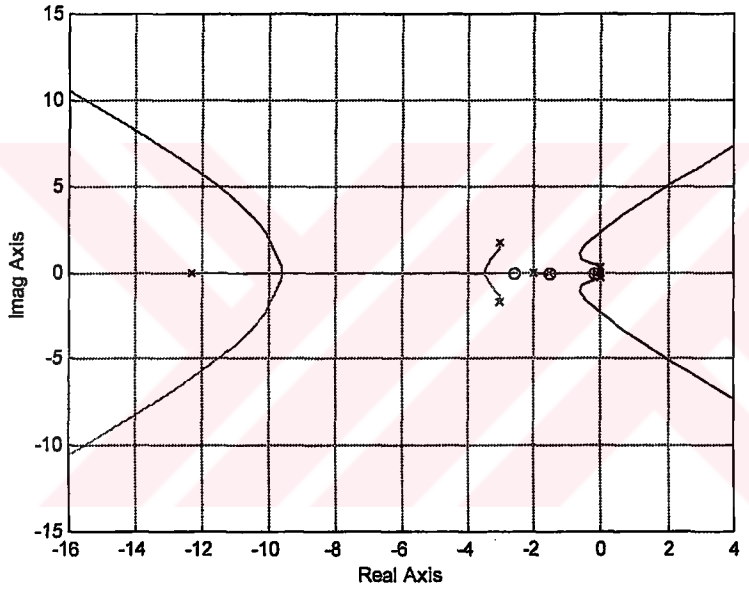

Figure 5.31 Root locus diagram of the outer loop of the Mach-hold autopilot

From Figure 5.31, it is observed that there is a very limited margin for the gain to make the closed loop system stable. By using root-locus diagram and trail and error method in unit-step response of the system, $K_V = 0.0225$ value is selected. The unit-step response of the system is given in Figure 5.32.

5.5 Summary

In this chapter, the automatic control system designed for hover, transition and cruise flight modes is presented. The tilt-duct VTOL UAV proposed is inherently unstable especially in hover and transition flight modes. Consequently, it requires a full authority automatic flight control system. The pitch stability

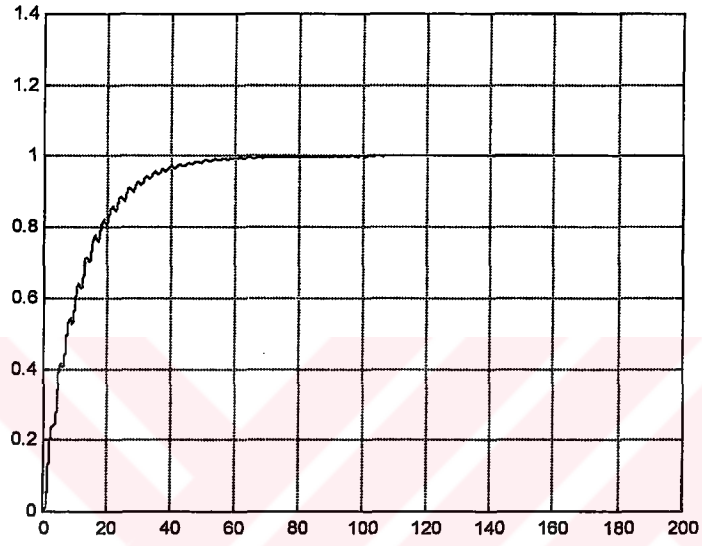

Figure 5.32 The unit-step response of the Mach-hold autopilot

augmentation systems designed for hover and the transition mode are given. Some examples of automatic flight control systems, which may be used in the cruise flight mode are designed and presented.

To verify the pitch stability augmentation systems designed for hover and transition flight modes, linear simulation models are built. The results are satisfactory. These models do not include flight path (guidance) loop.

CHAPTER 6

CONCLUSIONS

This study is a part of the research activity to develop an autonomously controlled tilt-duct VTOL UAV at the Middle East Technical University (METU). The project had started in 1998. The group is decided to work on UAVs due to the challenging issues and considerable interest on UAVs in Turkey and around the world. Thus, it is decided to undertake the development of a tilt-duct VTOL UAV, with autonomous flight capability for civilian uses such as aerial surveillance, reconnaissance, agricultural activities, traffic monitoring, air pollution control, meteorological data collection, early forest fire detection, pipeline survey, and etc.

The detailed summary of the conceptual design study of the proposed til-duct VTOL UAV is presented under related topics, such as airfoil and geometry selection, initial sizing, propulsion and fuel system integration, control policy and etc. The obtained geometric and performance characteristics are given in the relevant tables. Three view drawings in hover and cruise flight modes are presented. The stability derivatives are obtained by using Advanced Airplane Analysis (AAA) software. The methods used in this software are almost valid for conventional type of aircraft. In the transition mode, detailed wind tunnel tests are needed to calculate aerodynamic forces and moments. In order to model the drag force, component build-up and interpolation technique is proposed in this study.

For this aircraft, nonlinear equations of motion are developed for hover, cruise and transition flight modes. Then, trimmed flight problem is addressed and the numerical solution technique is proposed. Various trimmed flight conditions at hover, transition and cruise flight modes are obtained, using the trim program developed. These nonlinear longitudinal equations are linearized at these trim conditions and the longitudinal stability analysis for the tilt-duct VTOL UAV is carried out based on these linearized equations.

In the cruise flight mode, obtained eigenvalues showed that, the linearized equations are stable, and the tilt-duct VTOL UAV behaves in a classical manner with easily observable short period and phugoid modes. In hover mode, however, there is a follower force problem, the system is unstable, and stability augmentation is needed. The stability augmentation system designed is presented. The transition phase of the flight also needs a stability augmentation system. The stability augmentation system with gain scheduling is designed that covers the full transition flight mode. The blending technique between elevator setting and aft throttle setting is proposed. The linear quadratic regulator design is found to be most suitable for this kind of design.

As a future work, more detailed lateral-directional analysis shall be carried out and the autopilot design shall be checked against nonlinear simulations.

REFERENCES

[1] The information, given on the main web page and related links given on this page, about UAVs. The following web page is published by Air Force Flight Test Center (AFFTC), Edwards Air Force Base of USA. (http://afftc.edwards.af.mil:80/articles98/docs_html/splash/may98/cover/UAVmain.htm)

[2] D. P. Schrage, "Introduction to Vertical and Short Takeoff and Landing Aircraft", Georgia Institute of Technology, Unpublished Notes.

[3] E. Seckel, "Stability and Control of Airplanes and Helicopters", Academic Press, 1964.

[4] B. W. McCormick, "Aerodynamics, Aeronautics, and Flight Mechanics", Second Edition, John Wiley & Sons, Inc., 1995.

[5] E. B. Carlson, "Optimal Tiltrotor Aircraft Operations During Power Failure", Ph.D. Thesis, University of Minnesota, 1999.

[6] R. Decuypere, "Uninhabited Aerial Vehicles: From Science Fiction to Reality", Proceedings of the 2nd Ankara International Aerospace Conference, pp. 29-39, 1998.

[7] Ü. Kaynak, " Turkish Unmanned Air Vehicle Developments", NATO AGARD Conference Proccedings-591; Subsystem Integration for Tactical Missiles (SITM) and Design and Operation of Unmanned Air Vehicles (DOUAV), 1995.

[8] E. Torun, "UAV Requirements and Design Considerations", NATO-RTO Meeting Proceedings-44; Advances in Vehicle Systems Concepts and Integration, pp. B4.1-B4.8, 1999.

[9] D. P. Raymer, "Aircraft Design: A Conceptual Approach", 2nd Edition, AIAA Education Series, 1992.

[10] Ö. Armutcuoglu, M. Ş. Kavsaoğlu, O. Tekinalp, A. Okan, E. Tulunay, "Conceptual Design of a Tilt-Duct VTOL UAV", Proceedings of UAVs-15th Bristol International Conference, pp. 28.1-28.11, 2000.

[11] Shepard's Unmanned Vehicles Handbook, 1998.

[12] R. Eppler, "Airfoil Design and Data", Springer-Verlag, Heidelberg, 1990.

[13] T. S. Şen, N. Telçeker, "Design of Optimum Propellers", Final Project, AE 544 Advanced Airfoil and Propeller Theory, Instructor: M. Ş. Kavsaoğlu, June 1995.

[14] Jane's All The World's Aircraft, 1998.

[15] Limbach Flugmotoren, "Operating Manual L 275E / L 550E", Part No.: 905.275.010.000, Edition: 01.02.1999. & Technical Brochure about L 90 E.

[16] J. Roskam, "Airplane Design", 2nd Printing, Roskam Aviation and Engineering Corp., Parts I-VIII, 1990.

[17] Advanced Airplane Analysis (AAA) Program v. 2.2 User Manual, DAR Corporation, 1999.

[18] A. Okan, O. Tekinalp, M. Ş. Kavsaoğlu, Ö. Armutcuoğlu, E. Tulunay, "Flight Mechanics Analysis of a Tilt-Rotor UAV", Proceedings of the 1999 AIAA Atmospheric Flight Mechanics Conference and Exhibit, AIAA Paper 99-4255, 1999.

[19] D. McLean, "Automatic Flight Control Systems", Prentice Hall, 1990.

[20] R. C. Nelson, "Flight Stability and Automatic Control", McGraw-Hill, 1989.

[21] B. N. Pamadi, "Performance, Stability, Dynamics, and Control of Airplanes", AIAA Education Series, 1998.

[22] B. Etkin, L. D. Reid, "Dynamics of Flight-Stability and Control", Third Edition, John Wiley & Sons, Inc., 1996.

[23] B. L. Stevens, F. L. Lewis, "Aircraft Control and Simulation", John Wiley & Sons, Inc., 1992.

[24] MATLAB, The Language of Technical Computing, Using MATLAB, Version 5, The Mathworks Inc., 1996.

[25] A. Grace, Optimization Toolbox User's Guide, The Mathworks Inc., 1994.

[26] A. Ülkü, "Flight Control Law Design and HIL Simulation of a UAV", NATO-RTO Meeting Proceedings-44; Advances in Vehicle Systems Concepts and Integration, pp. B17.1-B17.6, 1999.

[27] J. H. Blakelock, "Automatic Control of Aircraft and Missiles", Second Edition, John Wiley & Sons, Inc., 1991.

APPENDIX A

STABILITY DERIVATIVES OBTAINED USING ADVANCED AIRPLANE ANALYSIS (AAA) SOFTWARE

The stability derivatives obtained using Advanced Airplane Analysis (AAA) software are listed below. These stability derivatives are used to calculate the aerodynamic forces and moments during cruise and transition flight mode of the tilt-duct VTOL UAV.

$$c_{L_\alpha} = 4.5909 \quad rad^{-1}$$

$$c_{L_{\dot{\alpha}}} = 3.1662 \quad rad^{-1}$$

$$c_{m_\alpha} = -0.8876 \quad rad^{-1}$$

$$c_{m_{\dot{\alpha}}} = -11.2784 \quad rad^{-1}$$

$$c_{m_q} = -33.682 \quad rad^{-1}$$

$$c_{m_{\delta_e}} = -3.4708 \quad rad^{-1}$$

$$c_{L_0} = 0.3164 \qquad c_{D_0} = 0.056 \qquad c_{m_0} = 0.0792$$

APPENDIX B

LINEAR SIMULATION MODEL USED TO VERIFY THE FULL-STATE FEEDBACK CONTROL SYSTEM DESIGN

In this model, system matrix, A and input matrix, B, given in Eqn. (5.4.8) and blending technique presented in Eqn. (5.4.26) are used. The full-state feedback control law, given in Eqn. (5.4.23) is applied. This process is repeated for different forward velocities. The input to the system used in full state variable feedback control system is u_1. Then, this input is separated into two inputs (i.e., aft throttle and elevator) by the help of the blending coefficient given in Eqn. (5.4.26).

The saturation of -0.1~0.1 is applied for three variables. These are the new input, u_1, aft throttle setting, $\tilde{\delta}_T^a$ and the elevator deflection, $\tilde{\delta}_e$. The simulation time is equal to 200 s.

The initial state is selected as $x(0) = \begin{bmatrix} 0 & 0.2 & 0 & 0 \end{bmatrix}^T$ that is, $\alpha(0)$ is chosen as 0.2 rad to model the vertical wind gust effect. The same initial state is used in the simulations and the results are presented in Appendix C.

The feedback gains obtained for each forward velocity are given in Figure 5.16 through Figure 5.19. The corresponding system and input matrices are used in the calculations.

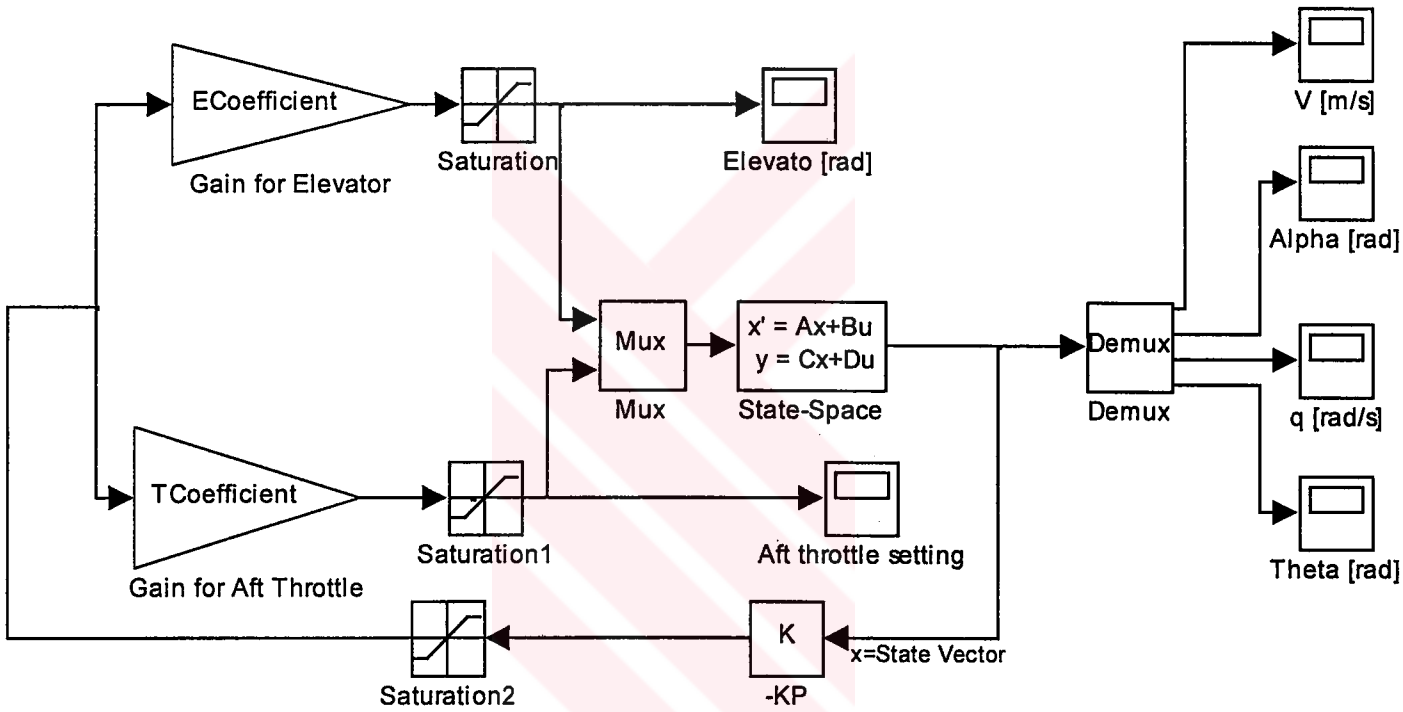

Figure B.1 The linear simulation model used to verify the full state feedback control system design with blending two inputs in transition flight mode

APPENDIX C

LINEAR SIMULATION RESULTS (THE FULL STATE FEEDBACK CONTROL SYSTEM DESIGN)

The simulation model given in Figure B.1 and simulation parameters defined in Appendix B are used in this application.

The following graphics are obtained for the specified forward velocities of the aircraft in transition flight mode.

The forward velocities, which are used in the simulations, are 5 m/s, 10 m/s, 15 m/s and 20 m/s respectively.

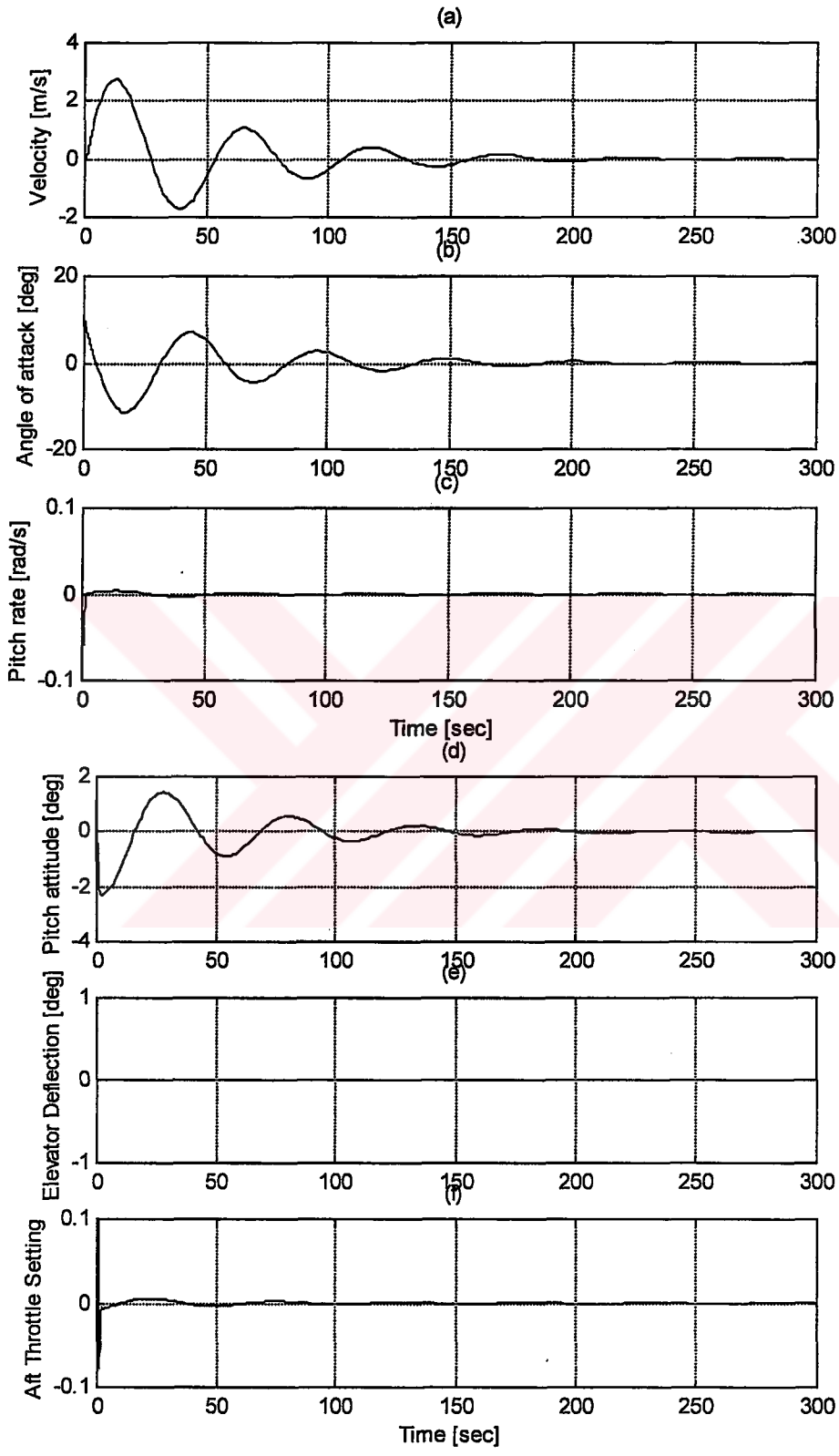

Figure C.1 Linear Simulation Results for $V = 5\,m/s$

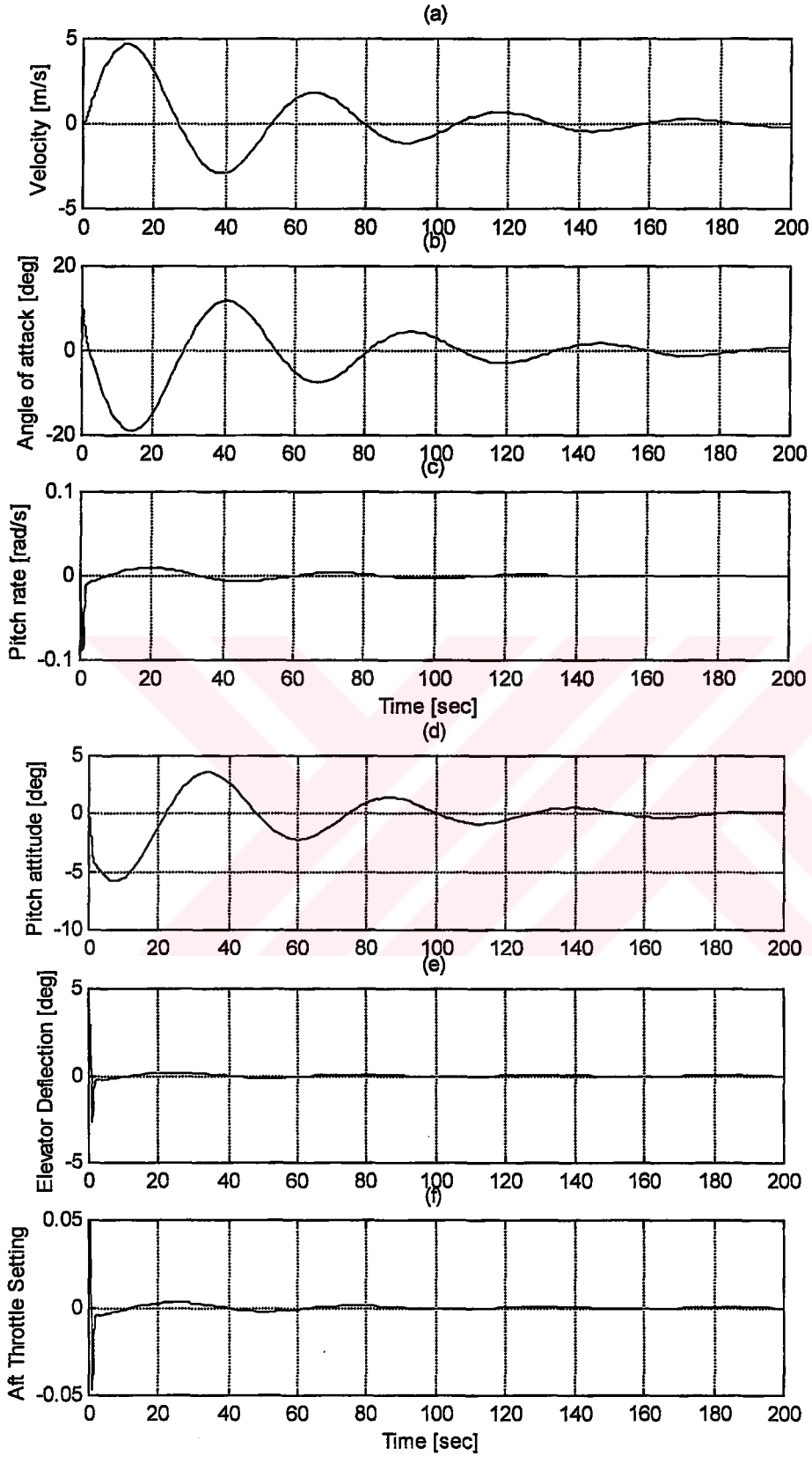

Figure C.2 Linear Simulation Results for $V = 10\,m/s$

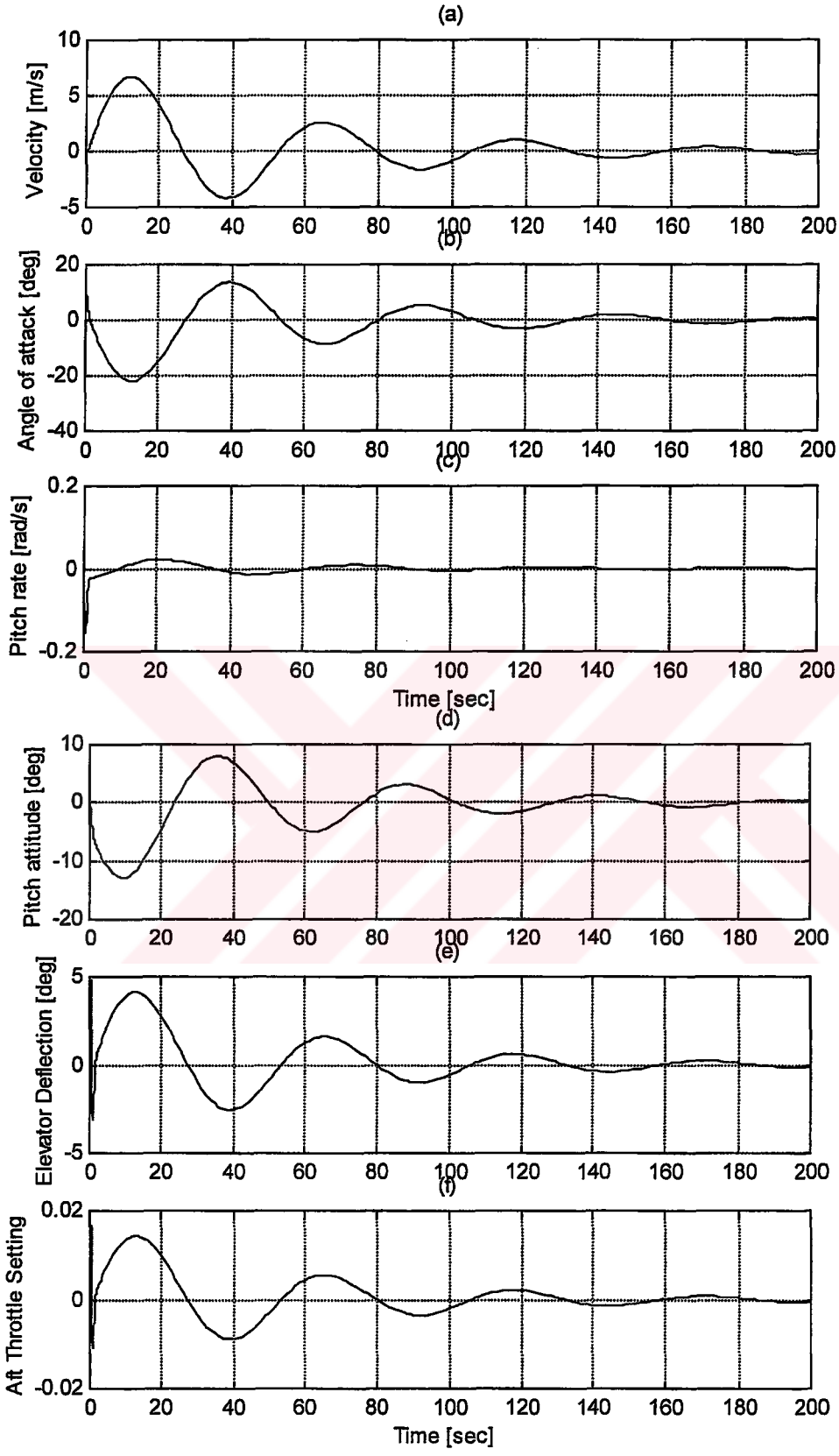

Figure C.3 Linear Simulation Results for $V = 15\,m/s$

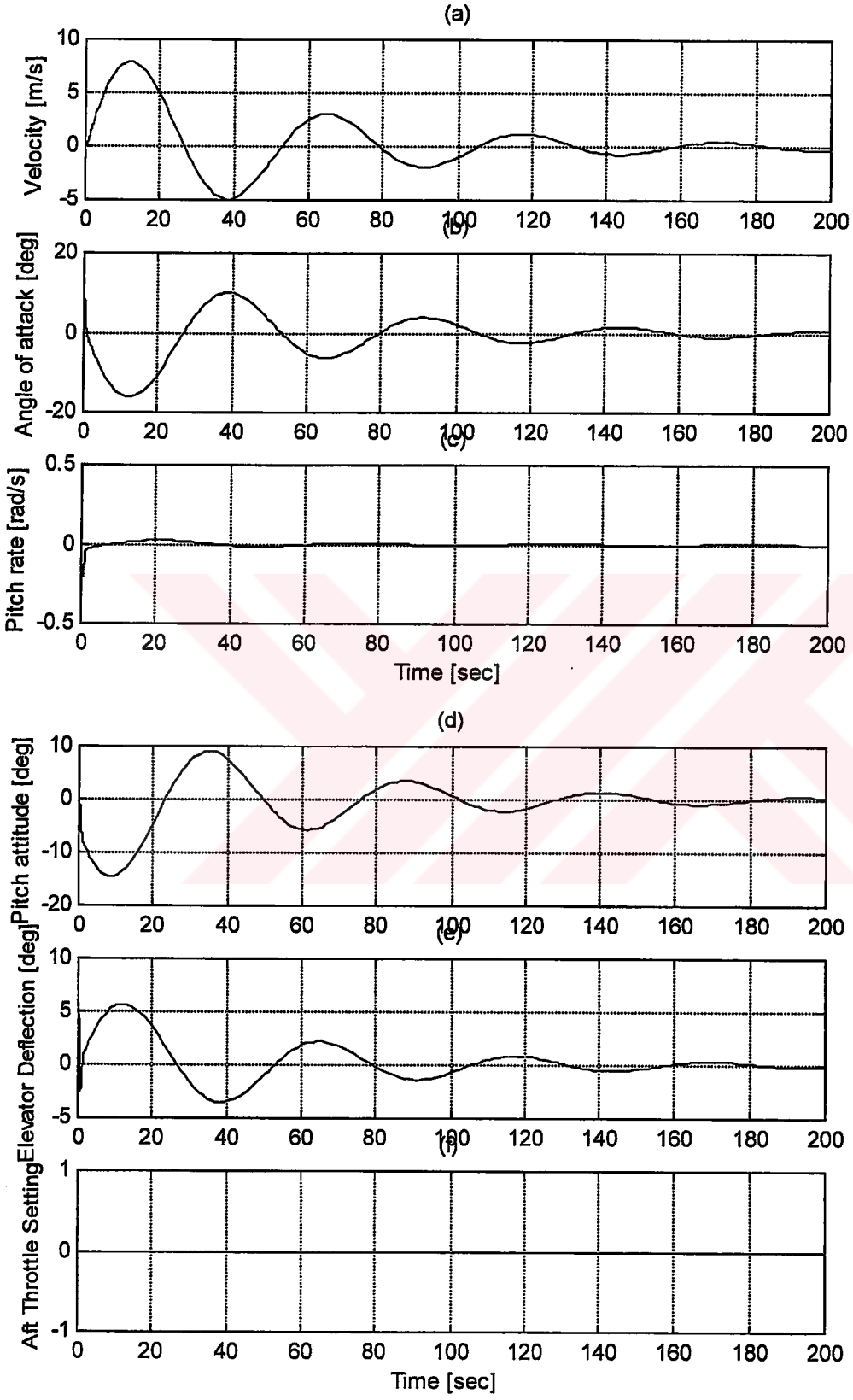

Figure C.4 Linear Simulation Results for $V = 20\,m/s$

APPENDIX D

SYSTEM MATRIX, INPUT MATRIX, LQR DESIGN GAIN MATRIX AND CORRESPONDING CLOSED LOOP EIGENVALUES

The matrices are presented in a special coding. A, B, K and Eig denotes, system matrix, input matrix, LQR design gain matrix and corresponding closed loop eigenvalues, respectively.

$\underline{V = 0.1\,m/s}$

$$A1 = \begin{bmatrix} -0.0006 & 0.0044 & 0 & -9.81 & -0.0484 \\ 0.409 & -0.0022 & 0.9919 & 0 & -15.44 \\ -0.0004 & -0.00003 & -0.0047 & 0 & -1.2973 \\ 0 & 0 & 1 & 0 & 0 \\ 0 & 0 & 0 & 0 & -0.14 \end{bmatrix} \quad B1 = \begin{bmatrix} 0 & 0 \\ 0 & 0 \\ -0.0001 & 0 \\ 0 & 0 \\ 0 & 0.14 \end{bmatrix}$$

$$K1 = \begin{bmatrix} 0 & 0 & 0 & 0 & 0 \\ 0.5908 & -0.3245 & -13.89 & -12.69 & 17.18 \end{bmatrix}$$

$$Eig1 = \begin{bmatrix} -0.6567 + 0.5937i \\ -0.6567 - 0.5937i \\ -0.2787 + 0.609i \\ -0.2787 - 0.609i \\ -0.6824 \end{bmatrix}$$

$V = 5\ m/s$

$$A2 = \begin{bmatrix} -0.039 & 0.1235 & 0 & -9.81 & -0.3767 \\ -0.0205 & -0.2350 & 0.9919 & 0 & -0.2998 \\ -0.0031 & -0.07 & -0.236 & 0 & -1.2978 \\ 0 & 0 & 1 & 0 & 0 \\ 0 & 0 & 0 & 0 & -0.14 \end{bmatrix}, B2 = \begin{bmatrix} 0 & 0 \\ 0 & 0 \\ -0.3376 & 0 \\ 0 & 0 \\ 0 & 0.14 \end{bmatrix},$$

$$K2 = \begin{bmatrix} 0 & 0 & 0 & 0 & 0 \\ 0.0307 & 0.2351 & -2.5277 & -1.446 & 5.9 \end{bmatrix},$$

$$Eig2 = \begin{bmatrix} -0.3415 + 0.3923i \\ -0.3415 - 0.3923i \\ -0.1846 + 0.2897i \\ -0.1846 - 0.2897i \\ -0.4245 \end{bmatrix}$$

$V = 7\ m/s$

$$A3 = \begin{bmatrix} -0.0642 & 0.3368 & 0 & -9.81 & -0.488 \\ -0.028 & -0.3463 & 0.9919 & 0 & -0.2096 \\ -0.0097 & -0.1055 & -0.3305 & 0 & -1.2982 \\ 0 & 0 & 1 & 0 & 0 \\ 0 & 0 & 0 & 0 & -0.14 \end{bmatrix}, B3 = \begin{bmatrix} 0 & 0 \\ 0 & 0 \\ -0.6617 & 0 \\ 0 & 0 \\ 0 & 0.14 \end{bmatrix}$$

$$K3 = \begin{bmatrix} 0.0048 & 0.035 & -0.1919 & -0.1820 & 00.3292 \\ 0.0188 & 0.1515 & -1.5507 & -0.8983 & 3.719 \end{bmatrix},$$

$$Eig3 = \begin{bmatrix} -0.4221 + 0.5578i \\ -0.4221 - 0.5578i \\ -0.126 + 0.1784i \\ -0.126 - 0.1784i \\ -0.4324 \end{bmatrix}.$$

$V = 10\ m/s$

$$A4 = \begin{bmatrix} -0.1135 & 0.9015 & 0 & -9.81 & -0.627 \\ -0.0376 & -0.5021 & 0.9919 & 0 & -0.1414 \\ -0.0128 & -0.1974 & -0.4721 & 0 & -1.2989 \\ 0 & 0 & 1 & 0 & 0 \\ 0 & 0 & 0 & 0 & -0.14 \end{bmatrix}, B4 = \begin{bmatrix} 0 & 0 \\ 0 & 0 \\ -1.3504 & 0 \\ 0 & 0 \\ 0 & 0.14 \end{bmatrix}$$

$$K4 = \begin{bmatrix} 0.0121 & 0.0876 & -0.4797 & -0.4549 & 0.823 \\ 0.0009 & 0.0261 & -0.0853 & -0.0762 & 0.4474 \end{bmatrix}$$

$$Eig4 = \begin{bmatrix} -0.6362 + 0.585i \\ -0.2331 - 0.2912i \\ -0.2331 + 0.2912i \\ -0.2331 - 0.2912i \\ -0.1996 \end{bmatrix}$$

$V = 15\ m/s$

$$A5 = \begin{bmatrix} -0.1911 & 2.008 & 0 & -9.81 & -0.709 \\ -0.0435 & -0.7346 & 0.9919 & 0 & -0.0917 \\ -0.0112 & -0.8424 & -0.7081 & 0 & -1.2993 \\ 0 & 0 & 1 & 0 & 0 \\ 0 & 0 & 0 & 0 & -0.14 \end{bmatrix}, B5 = \begin{bmatrix} 0 & 0 \\ 0 & 0 \\ -3.039 & 0 \\ 0 & 0 \\ 0 & 0.14 \end{bmatrix}$$

$$K5 = \begin{bmatrix} 0.008 & 0.1246 & -0.3354 & -0.4147 & 0.247 \\ 0.00002 & 0.0005 & -0.0005 & -0.0005 & 0.0166 \end{bmatrix}$$

$$Eig5 = \begin{bmatrix} -1.0474 + 1.0023i \\ -1.0474 - 1.0023i \\ -0.279 + 0.445i \\ -0.2331 - 0.2912i \\ -0.1423 \end{bmatrix}$$

$V = 20\ m/s$

$$A6 = \begin{bmatrix} -0.1857 & 2.9174 & 0 & -9.81 & -0.545 \\ -0.035 & -0.946 & 0.9919 & 0 & -0.072 \\ -0.008 & -2.1739 & -0.9442 & 0 & -1.2985 \\ 0 & 0 & 1 & 0 & 0 \\ 0 & 0 & 0 & 0 & -0.14 \end{bmatrix}, \quad B6 = \begin{bmatrix} 0 & 0 \\ 0 & 0 \\ -5.4 & 0 \\ 0 & 0 \\ 0 & 0.14 \end{bmatrix}$$

$$K6 = \begin{bmatrix} 0.007 & 0.1848 & -0.3110 & -0.4381 & 0.1261 \\ 0 & 0 & 0 & 0 & 0 \end{bmatrix}$$

$$Eig6 = \begin{bmatrix} -1.5535 + 1.4322i \\ -1.5535 - 1.4322i \\ -0.3245 + 0.4421i \\ -0.3245 - 0.4421i \\ -0.14 \end{bmatrix}$$

$V = 23\ m/s$

$$A7 = \begin{bmatrix} -0.1651 & 3.3591 & 0 & -9.81 & -0.4293 \\ -0.0295 & -1.066 & 0.9919 & 0 & -0.0646 \\ -0.0109 & -3.125 & -1.0858 & 0 & -1.298 \\ 0 & 0 & 1 & 0 & 0 \\ 0 & 0 & 0 & 0 & -0.14 \end{bmatrix}, \quad B7 = \begin{bmatrix} 0 & 0 \\ 0 & 0 \\ -7.144 & 0 \\ 0 & 0 \\ 0 & 0.14 \end{bmatrix}$$

$$K7 = \begin{bmatrix} 0.0071 & 0.211 & -0.2944 & -0.4417 & 0.1002 \\ 0 & 0 & 0 & 0 & 0 \end{bmatrix}$$

$$Eig7 = \begin{bmatrix} -1.8647 + 1.6186i \\ -1.8647 - 1.6186i \\ -0.3456 + 0.4105i \\ -0.3456 - 0.4105i \\ -0.14 \end{bmatrix}$$

$V = 25\ m/s$

$$A8 = \begin{bmatrix} -0.1553 & 3.39 & 0 & -9.81 & -0.382 \\ -0.0267 & -1.1447 & 0.9919 & 0 & -0.0599 \\ -0.0113 & -3.8 & -1.18 & 0 & -1.2979 \\ 0 & 0 & 1 & 0 & 0 \\ 0 & 0 & 0 & 0 & -0.14 \end{bmatrix}, \quad B8 = \begin{bmatrix} 0 & 0 \\ 0 & 0 \\ -8.44 & 0 \\ 0 & 0 \\ 0 & 0.14 \end{bmatrix}$$

$$K8 = \begin{bmatrix} 0.0074 & 0.2228 & -0.289 & -0.4452 & 0.0872 \\ 0 & 0 & 0 & 0 & 0 \end{bmatrix}$$

$$Eig8 = \begin{bmatrix} -2.0981 + 1.7083i \\ -2.0981 - 1.7083i \\ -0.36 + 0.394i \\ -0.36 - 0.394i \\ -0.14 \end{bmatrix}$$

$V = 30\ m/s$

$$A9 = \begin{bmatrix} -0.1172 & 3.7466 & 0 & -9.81 & -0.262 \\ -0.02 & -1.342 & 0.9919 & 0 & -0.05 \\ -0.0178 & -5.69 & -1.4163 & 0 & -1.2976 \\ 0 & 0 & 1 & 0 & 0 \\ 0 & 0 & 0 & 0 & -0.14 \end{bmatrix}, \quad B9 = \begin{bmatrix} 0 & 0 \\ 0 & 0 \\ -12.15 & 0 \\ 0 & 0 \\ 0 & 0.14 \end{bmatrix}$$

$$K9 = \begin{bmatrix} 0.0091 & 0.2525 & -0.284 & -0.467 & 0.067 \\ 0 & 0 & 0 & 0 & 0 \end{bmatrix}, \quad Eig9 = \begin{bmatrix} -2.7626 + 1.81i \\ -2.7626 - 1.81i \\ -0.41 + 0.349i \\ -0.41 - 0.349i \\ -0.14 \end{bmatrix}$$

APPENDIX E

LINEAR SIMULATION MODEL USED TO VERIFY THE LINEAR QUADRATIC REGULATOR (LQR) DESIGN IN TRANSITION FLIGHT MODE

In this model, system matrix, A and input matrix, B, presented in Eqn. (5.4.29) and blending technique presented in Eqn. (5.4.26) are used. The full-state feedback control law is applied given in Eqn. (5.4.31). This process is repeated for different forward velocities. The state and input variables are in variational parameter mode.

The saturation of -0.1~0.1 is applied for two variables. These are commanded aft throttle setting, $\tilde{\delta}_{Tc}^{a}$ and the elevator deflection, $\tilde{\delta}_{e}$. Thus, $\pm\%10$ authority in the aft throttle and $\pm 5.73^{0}$ authority in the elevator is taken. The simulation time is equal to 75 s.

The initial state is selected as $x(0) = [0 \quad 0.2 \quad 0 \quad 0]^{T}$ that is, $\alpha(0)$ is chosen as 0.2 rad to model the vertical wind gust effect. The same initial state is used in the simulations and the results are presented in Appendix F.

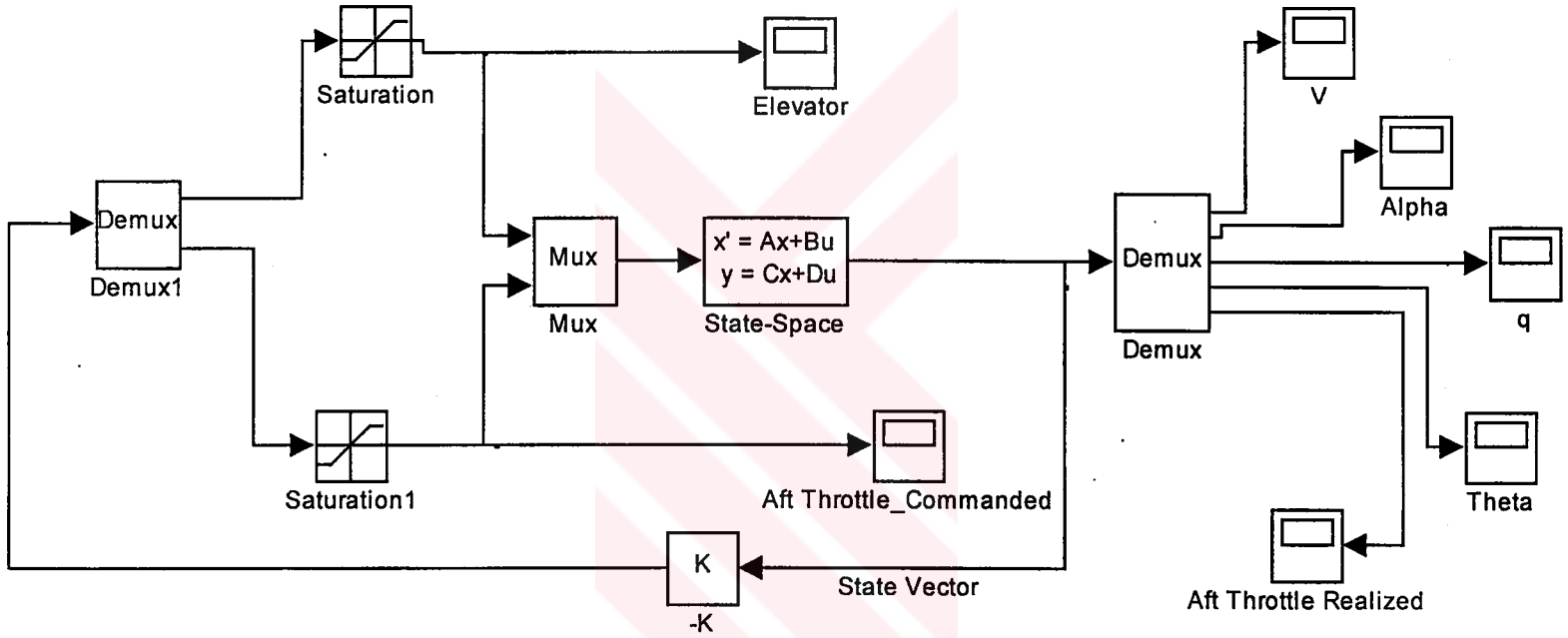

Figure E.1 The linear simulation model used to verify the linear quadratic regulator (LQR) design in transition flight mode

APPENDIX F

LINEAR SIMULATION RESULTS OF THE OVERALL SYSTEM DESIGNED WITH THE LINEAR QUADRATIC REGULATOR (LQR)

The simulation model given in Figure E.1 and simulation parameters defined in Appendix E are used in this application.

The following graphics are obtained for the specified forward velocities of the aircraft in transition flight mode.

The forward velocities, which are used in the simulations, are 5 m/s, 7 m/s, 10 m/s, 15 m/s, 20 m/s and 23 m/s respectively.

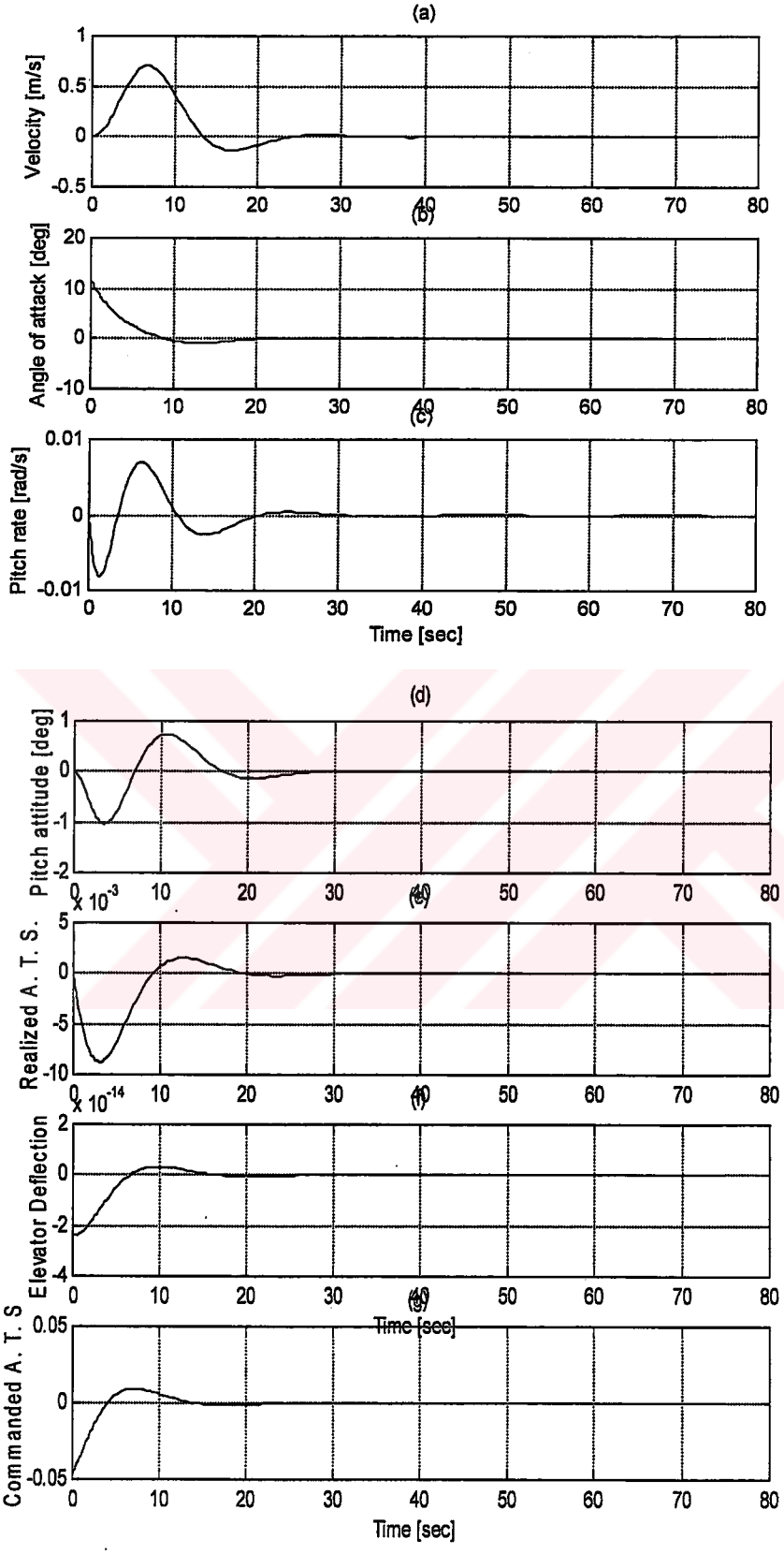

Figure F.1 Linear Simulation Results for $V = 5m/s$

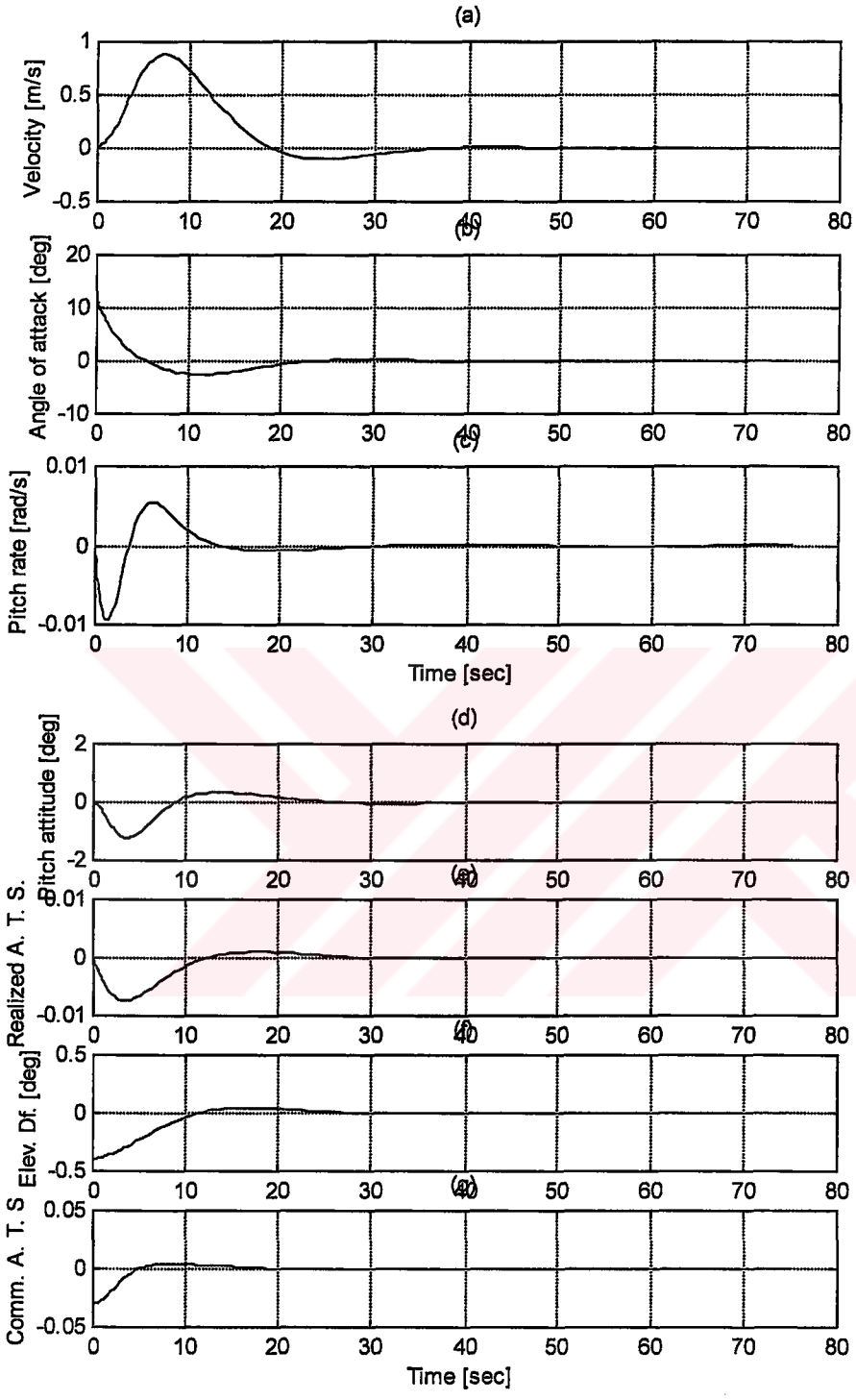

Figure F.2 Linear Simulation Results for $V = 7\,m/s$

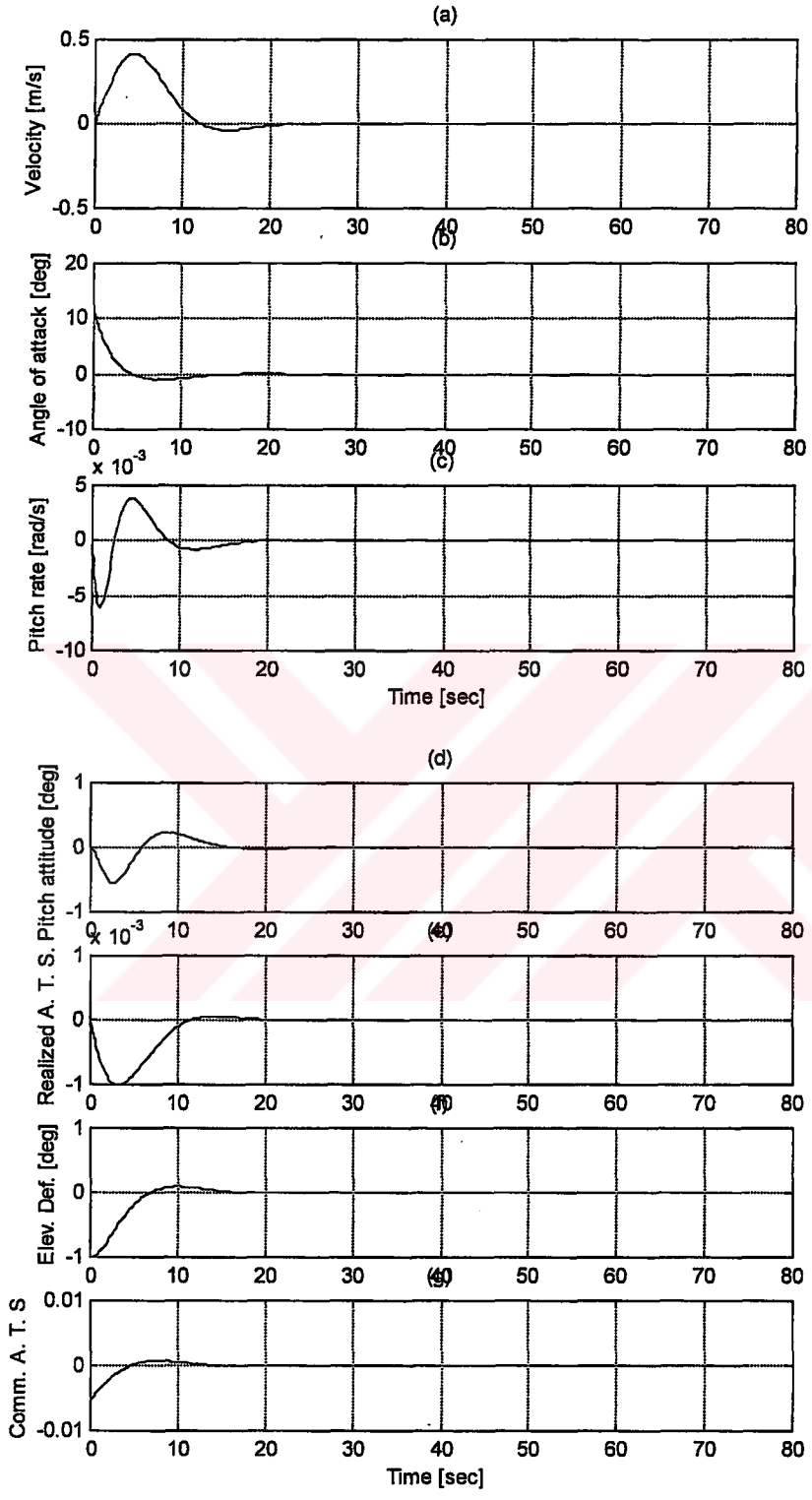

Figure F.3 Linear Simulation Results for $V = 10\,m/s$

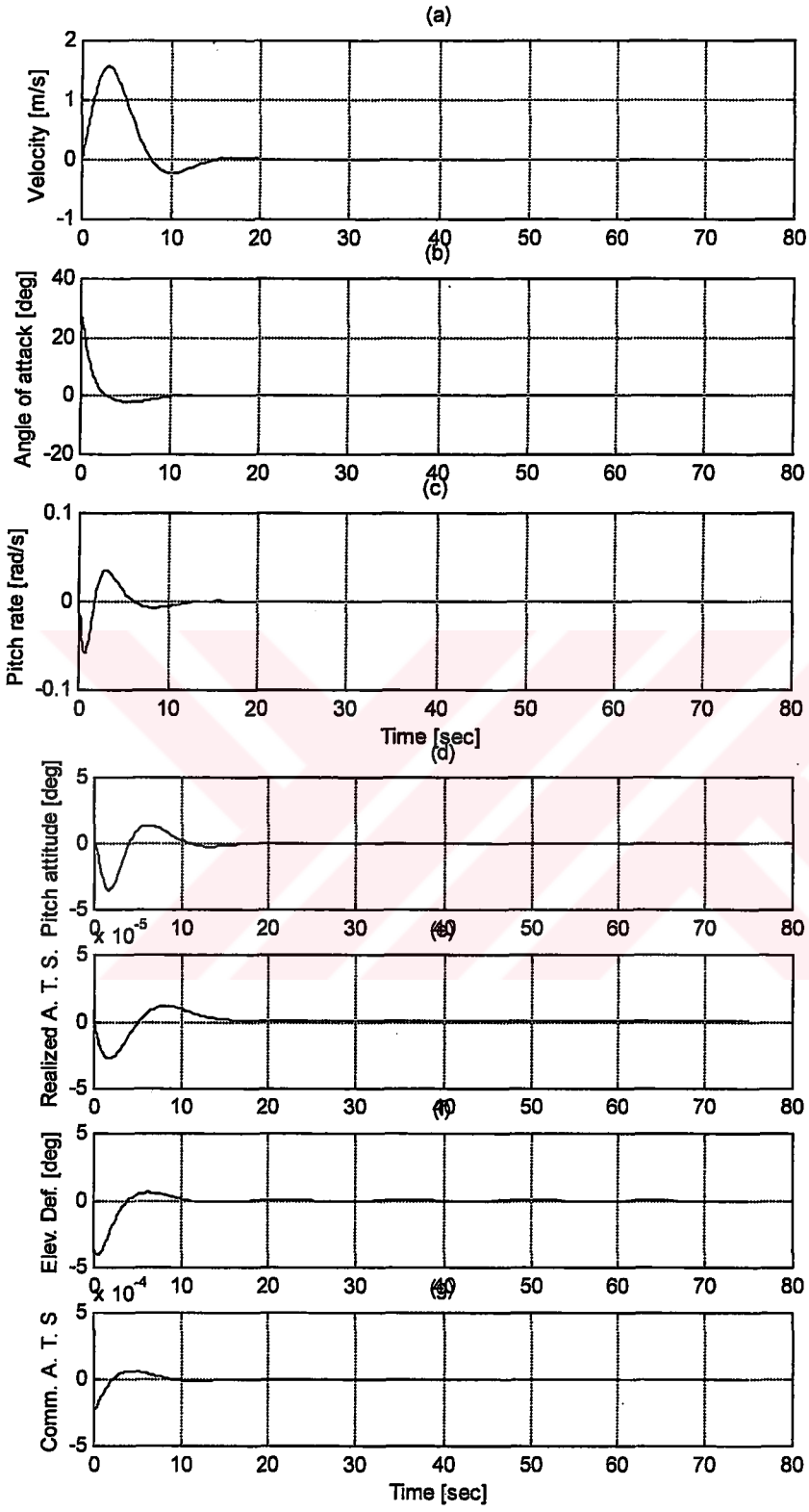

Figure F.4 Linear Simulation Results for $V = 15\,m/s$

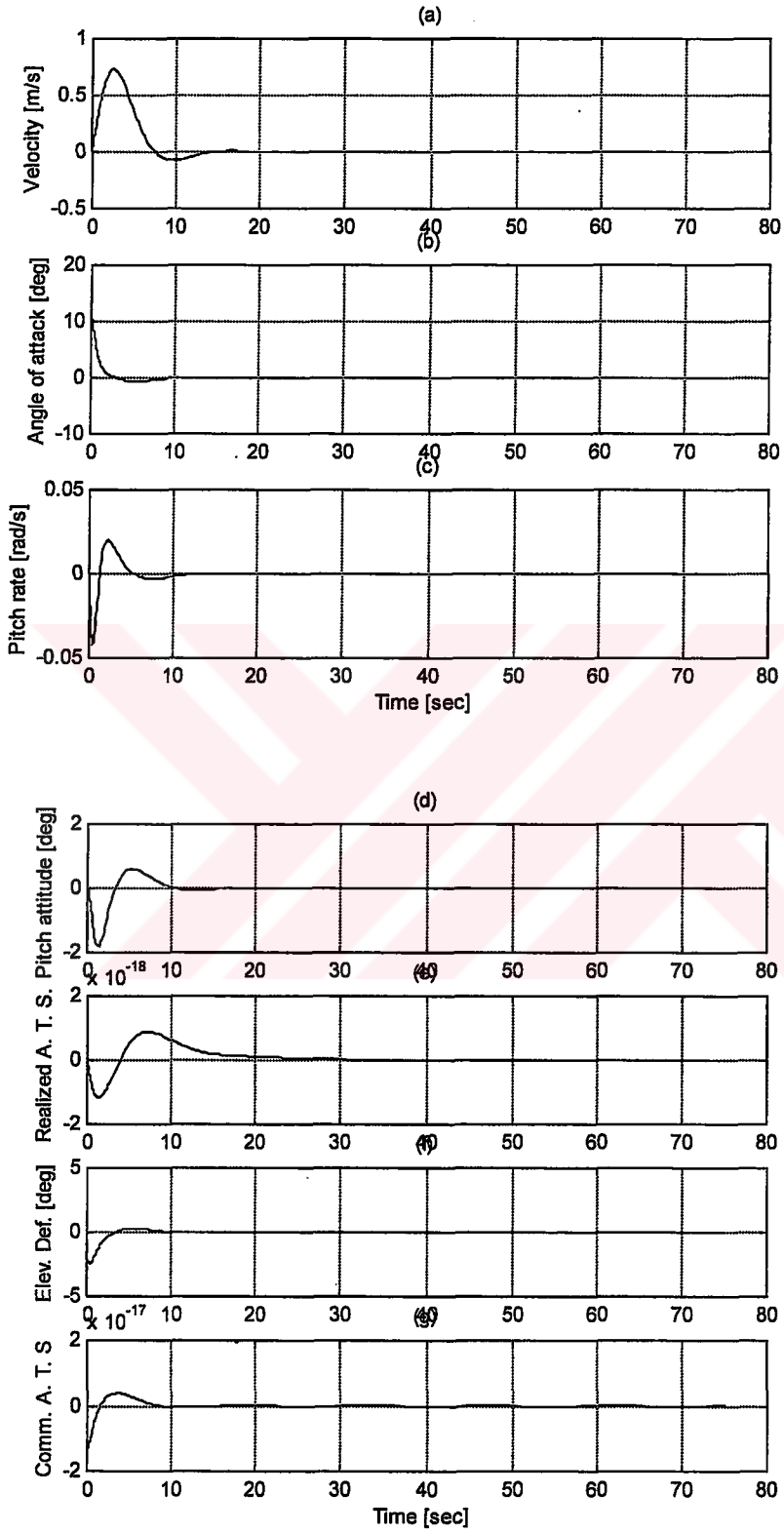

Figure F.5 Linear Simulation Results for $V = 20\,m/s$

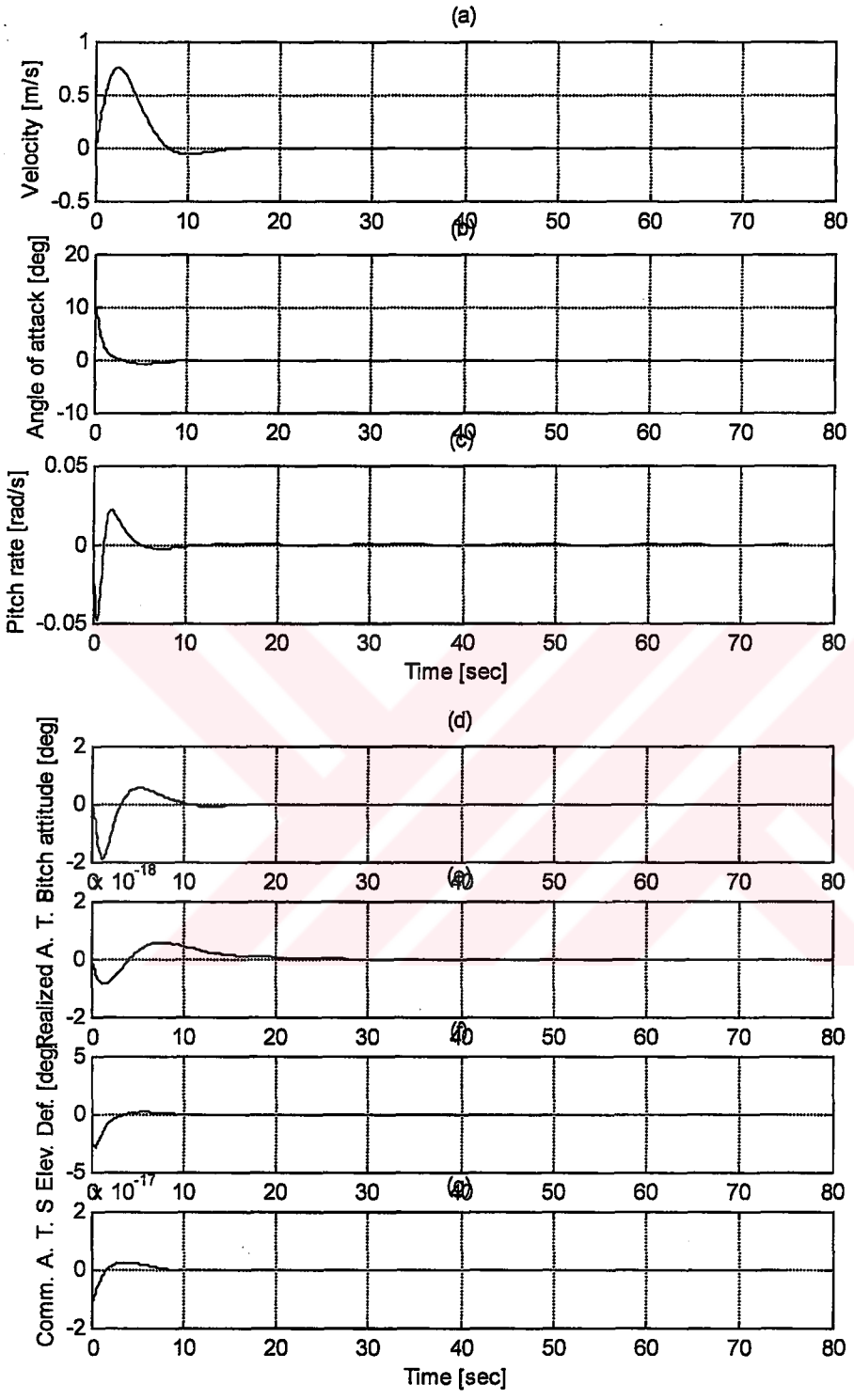

Figure F.6 Linear Simulation Results for $V = 23\,m/s$